2009

Studies of G-Protein Coupled Receptors Incorporated Into a Novel, Nanoscale, Membrane-Mimetic System

Sourabh Banerjee

STUDIES OF G PROTEIN-COUPLED RECEPTORS INCORPORATED INTO A NOVEL, NANOSCALE, MEMBRANE-MIMETIC SYSTEM

A Thesis Presented to the Faculty of

The Rockefeller University

in Partial Fulfillment of the Requirements for

the degree of Doctor of Philosophy

by

Sourabh Banerjee

June 2009

STUDIES OF G PROTEIN-COUPLED RECEPTORS INCORPORATED INTO A NOVEL, NANOSCALE, MEMBRANE-MIMETIC SYSTEM

Sourabh Banerjee, Ph.D.

The Rockefeller University 2009

From first principles of phospholipid – apolipoprotein A-I (apo A-I) interactions, we hypothesized that the amino acid sequence of apo A-I derived from a different species may exhibit improved properties compared to human apo A-I for the purpose of incorporation of G protein-coupled receptors (GPCRs) into homogeneous discoidal lipoprotein particles. We generated apolipoprotein A-I DNA derived from zebrafish (*Danio rerio*) using molecular cloning techniques and optimized a heterologous bacterial expression system, and protein purification and labeling scheme for obtaining high-yields of pure zebrafish apo A-I. We demonstrated that zebrafish apo A-I forms stable, homogeneous discoidal lipoprotein particles, which we termed as Nanoscale Apolipoprotein Bound Bilayers (NABBs).

Using bovine rhodopsin as a model system, we developed a novel method of rapidly incorporating GPCRs into NABBs – a significant improvement over traditional methods – requiring less time and materials for receptor reconstitution. The method was generalized for incorporation of heterologously expressed GPCRs in mammalian cells available at comparatively lower levels of receptor concentration and purity. A novel

ELISA technique was developed for high-throughput quantification of the incorporated GPCR in NABBs. We also developed methods to control the ratio of receptor to NABB and imaged the rhodopsin-NABBs using electron microscopy (EM) to measure stoichiometry and receptor orientation.

Using a combination of EM imaging and biochemical analyses, we correlated stability and signaling efficiency of rhodopsin in NABBs with either one or two receptors. We discovered that the specific activity of G protein coupling for single rhodopsins sequestered in individual NABBs was nearly identical to that of two rhodopsins per NABB under conditions where stoichiometry and orientation could be inferred by electron microscopy imaging. Thermal stability of rhodopsin and CCR5 in NABBs was superior to the receptors in various detergents commonly used for membrane protein work. CCR5 in NABBs retained its ability to activate G protein. This work highlights the NABBs as a promising tool for *in-vitro* manipulation of GPCR stoichiometry and biophysical studies of GPCRs in an isolated, native-like, cell-free system.

The important thing in science is not so much to obtain new facts

as to discover new ways of thinking about them.

-William Lawrence Bragg

ACKNOWLEDGEMENTS

The work presented in this thesis would not have been possible without the guidance and help of the people mentioned here. First and foremost, my thesis advisor Dr. Thomas P. Sakmar for his timely advice, motivation and guidance. He has treated me more like a colleague than a student, which made me gain independence at the bench from the very first day and confidence shortly thereafter. Also, the members of my thesis advisory committee have consistently provided me with constructive feedback during my faculty advisory committee meetings.

I would also like to acknowledge all the members of the Sakmar Lab 2004-08 who have been brilliant colleagues and great friends. Most notably, Thomas Huber who has always stimulated my thinking, challenged my assumptions and inspired me to design experiments as elegantly as himself. Manija Kazmi for teaching me the basics of molecular cloning, Santosh Menon for teaching me protein expression, purification and activity assays, Pallavi Sachdev for introducing me to mammalian cell culture techniques and antibody based work, Shixin Ye for PCR troubleshooting ideas that worked and Amy Grunbeck for helping out with some of the CCR5-NABB experiments. I also thank Tom Haines, Cecille Unson-O'Brien, Jay Janz, Fabien Decalloit, Neeraj Kapoor, and Christoph Seibert for helpful discussions.

I am grateful to the following people at the New York Structural Biology Center (NYSBC) for patiently teaching me electron microscopy techniques- John Berriman, KD Derr, Ruben Diaz, William Rice and David Stokes. Several people were indirectly involved by providing us with materials vital to our experiments: Dr. Stephen G. Sligar (UIUC) for MSP1 protein during the early phase of this work, Dr. James Hudspeth (RU) provided us with zebrafish RNA, and Dr. Maurine Linder (WUSTL) for NMT1 and Gi1-alpha expression vectors.

My training would not have been successful without generous funding support from the tri-institutional Training Program in Chemical Biology (TPCB) and the David Rockefeller Graduate Program, which among other things, enabled me to attend a molecular microscopy workshop at the Scripps Research Institute, CA, and travel to attend conferences.

Finally, I would like to thank my family for their constant encouragement and my wife for her support and understanding, which was duly tested before many submission deadlines and presentations.

TABLE OF CONTENTS

LIST OF FIGURES

LIST OF TABLES

ABBREVIATIONS

Apo A-I	Apolipoprotein A-I
BRET	Bioluminescence Resonance Energy Transfer
CCR5	Chemokine Receptor 5
CD	Circular Dichroism
CV	Column Volume
DM	*n*-dodecyl-β-D-maltopyranoside
EDTA	Ethylenediaminetetraacetic acid
EM	Electron microscopy
FRET	Fluorescence Resonance Energy Transfer
Gn.HCl	Guanidine hydrochloride
GPCR	G protein-coupled receptor
Gt	Holotransducin
Hap1	Hexahistidine tagged human apolipoprotein A-I
HDL	High-density lipoprotein
ITC	Isothermal titration calorimetry
LRB-DOPE	*N*-(lissamine rhodamine B sulfonyl)-1,2-dioleoyl-*sn*-glycero-3-phosphatidylethanolamine
NABB	Nanoscale Apolipoprotein Bound Bilayer

OG	*n*-octyl-β-D-glucopyranoside
POPC	1-palmitoyl-2-oleoyl-*sn*-glycero-3-phosphatidylcholine
Rho	Rhodopsin
ROS	Rod outer segment
RT	Reverse transcriptase
SUV	Small unilamellar vesicle
UA	Uranyl acetate
Zap1	Hexahistidine tagged zebrafish apolipoprotein A-I

1.0

Introduction

1.1 G Protein-Coupled Receptors

G Protein-Coupled Receptors (GPCRs) are integral transmembrane proteins that are known to transduce extracellular signals into intracellular functions and pathways (Filipek, Stenkamp *et al.* 2003). They form the largest and one of the most diverse groups of receptor proteins and are encoded by more than 1,000 genes in the human genome (Howard, McAllister *et al.* 2001). The signal transduction machinery in a cell is triggered by binding of an agonist ligand (or activation by light in the case of rhodopsin) at the extracellular side, followed by binding and activation of a guanine-nucleotide binding regulatory protein (G Protein) at the cytoplasmic side. A variety of chemical transmitters can elicit a cellular response via their related GPCR. These include biogenic amines (neurotransmitters), amino acids, peptides, lipids, nucleosides and large polypeptides. GPCRs thus control a wide range of physiological processes such as neurotransmission, cellular metabolism, secretion, cellular differentiation and growth, and inflammatory and immune responses (Bouvier 2001).

Figure 1-1. Signal Transduction by G Protein-Coupled Receptors

G-Protein Coupled Receptors (GPCRs) are seven-transmembrane helix containing proteins. GPCRs activate a heterotrimeric guanine-linked protein (G-protein) inside the cell. In the inactive state the G-protein contains a GDP bound to its α-subunit (Step 1). The GPCR is activated by an extracellular ligand, or in case of rhodopsin, by light (Step 2). A conformational change during activation of the GPCR (Step 3) catalyzes an exchange of GDP for GTP by the α-subunit of the G-protein (Step 4). Uptake of GTP causes the heterotrimeric G-protein to dissociate into the GTP-bound α-subunit and the βγ-subunits (Step 5). The α and/ or βγ-subunits interact with downstream proteins to manifest their action, which is dependent on the G-protein sub-type. The GTP bound to the α-subunit is converted to GDP by the intrinsic enzymatic hydrolysis activity of the α-subunit, and controlled by accessory proteins (Step 6). In the GDP bound state, the α-subunit reassociates with the βγ subunits to form the G-protein heterotrimer. The G-protein heterotrimer is then ready to couple with another GPCR (Step 6).

Image adapted from http://en.wikipedia.org/wiki/G_protein

Figure 1-1

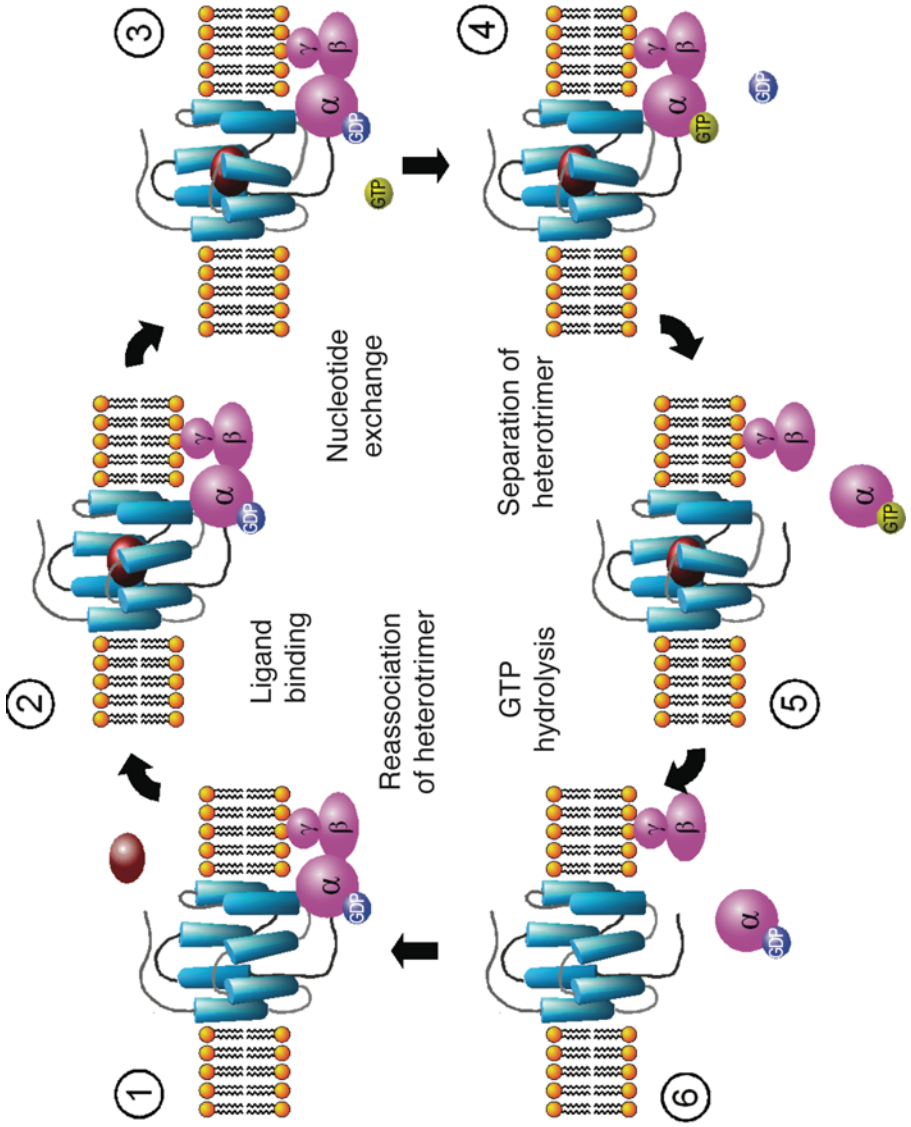
1
2
3
4
5
6
Ligand binding
Nucleotide exchange
Separation of heterotrimer
GTP hydrolysis
Reassociation of heterotrimer
α
β
γ
GDP
GTP

Not surprisingly, GPCRs are targets of a large number of therapeutic agents. It is estimated that 50% of all modern drugs (Howard, McAllister *et al.* 2001) and almost one-quarter of the top 200 best-selling drugs in the year 2000 modulated GPCR activity (George, O'Dowd *et al.* 2002).

The membrane topology of GPCRs consists of a characteristic hydrophobic core of seven transmembrane α-helices (Suryanarayana, von Zastrow *et al.* 1992), an extracellular amino-terminal segment and a cytoplasmic carboxy-terminal tail. Some GPCRs bear amine-linked glycosylation sites near their amino terminal tails. Ligand binding to GPCRs involves multiple interactions between functional groups and specific amino acids in the extracellular domains and/or the hydrophobic transmembrane core. Till recently, these interactions were well defined for only a few GPCRs (Bockaert and Pin 1999). Over the last year, there have been an increasing number of reports of high resolution X-ray crystal structures of GPCRs (Cherezov, Rosenbaum *et al.* 2007; Jaakola, Griffith *et al.* 2008; Scheerer, Park *et al.* 2008; Shimamura, Hiraki *et al.* 2008; Warne, Serrano-Vega *et al.* 2008). These structures have confirmed some key differences in structural elements compared with the prototypical GPCR – bovine rhodopsin (Palczewski 2000; Huber, Menon *et al.* 2008), but have not been able to adequately explain the dynamic regulation and mechanism of action of the active state of the GPCR.

Classically, the basic unit of signal transduction comprises the receptor, a heterotrimeric G protein and a downstream effector component. Binding of a

ligand promotes allosteric interactions between the receptor cytoplasmic side and the GDP-bound trimeric G protein leading to the release of GDP and binding of GTP to the α-subunit. This destabilizes the trimeric complex, causing the dissociation of the G_{α}.GTP and the $G_{\beta\gamma}$ dimer. The G_{α}.GTP, the $G_{\beta\gamma}$ dimer or both, in turn interact with and modulate the effector component, often involving a second messenger. Termination of the signal occurs upon hydrolysis of GTP to GDP due to the GTPase activity of the Gα subunit, aided by other GTPase activating proteins (GAPs). The signaling state of the receptor may be turned off either by ligand dissociation from the active conformation of the GPCR (in the case of rhodopsin), or phosphorylation of the cytoplasmic side followed by binding of a protein that is not G protein, or by receptor internalization into the cell.

GPCRs have been classified into various subclasses based upon differences in the N and C-terminal regions and insertions in the cytoplasmic loop regions (Bockaert and Pin 1999). Rhodopsin is a defining member of family 1 (or family A) GPCRs characterized by comparatively short N- and C-termini. This family includes β_2-adrenergic receptor, chemokine receptors, dopamine receptors and serotonin (5-HT) receptors. Most of the family A GPCRs have a palmitoylated cysteine in the C-terminal tail which serves as an anchor to the membrane. Family A GPCRs were all initially assumed to be monomeric, but some were able to form homodimers or heterodimers with another GPCR of the same class via their C-termini, or via contacts between the two 7TM cores (Chabre and le Maire 2005). Family 2 (or family B) GPCRs have a relatively long

N-terminal region which contains several cysteines forming a network of disulfide bridges, e.g- glucagon receptor. They are not palmitoylated at the C-terminus, unlike family 1. Family 3 (or family C) GPCRs have a long N-terminal extension folded in a separate extracellular domain as well as a C-terminal extension, e.g.- metabotropic glutamate receptor and the $GABA_B$ receptor. Family C GPCRs form constitutive homo or heterodimers, linked by disulfide bridges and associated mainly by their large extracellular domains, which include the ligand binding site.

Figure 1-2. Rhodopsin Photocycle and Crystal Structure

Rhodopsin in the dark state has 11-*cis*-retinal bound to Lys 296 via a protonated Schiff-base linkage with Glu-113 serving as the counterion. The retinal chromophore is a derivative of vitamin A_1. The structure in the center of the cycle represents rhodopsin in its dark state (adapted from (Sakmar 2002)). Photoisomerization of 11-*cis*-retinal occurs on an ultrafast timescale. The photolyzed pigment then proceeds through a series of spectral intermediates (Lewis and Kliger 2000). The Schiff-base imine remains protonated due to stabilization by its counterion Glu-113, through metarhodopsin-I (Meta-I). Under physiological conditions, Meta-I is in a dynamic equilibrium with Meta-II, which is characterized by a de-protonated Schiff base imine and a blue-shifted absorbance at 380nm. Meta-II is the 'active' state of the GPCR and is able to catalyze GTP uptake by its cognate G protein, transducin. Meta-II eventually decays to free all-*trans*-retinal and free opsin apoprotein.

This figure was adapted from Menon *et al.* (Menon, Han *et al.* 2001).

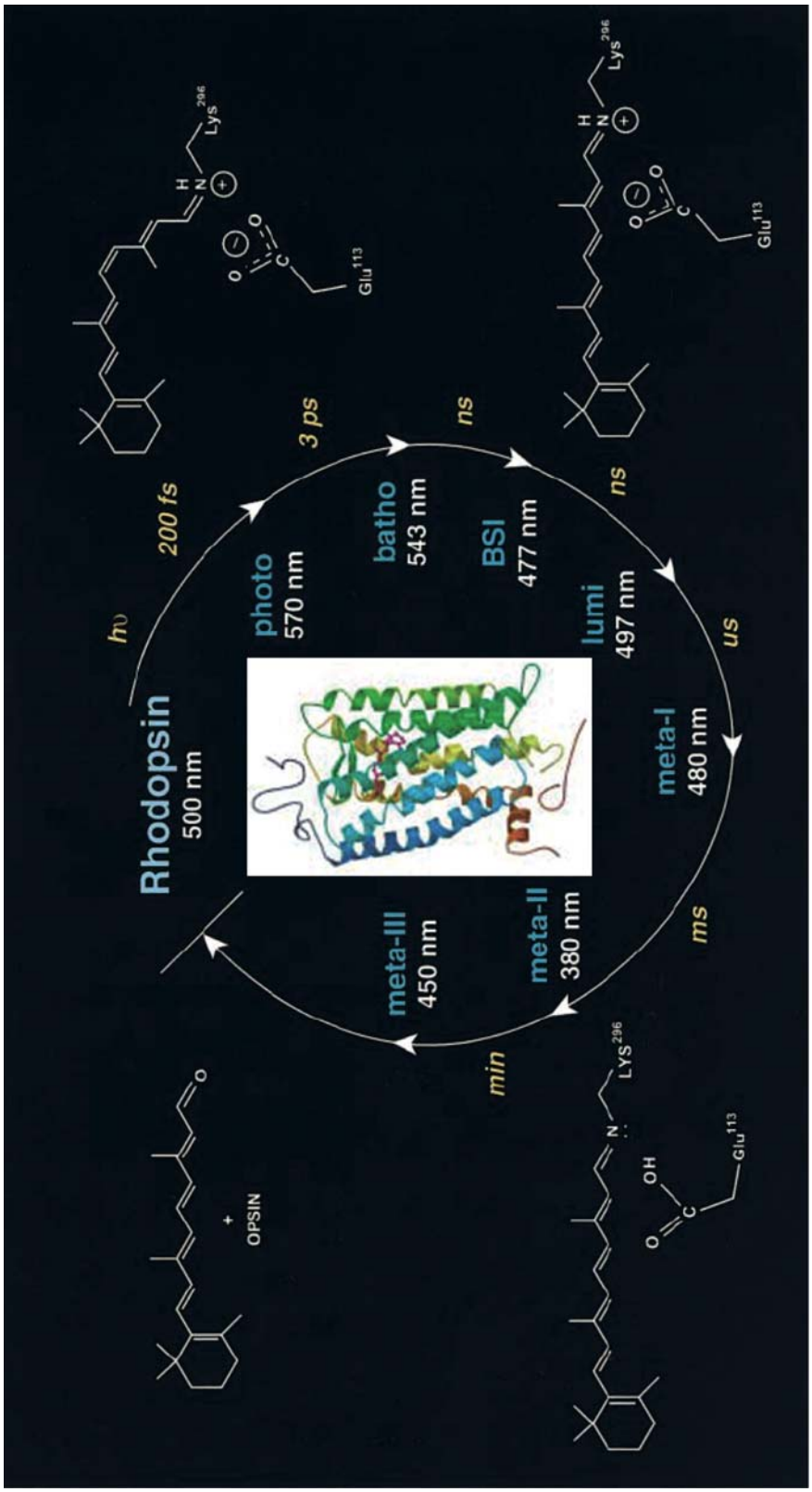
Rhodopsin
500 nm
hυ
200 fs
photo
570 nm
3 ps
batho
543 nm
ns
BSI
477 nm
ns
lumi
497 nm
μs
meta-I
480 nm
ms
meta-II
380 nm
min
meta-III
450 nm
OPSIN
Lys296
Glu113

Figure 1-2

1.1.1 Rhodopsin as the prototypical GPCR

The dim-light visual receptor rhodopsin stands out as a model system for GPCRs, both in terms of GPCR structure and the downstream G protein signaling mechanism. Rhodopsin is located in the outer segments of retinal rod cells. Bovine rhodopsin is easily accessible, available in relatively large amounts and has an available high-resolution structure solved by X-ray crystallography (Palczewski, Kumasaka *et al.* 2000; Filipek, Teller *et al.* 2003). Rhodopsin in its dark state has the chromophore 11-*cis*-retinal covalently linked with Lys296 on helix 7 via a protonated Schiff base linkage, with Glu113 serving as the counter-ion for the Schiff Base (Menon, Han *et al.* 2001). 11-*cis*-retinal serves as an inverse agonist and keeps the receptor in the inactive conformation in the dark. Bovine rhodopsin is sufficiently stable in the dark to be further purified by various chromatographic procedures and is thermally stable in solubilized form in a variety of detergents (De Grip 1982; Okada, Takeda *et al.* 1998).

Upon absorption of a photon, the bound chromophore 11-*cis*-retinal undergoes a *cis*-trans conformational switch, which brings about a shift in the transmembrane helices. The isomerization of retinal leads to a series of conformational changes in the transmembrane helices (Farrens, Altenbach *et al.* 1996), which include a counter-ion switch from Glu113 to Glu181 (Yan, Kazmi *et al.* 2003) to form metarhodopsin I (pre-active state), deprotonation of the Schiff Base to form the active state- metarhodopsin II (**Fig. 1-2**) and the disruption of a critical salt-bridge between Lys296 and Glu113 (Cohen, Oprian *et al.* 1992) to

form opsin. Metarhodopsin II (Meta-II) interacts with a G protein, called transducin, and activates it. This in turn activates (by de-inhibiting) a photoreceptor cGMP-specific phosphodiesterase (Stryer, Hurley *et al.* 1983).

It is anticipated that the phototransduction signaling pathway involving rhodopsin and transducin will be the first G protein-coupled pathway for which a complete molecular description is ultimately available (Ridge, Abdulaev *et al.* 2003).

1.1.2 Chemokine Receptors

Chemokine receptors are members of family A GPCRs and of significant clinical importance. Chemokines (chemotactic cytokines) constitute a superfamily of structurally related small proteins, less than 100 residues in length that are implicated in the control of a large variety of biological processes including inflammation, immunosurveillance, viral infection and cancer (Gerard and Rollins 2001). Chemokines mediate their effects by binding to the chemokine receptors (Berger, Murphy *et al.* 1999; Rossi and Zlotnik 2000). The CXC and CC chemokines belong to different subfamilies where the two N-terminal cysteines are separated by a single amino acid and are adjacent to each other respectively. Examples of CC-chemokines include MIP-1α (Macrophage Inflammatory Protein-1α), MIP-1β and RANTES (Regulated on Activation, Normal T-Cell Expressed and Secreted). All of these CC-chemokines bind non-selectively to CCR5 (Rossi and Zlotnik 2000).

CCR5 is an important co-receptor that is exploited for entry of HIV-1 (Human Immunodeficiency Virus type 1) and is critical for the transmission of this virus in the body (Berger, Murphy *et al.* 1999) (**Fig. 1-3**). A naturally occurring CCR5 mutant (CCR5Δ32) results in a truncated receptor which leads to protection against HIV-1 in homozygous individuals and markedly reduced progress towards AIDS in individuals heterozygous for this mutation (Liu, Paxton *et al.* 1996; Samson, Libert *et al.* 1996; O'Brien and Moore 2000). No adverse health effects have been linked to the non-functional CCR5 in these individuals, which makes CCR5 a very attractive target for pharmaceutical intervention for the prevention of HIV/AIDS (O'Brien and Moore 2000). CCR5 homo and heterodimerization has been reported to have effects on CCR5 mediated HIV entry into cells. The dominant-negative phenotype of CCR5Δ32 over its wild-type counterpart have been attributed to the propensity of CCR5Δ32 to dimerize with wild-type CCR5 in the ER, thereby promoting intra-cellular retention of the heterodimers (Benkirane, Jin *et al.* 1997). An anti-CCR5 antibody that promotes dimerization has been reported to activate receptor dependent calcium mobilization and cell migration, but inhibit its use by HIV as a co-receptor for virus entry (Vila-Coro, Mellado *et al.* 2000). Heterodimerization of CCR5 with CCL2 has also been reported to block HIV entry (Rodriguez-Frade, del Real *et al.* 2004).

A CCR5 to CXCR4 switch has also been reported to accompany the onset of AIDS (Berger, Murphy *et al.* 1999). SDF-1 (Stromal cell-Derived Factor-1) is a CXC-chemokine and is expressed as two functionally identical, alternative

splice variants: SDF-1α and SDF-1β (Rossi and Zlotnik 2000), and binds to CXCR4. CXCR4 is expressed in hematopoeitic cell-lines (Zou, Kottmann *et al.* 1998) and is thought to be involved in signaling responsible in part for stem-cell maturation, naive T-cell migration to spleen for antigen presentation and other developmental signaling (Proudfoot 2002). The SDF-1/CXCR4 system has been implicated in breast and ovarian cancers (Muller 2001; Scotton, Wilson *et al.* 2002) and brain tumors (Rubin, Kung *et al.* 2003).

Figure 1-3. Amino-acid sequence of CCR5 and its role in HIV entry

Secondary structure of CCR5 is arranged in the form of putative transmembrane helices. The membrane is depicted by the gray box. Amino acids considered critical for CCR5 function are shown by filled circles. Illustration taken from Oppermann *et al.* (Oppermann 2004). CCR5 is an important co-receptor for HIV entry into cells. The HIV protein gp120 binds first to CD4 and then with CCR5 (or CXCR4). Binding to the chemokine receptor (co-receptor) triggers the formation of a helix bundle in gp41, which eventually leads to insertion of a fusion peptide in the membrane and membrane fusion to facilitate HIV entry. Image adapted from Doms *et al.* (Doms and Trono 2000).

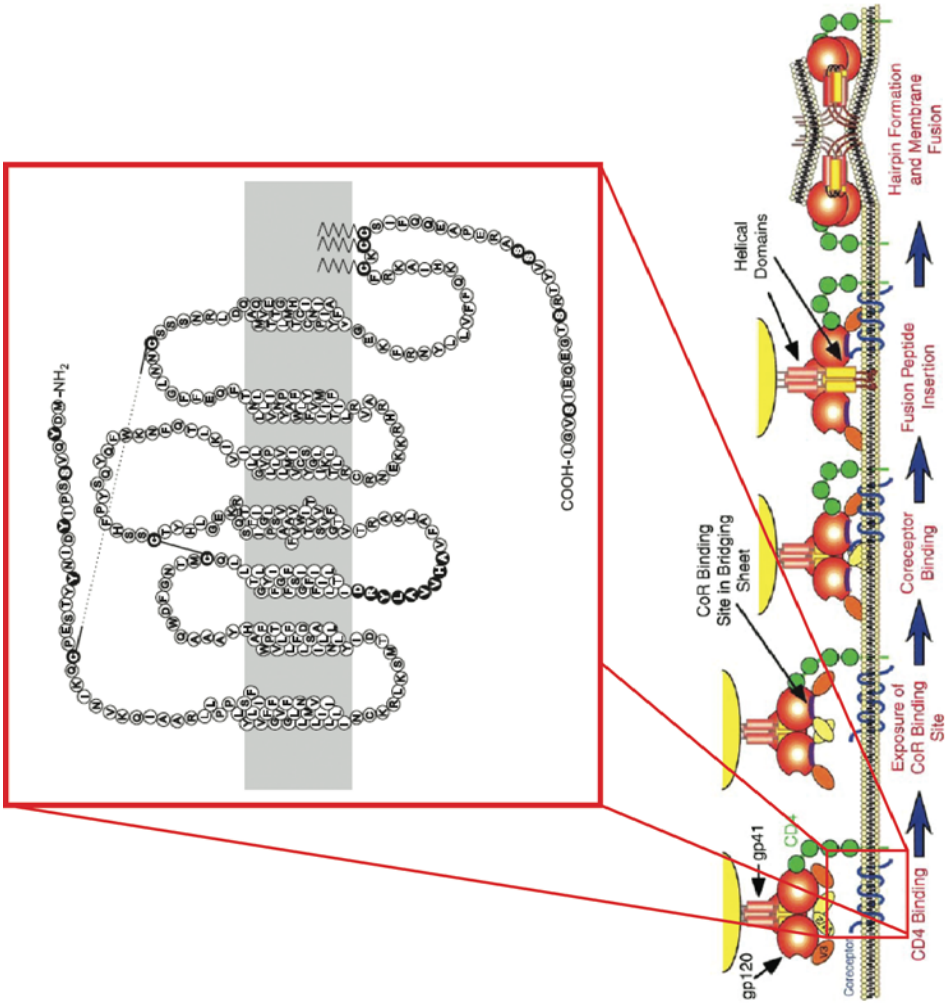
COOH-
gp120
gp41
CD4
CD4 Binding
Exposure of CoR Binding Site
CoR Binding Site in Bridging Sheet
Coreceptor Binding
Fusion Peptide Insertion
Helical Domains
Hairpin Formation and Membrane Fusion

Figure 1-3

1.2 Rhodopsin Dimerization

Despite an increasing number of reports of GPCR dimerization, the idea of rhodopsin existing as dimers in its native state remains one of the most controversial issues in the GPCR field. In this section, we review some of the notable experiments performed with rhodopsin pertaining to the nature of its organization in native and reconstituted systems. A comparison of key assays, and their possible pitfalls, used to detect dimerization in other GPCRs is also reviewed (see also section 5.3.4).

Rhodopsin has been historically considered a monomer. One of the first reports of rhodopsin forming monomers in detergents came from rhodopsin solubilized in Triton X-100 (H. Beverley Osborne 1974) where it was determined, using ion-exchange chromatography and analytical ultracentrifugation, that protein-detergent complexes contained a single protein in approximately 80 detergent molecules. The methods used in this study however, could not differentiate between a monomer or dimer in a detergent micelle. Determinations of protein molecular mass in other detergents by small-angle neutron scattering (Osborne, Sardet *et al.* 1978) have pointed at monomeric rhodopsin. The study also found that flash photoactivation of rhodopsin in certain types of polar detergents induced possible dimerization on a timescale of minutes. The slow

dimerization was followed by further oligomerization and eventual precipitation- a sign of protein denaturation in detergent. Dimerization and oligomerization of rhodopsin has not been observed in the native ROS membranes in the absence of detergents using small-angle neutron scattering (Saibil, Chabre *et al.* 1976). Formation of rho monomers or oligomers was shown to be dependent on the type of detergent used for solubilization of ROS (McCaslin and Tanford 1981). The oligomeric nature could be altered by varying the concentration of these detergents. In terms of G protein activation, it has been reported that photoactivated rho and holotransducin form a 1:1 complex in detergent, and that the photoactivated rho can activate hundreds of transducin molecules (Vuong, Chabre *et al.* 1984).

The issue of rhodopsin dimerization came to the forefront of GPCR research primarily due to observations of associated rhodopsins as a row of dimers in AFM images of intact mouse disk membranes (Fotiadis, Liang *et al.* 2003) (**Fig. 1-4**) and structural characterizations of crystal structures of rhodopsin (Salom, Lodowski *et al.* 2006). The dimerization reports have been contested as sample preparation (lipid phase change induced) problems (Chabre, Cone *et al.* 2003) or crystallography artifacts. It has also been reported that transducin activity by rhodopsin dimers and olimers in detergents is significantly higher than by rhodopsin monomers (Jastrzebska, Maeda *et al.* 2004; Jastrzebska, Fotiadis *et al.* 2006). Moreover, opsin has been reported to be present as dimers on the surface of heterologously expressing COS cells (Kota, Reeves *et al.* 2006). Although the claims of rhodopsin dimerization, and the biological relevance of

this putative dimerization have been contested (Chabre and le Maire 2005; Ernst, Gramse *et al.* 2007), lack of an appropriate system for the study of one and two rhodopsins free from detergent-related aggregation artifacts and cellular overexpression have made the answer elusive.

In order to investigate the existence of GPCR dimers in living cells, several groups have used biophysical assays based on light resonance energy transfer methods which are fluorescence resonance energy transfer (FRET) that uses fluorophores, or bioluminescent resonance energy transfer (BRET) using luciferase or green fluorescent protein (GFP) containing GPCR constructs (Bouvier 2001; Bartfai, Benovic *et al.* 2004). Close proximity between GPCRs containing complementary labels causes energy transfer from a donor to an acceptor molecule resulting in the appearance (in BRET) or enhancement of the emission signal (in FRET) of the acceptor molecule. It is plausible that using comparatively large labels like luciferase and GFP (~25 kD) on GPCRs (~40 kD) may itself influence trafficking of the GPCR as well as dimerization either directly or via accessory proteins. Further, constraints on the assumed distance dependency of these methods have been seen. Heterodimerization between β_2-adrenergic receptor and δ-opioid receptors were detected with co-immunoprecipitation but not with BRET and FRET, whereas homodimerization could be detected with all three methods (McVey, Kellet *et al.* 2001). Overexpression of GPCRs in cells has been reported to cause significant BRET signal attributed to transient, non-specific interactions (James, Oliveira *et al.* 2006). Finally, the issue of interpreting ligand-mediated dimerization of GPCRs

in cells is non-trivial. Both BRET and FRET are sensitive to the dipole orientation of their respective labels and conformational changes induced by ligand binding may change the dipole orientation such that a signal is seen independent of any change in the distance between the receptors (Bouvier 2001).

Investigation of dimerization of GPCRs therefore, will benefit from validation of cell-based assays using a combination of ensemble biochemistry, single-particle imaging and novel receptor assays in a cell-free system.

Figure 1-4. AFM Image and Models for Rhodopsin Dimerization

(A) Topographic image of the cytoplasmic side of rhodopsin obtained by Atomic Force Microscopy (AFM) on native disc membranes. Rows of rhodopsin dimers are seen in a paracrystalline array. The dashed ellipse shows isolated dimers and the arrows show rho monomers. The scale bar is 15nm. Image adapted from Fotiadis *et al.* (Fotiadis, Liang *et al.* 2003). **(B)** Model of the side view model of a rho dimer. Contact between the monomers is formed by transmembrane helices IV (yellowish-green) and V (yellow). The dimer interface consists of hydrophobic interactions and hydrogen bonds. Model taken from Fotiadis *et al.* (Fotiadis, Liang *et al.* 2004). **(C)** Model of the packing arrangement of rho in paracrystalline arrays. Rho assembly in a 'row of dimers' state by contacts between helices IV and V (contact 1). The rows formed by dimers are highlighted by blue bands. The rows are thought to be formed due to contacts between the cytoplasmic loop connecting helices V and VI (C 3) on one dimer and helices I and II (C 1) on the other dimer (contact 2). Rows form paracrystals by extracellular contacts through helix I (contact 3). Image taken from Liang *et al.* (Liang, Fotiadis *et al.* 2003). **(D)** Another depiction of the 'row of dimers' model. Helix ends are shown in different colors. Image taken from Fotiadis *et al.* (Fotiadis, Liang *et al.* 2004).

Figure 1-4

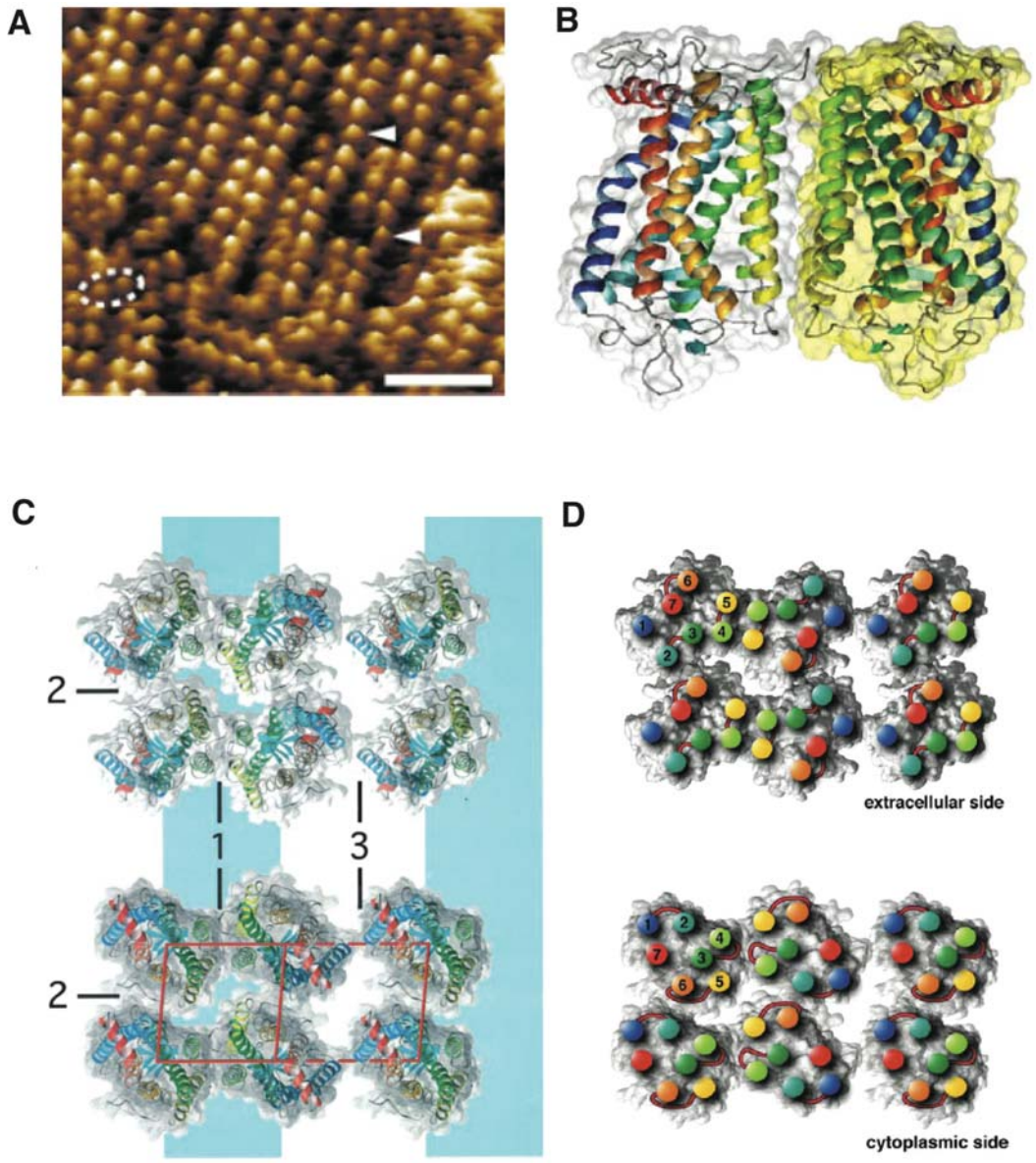

1.3 The Importance of Lipids

Lipids as a class of molecules display a wide diversity in both structure and biological function. The propensity of hydrophobic lipid tails to self-associate (entropically driven by water), and the tendency of the hydrophilic moieties to interact with aqueous environments and with each other, is the physical basis of the spontaneous formation of the lipid bilayer membrane. The membrane is the supporting matrix for a wide spectrum of proteins involved in many cellular processes. Lipids also allow particular proteins in membranes to aggregate, and others to disperse. Approximately 20-35% of all proteins are integral membrane proteins, and probably half of the remaining proteins function at or near a membrane surface. Because of their relatively reduced state, lipids are used for energy storage in lipid droplets as triacylglycerol and steryl esters (van Meer, Voelker *et al.* 2008). Lipids may also act as first and second messengers in signal transduction and molecular recognition processes. The adaptability and flexibility exhibited in membrane structure and function is possible only with a broad spectrum of lipid mixtures (Dowhan 1997). Therefore, the physical and chemical properties of the membrane directly affect most cellular processes making the role of lipids dynamic with respect to cell function rather than simply defining a static barrier.

Figure 1-5. Apo A-I and Reverse Cholesterol Transport

Discoidal HDL particles play a physiologically vital role in reverse cholesterol transport. Delipidated apo A-I interacts with cholesterol-loaded plasma membranes forming lipid-poor particles called pre β HDL. These lipid-poor particles fuse with each other and with small discoidal HDL particles while gathering free cholestrol (FC) and phospholipids (PL) from the surface of peripheral cells. The discoidal HDL particle increases in diameter, presumably by addition of FC and PL, catalyzed by Phospholipid Transfer Protein (PLTP). The mature discoidal HDL with apo A-I still attached enters the plasma where it interacts with Lecithin Cholesterol Acyl Transferase (LCAT). LCAT activity converts discoidal HDL to spheroidal HDL. Apo A-I shows lower affinity for spheroidal HDL and dissociates from the complex and is recycled.

The inset shows an EM image of reconstituted HDL particles prepared using purified human apo A-I and egg-PC lipids. The particles were purified using density gradient centrifugation, at densities similar to that of native HDL particles. Extensive stacking between the planar discs can be seen.

Illustration adapted from Fielding *et al.* (Fielding and Fielding 1995). EM image of HDL particles taken from Matz *et al.* (Matz and Jonas 1982)

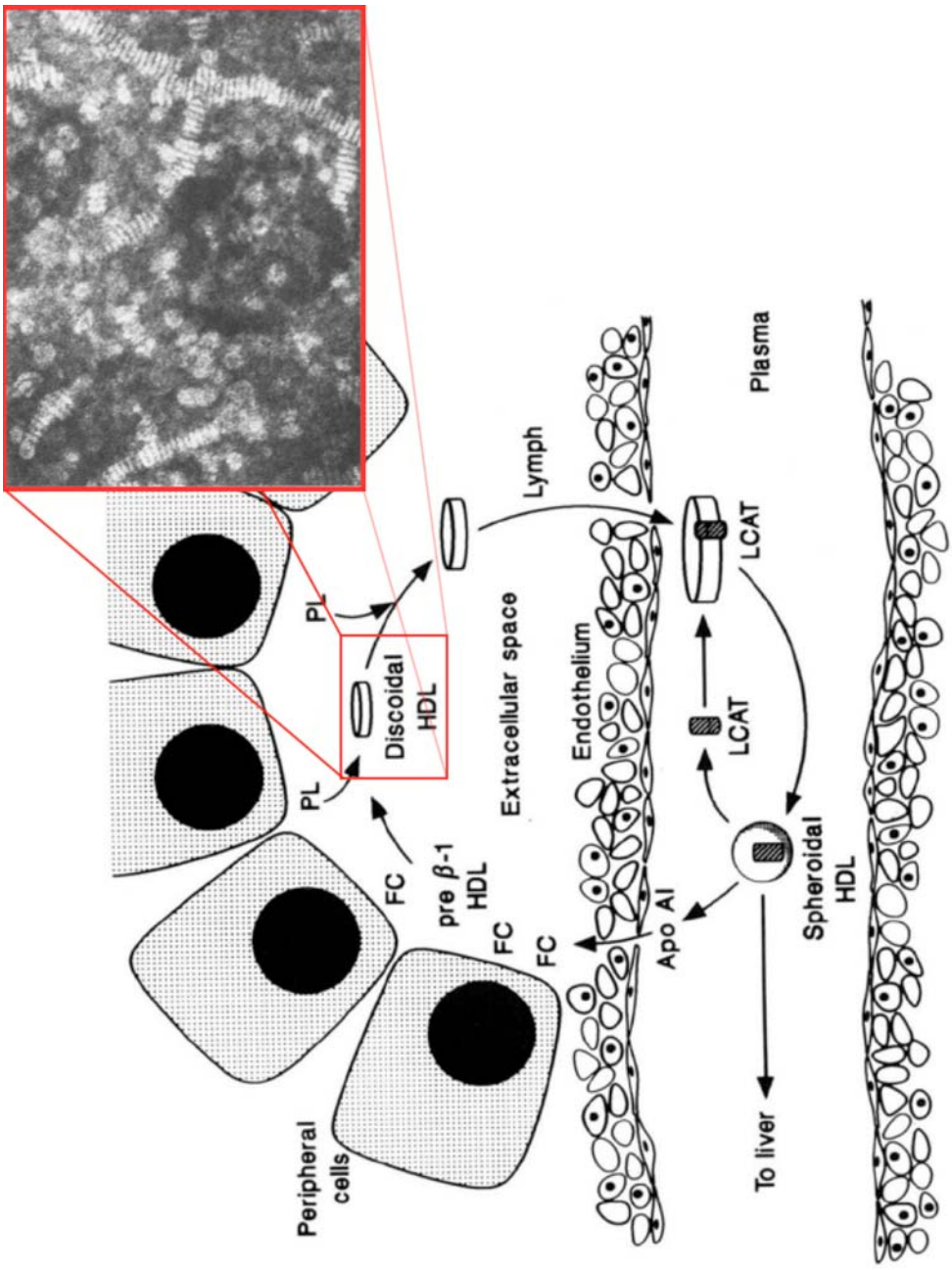
Peripheral cells
FC
pre β-1 HDL
FC
FC
PL
PL
Discoidal HDL
Extracellular space
Lymph
Endothelium
Apo AI
LCAT
LCAT
Plasma
Spheroidal HDL
To liver

Figure 1-5

1.3.1 Discoidal HDL Particles to Study Membrane Proteins

The formation of discoidal structures of lipids surrounded by human apolipoprotein A-I (apo A-I) was first demonstrated in 1980 (Jonas and Drengler 1980), after similar structures were implicated in transport of cholesterol by High Density Lipoproteins (HDL) in the serum (Jonas, Krajnovich *et al.* 1977). More recently, an engineered N-terminal truncated form of human apo A-I was used in a similar manner to incorporate peripheral and integral membrane proteins into such bilayer nano discs (Bayburt, Grinkova *et al.* 2002; Bayburt and Sligar 2002; Bayburt and Sligar 2003).

Nanoscale discoidal lipoproteins with incorporated GPCRs are an ideal system for spectroscopy. The discrete lipid discs prevent aggregation phenomena as seen with detergent micelles, light-scattering of lipid vesicles and provide a system that can be isolated in monodisperse form with the phospholipid-protein native structure and function maintained. The nanoscale lipid disc with embedded protein can be versatilely adapted for assays involving either immobilization or constant flow of the discs over a surface. The protein-lipid complex will behave more or less like normal proteins in solution without foaming or sedimentation problems associated with detergents and vesicles.

Figure 1-6. X-Ray Crystal Structures of Human Apo A-I

High-resolution x-ray structures are available for human apo A-I (1-43 amino acids truncated) as well as full-length protein. **(A)** 4Å structure of residues 44-243 of human apo A-I from Borhani *et al.* (Borhani, Rogers *et al.* 1997). N-terminal truncation of apo A-I resulted in crystallization of a tetramer in a unit cell shown in the right panel. Apo A-I monomer (left) and dimer (center) are also shown. Dimeric crystal contacts were formed along helix 10 of two anti-parallel apo A-I molecules (center). **(B)** Domain representation of human apo A-I from Li *et al.* (Li, Chen *et al.* 2004). The N-terminal 43 amino-acids are considered to form a globular, flexible domain and important for activation of Lecithin Cholesterol Acyl Transferase (LCAT) enzyme in the reverse cholesterol transport pathway. **(C)** Domain representation and x-ray structure of full-length human apo A-I adapted from Ajees *et al.* (Ajees, Anantharamaiah *et al.* 2006). The N-terminus forms a helix among a four helix bundle. Notably, the structure shows six total helices, indicating that every proline residue in the sequence may not always cause kinks in the helices.

Figure 1-6

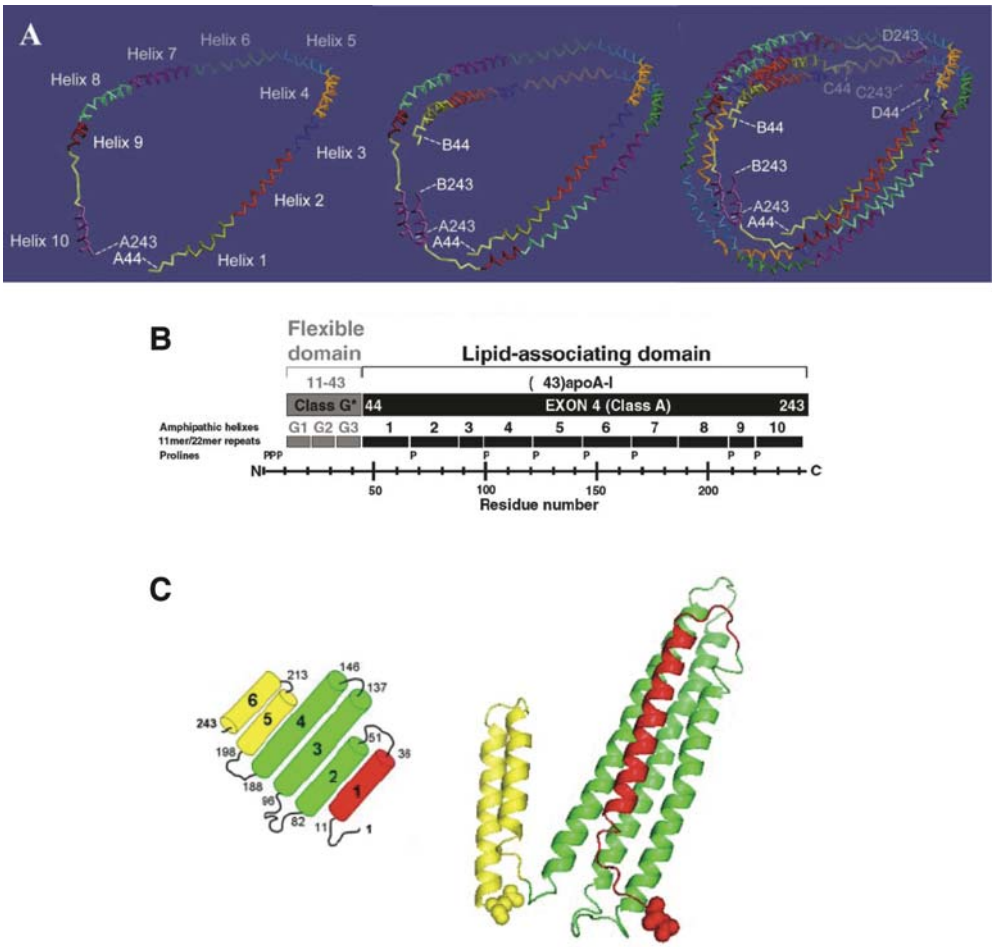
A
Helix 8
Helix 7
Helix 6
Helix 5
Helix 4
Helix 9
Helix 3
Helix 2
Helix 10
A243
A44
Helix 1
B44
B243
A243
A44
D243
C44
C243
D44
B44
B243
A243
A44
B
Flexible domain
Lipid-associating domain
11-43
(43)apoA-I
Class G*
44
EXON 4 (Class A)
243
Amphipathic helixes
11mer/22mer repeats
Prolines
G1 G2 G3
1 2 3 4 5 6 7 8 9 10
PPP
P P P P P P P P
N
C
50
100
150
200
Residue number
C
213
146
137
243
6
5
4
3
2
1
51
38
198
188
96
82
11
1

In-vitro assays avoid several artifacts and assumptions inherent to *in-vivo* systems. Detergents offer the first choice to isolate transmembrane proteins from their cellular context. In a sense, both detergents and lipids are surfactants. What distinguishes one from the other are the concentration regimes for self-association and the kinds of multimolecular structures each can make. The problem of isolating native membrane proteins from lipid bilayers and then subsequently manipulating them is, in essence, a problem of dealing with mixed surfactant systems. However most GPCRs retain function in only a limited number of detergents, which typically have a relatively low critical micelle concentration and a relatively large micelle size. This gives rise to aggregation phenomena (Jastrzebska, Maeda *et al.* 2004) and is a potential source of irreproducibility while performing spectroscopic measurements. Vesicles form closed structures and the chemical composition of the lumen is difficult to alter. Lipid vesicles are also prone to light scattering artifacts in optical spectroscopy and a precise control of the number of receptors per vesicle, and heterogeneity of vesicle sizes, are difficulties. A further complication, when the GPCR is reconstituted in a vesicle, arises from the 'sidedness' of GPCR interactions with ligands and G proteins respectively.

Figure 1-7. Double-belt Model and Salt-Bridging in Discoidal Lipoprotein Particles

(A) Molecular model of a 'double-belt' conformation of N-terminal 1-43 amino-acid truncated version of human apo A-I with a simulated POPC bilayer, from Segrest *et al.* (Segrest, Jones *et al.* 1999). The helical ribbons are based on the x-ray structure of N-terminally truncated human apo A-I (Borhani, Rogers *et al.* 1997) and arranged antiparallel with respect to each other with helix 5 of monomer 1 associated with helix 5 of monomer 2 (LL5/5 configuration). **(B)** Space-filling molecular graphics model of human apo A-I Δ1-43, from Segrest *et al.* (Segrest, Li *et al.* 2000). The apo A-I is viewed with the plane of the disc parallel to the paper. Hydrophobic residues are indicated in orange, prolines in green, basic residues in blue and acidic residues in red. The amphipathic nature of the α-11/3 ring can be clearly seen in this depiction. **(C)** Molecular Dynamics simulation at 4.5 nsec of a single bacteriorhodopsin embedded in a HDL particle containing DPPC lipids. The two molecules of human apo A-I Δ1-43 are shown in blue and red in this figure from Shih *et al.* (Shih, Denisov *et al.* 2005). **(D)** Structure and interhelical salt bridging between apo A-I helices arranged in the LL5/5 configuration, taken from Segrest *et al.* (Segrest, Jones *et al.* 1999). **(E)** Weighed interhelical salt-bridging score analysis of the C-terminal 200 amino acids of human apo A-I and zebrafish apo A-I. 2 molecules of apo A-I were considered to be in α-11/3 helical conformation and the salt bridging score was computationally calculated using the ALIGN program in this figure adapted from Segrest *et al.* (Segrest, Jones *et al.* 1999). **(F)** An example of a salt-bridging triad observed in a apo A-I rotamer by MD simulation, from Klon *et al.* (Klon, Segrest *et al.* 2002).

Figure 1-7

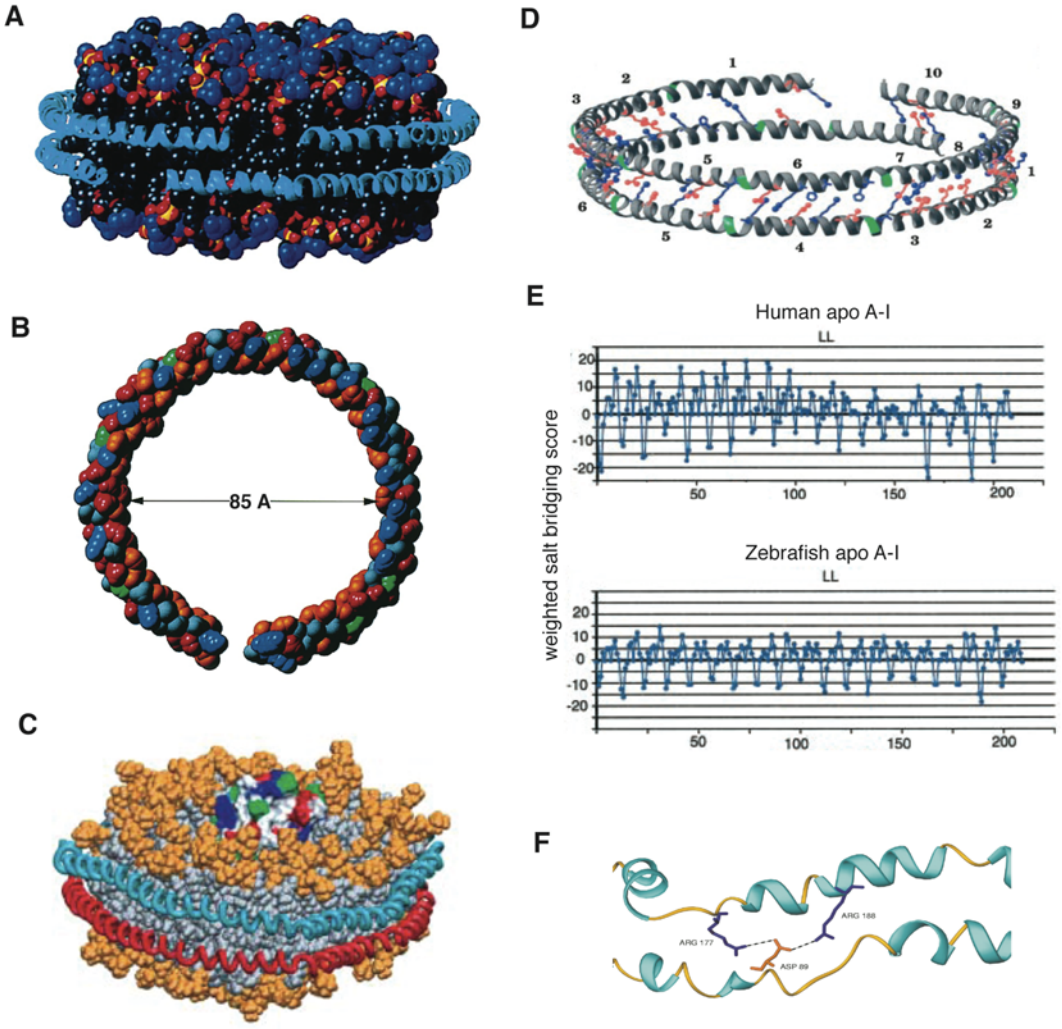
A
B
85 A
C
D
1
2
3
4
5
6
7
8
9
10
E
Human apo A-I
LL
20
10
0
-10
-20
50
100
150
200
Zebrafish apo A-I
LL
weighted salt bridging score
F
ARG 188
ARG 177
ASP 89

1.4 Signal Transduction Events Proximal to the GPCR

There are no known prokaryotic homologs of GPCRs (unlike ion-channels), hence the closest substitute to their native environment has been assumed to be the cell membrane of eukaryotic cell lines like HEK293, Sf9, COS and CHO cells. Cell-based assays, for example those measuring second messenger levels, like cAMP, Ca^{2+} or IP_3 in response to stimulation of a GPCR, monitor signaling at very distal points but do not provide direct information about the events going on more proximally; that is, at the G protein level. In fact, ligand efficacies and potencies measured at the G protein level and at the effector level in a given signaling cascade can be quite different (Seifert, Wenzel-Seifert *et al.* 1999). GPCR-dependent functions other than ligand-receptor binding might give a signal that might be construed as an affirmative response to ligand binding. These signals may be due to compounds acting on GPCRs like regulator of G protein signaling-4 (RGS4), accessory proteins like receptor-activity-modifying proteins (RAMPs), or receptor dimerization. Overexpression of the receptor can lead to aberrant responses due to inappropriate stoichiometry of these proteins. There may be a lack of reproducibility *in-vivo*, in particular regarding signaling from cells transfected with high levels of a GPCR. Finally, it is entirely possible that GPCR signaling *in-vivo* is influenced by its location within signaling complexes that are cell-type specific (Steinberg and Brunton 2001; Luttrell and Lefkowitz 2002). Cell based assays have the advantage that they can be adapted in a relatively straightforward way for high throughput screening of compounds;

by binding competition assays for instance. An alternative system for studying ligand-receptor, or receptor-G protein phenomena will have to discard the presence of 'interfering' players and phenomena mentioned above, while maintaining the native-like lipid environment for the receptor and preserving the advantages of simplicity and high-throughput screening. GPCRs, like most other complex membrane proteins, are dependent on a lipid environment for structural stability and integrity. The importance of a lipid environment is exemplified in literature reports which exemplify profound effects of different membrane lipids on functional parameters of rhodopsin (Botelho, Gibson *et al.* 2002; Botelho, Huber *et al.* 2005). Furthermore, a lipid environment has been reported to enhance G protein binding to the activated GPCR compared with detergents (Melia, Malinski *et al.* 2000; Zhang, Melia *et al.* 2004).

Biophysical studies of GPCRs have been indispensable in providing knowledge of ligand-dependent conformational states of a receptor (Imamoto, Kataoka *et al.* 2000; Ghanouni 2001; Devanathan, Yao *et al.* 2004), intermediate conformations adopted by the receptor upon activation (Palanche 2001; Swaminath 2004) and receptor oligomerization (Bouvier 2001; George, O'Dowd *et al.* 2002; Mercier, Salahpour *et al.* 2002; Fotiadis, Liang *et al.* 2004). The majority of the biophysical studies on GPCRs have been done on receptors solubilized in detergent micelles, reconstituted in lipid vesicles or overexpressed on the cell surface. A monodisperse, soluble form of the receptor, although convenient for *in-vitro* assays, does not usually provide a native environment of the receptor and thereby makes an underestimation of the role of native membrane

lipids in the modulation of GPCR function. Molecular assays that directly report G protein activation and conformational changes undergone by the receptor in a controlled lipid environment could bridge the gap between the limited information obtained from simple binding assays in detergents and the complexity of cell-based systems.

A crystal structure provides a high-resolution snapshot of a single receptor conformation, often with some artifactual elements. Although it gives a wealth of information, x-ray crystallography alone is unlikely to be sufficient in elucidating the dynamic picture of agonist binding, receptor oligomerization and G protein interactions in the native state of the GPCR. The organization of GPCR systems and signaling complexes is still an open question. Even in the case of rhodopsin, the field is sharply divided on the question of whether it is dimeric in its native membrane. Therefore, we developed the NABB system as a platform to study G protein activation by either one (monomer) or two (putative dimer) rhodopsins isolated and purified in a soluble lipid bilayer. We performed characterization experiments, including electron microscopy imaging of the particles with one or two rhodopsins and we proposed the relative limits of G protein activity of a putative rhodopsin dimer with respect to that of the monomer. We also show that our strategy of GPCR reconstitution may be applied to a different heterologously expressed GPCR – called CCR5, and that CCR5 reconstituted in NABBs retain their native conformation and G protein activity.

2.0

Materials and Methods

2.1 Reagents and Buffers

Oligonucleotide primers were obtained from GeneLink (NJ), restriction endonucleases from New England Biolabs (Ipswich, MA). Lipids were obtained from Avanti Polar Lipids (Alabaster, AL). Detergents were obtained from Anatrace Inc (Maumee, OH). Fluorescent dyes were obtained from Invitrogen (Carlsbad, CA). All buffer reagents obtained from Sigma-Aldrich Inc. (St. Louis, MO). Electron microscopy stains and grids were obtained from Electron Microscopy Sciences (Hatfield, PA). All UV-visible absorption spectroscopy experiments were performed in a Perkin-Elmer Lamda 800 UV-visible spectrophotometer.

The following buffers were used in the methods followed in this project:

Buffer T: 25 mM Tris pH 8, 125 mM NaCl, 1 mM NaN_3.

Buffer H1: 25 mM HEPES-MES-KOH pH 6.9, 125 mM KCl, 2 mM $MnCl_2$, 2 mM $CaCl_2$, 1 mM EDTA.

Buffer H2: 10 mM HEPES-MES-KOH, 100 mM KCl. pH adjusted from 6.9 by using either 1 N HCl (more acidic pH) or 1 N KOH (more basic).

Buffer N1: 20 mM Tris pH 7, 0.1 M $(NH_2)SO_4$, 10% glycerol, 0.07% CHS, 0.018% DOPC, 0.008% DOPS, 0.33% DM.

Buffer P1: 20 mM Tris pH 8, 1% (w/v) POPC, 0.01% (w/v) NBD-DPPE, 1% (w/v) CHAPS.

Buffer P2: 20 mM Tris pH 8, 0.6% (w/v) POPC, 0.4% POPS, 0.01% (w/v) NBD-DPPE, 1% (w/v) CHAPS.

Buffer G1: 20 mM HEPES-MES-KOH pH 6.9, 0.3 M NaCl, 5 mM $MgCl_2$, 5 μM GDP.

Buffer G2: 20 mM Tris pH 8, 0.3 M NaCl, 5 mM $MgCl_2$, 5 μM GDP, 1 mM DTT.

Buffer GM1: 50 mM Tris pH 8, 1 mM EDTA, 1 mM DTT.

Buffer GM2: 50 mM Tris pH 8, 1 mM EDTA, 1 mM DTT, 1.2 M $(NH_4)_2SO_4$, 25 μM GDP.

Buffer GM3: 50 mM Tris pH 8, 1 mM EDTA, 1 mM DTT, 35% glycerol, 25 μM GDP.

Buffer R1: 30% (w/w) sucrose, 10 mM Tris-acetate pH 7.4, 130 mM NaCl, 0.4 mM $MgCl_2$, 0.4 mM EDTA.

Buffer ISO: 20 mM Tris pH 7.1, 120 mM KCl, 60 mM NaCl, 10 mM $MgSO_4$, 2 mM DTT, 0.1 mM PMSF.

Buffer HYPO: 5 mM Tris pH 7.1, 5 mM $Mg(CH_3COO)_2$.

Buffer BG1: 10 mM sodium phosphate pH 6.5, 2 mM $MgCl_2$, 0.1 mM EDTA, 1 mM DTT, 10% (w/v) glycerol.

2.2 Isolation and Purification of Rhodopsin

Rod Outer Segment (ROS) membranes were isolated from frozen dark-adapted bovine retinae (W.L. Lawson Co., NE; Ph: 402-466-0492) using a modification of previously reported procedure (Papermaster 1982). All steps were carried out in the dark or under dim red light. Foil-wrapped vials containing 100 retinae were thawed in a water bath for 1 h. The retinae were placed in a dounce homogenizer and flushed with Ar for 5 min. 60 mL of buffer R1 was added to the retinae and the solution was homogenized 10 times very slowly with Ar flush between the strokes. The retina solution was transferred to Ti-45 centrifuge tubes (50mL per tube), flushed with Ar and centrifuged at 4k rpm, 20 min, 4°C. The supernatant was collected and the pellet was re-homogenized by adding equal volume of buffer R1 and applying 6-8 strokes of the homogenizer, and the centrifugation repeated. The supernatants were combined in a beaker on ice and 2 volumes of 10 mM Tris-acetate pH 7.4 were added while stirring the solution under Ar. The combined supernatants were centrifuged in a Ti-45 rotor at 7k, 50 min, 4°C. The pellet was preserved. A three-step sucrose gradient was prepared in polyallomer centrifuge tubes for the Beckman SW-28 rotor. Sucrose densities of 1.15 g/mL (8mL), 1.13 g/mL (10mL) and 1.11 g/mL (10 mL) were used. 1.10

g/mL sucrose solution was used to resuspend the ROS pellet in a total of 25mL and this solution was distributed to bring the polyallomer tubes to final volume. The tubes were flushed with Ar and the SW-28 rotor was centrifuged at 24k, 1 h, 4°C. The band at the interface of 1.11/1.13 g/mL sucrose was harvested (highest purity of ROS). The collected bands were pooled and diluted with 2 volumes of water and distributed to Ti-45 tubes, flushed with Ar and centrifuged at 25k, 30 min, 4°C. The pellet was washed with water and the centrifugation repeated twice. After the final wash, the pellet was resuspended in 67 mM sodium phosphate pH 7.0. The ROS was dispensed as 500μL aliquots and stored wrapped in foil at –80°C. Using this protocol, approximately 45 mg of ROS was obtained at 5.6 mg/mL rhodopsin at a A280/A500 ratio of 3.

To purify rhodopsin from ROS, a membrane aliquot was thawed and solubilized with 2.5mL of 1.5% Octyl Glucoside (OG) containing buffer H1 (Solubilization buffer) for 2-3 hours at 4°C on a nutator. The solution was then centrifuged in a Beckman Type 50 rotor at 34,000 rpm for 10 min at 4°C. The supernatant was added to 1mL cross-linked ConA-sepharose beads and nutated for 1 h at 4°C. The beads were washed with Solubilization buffer and elution was done using 100mM α-methyl mannoside in 1.5% OG containing buffer H1.

2.3 Site-specific Labeling of Rhodopsin with Fluorophores

Fluorophore labeling of rhodopsin was done on ROS membranes with fluorophores functionalized with a maleimide group. The ROS used had a rhodopsin concentration of 187 μM and absorbance 280nm/500nm ratio of 2.0. The labeling reactions were carried out in a dark room under dim red light. The fluorophores were stored as a 22 mM stock in DMSO at –20°C. The optimal fluorophore to rhodopsin ratio at the start of the labeling reaction was determined experimentally for different fluorophores. Typically, three different molar ratios of dye to rhodopsin were used- 1:1, 3:1, 9:1. Each labeling reaction had ROS containing 1.2 mg rhodopsin (163μL aliquot of the ROS) in 0.6mL tubes. After addition of the appropriate volume of fluorophore stock, the tubes were flushed with Ar and incubated for 12.5 h at 28°C with shaking in a thermomixer. The reaction was terminated by adding 5 mM DTT to each tube and incubating on ice for 10-15 min. The excess label was washed from the ROS using three washes of 1% BSA containing buffer H1. The ROS was then transferred to a 15mL tube containing 2mL of 1.5% OG containing buffer H1 (Solubilization buffer) and kept on a nutator for 1 h at 4°C. The solution was then transferred to centrifuge tubes and centrifuged in a Beckman Type 50 rotor at 34,000 rpm for 10 min at 4°C. The supernatant was added to 1mL cross-linked ConA-sepharose beads and nutated for 1 h at 4°C. The beads were washed with Solubilization buffer 4-5 times, or till coincident UV-vis spectra were obtained from subsequent washes. The rho was eluted from the ConA beads using 100mM α-methyl mannoside in 1.5% OG

containing buffer H1, then pooled and concentrated using a centrifugal concentrator with 10k MWCO. The final rho concentration was determined by UV-vis difference spectral scan from 700nm to 250nm before and after photobleaching the sample with yellow light. The stoichiometry of labeling was determined by comparing the molar concentration of label and rho in the cuvette.

Site-specificity of labeling at a single accessible cysteine was confirmed by digestion of labeled rhodopsin by V8 protease (Farrens, Altenbach *et al.* 1996) and detecting labeled fragments on SDS-PAGE. V8 protease was added to rho in 1.5% OG buffer H1 at a molar ratio of 1:30. The mixture was incubated for 1.5 h at 30°C and the fractions were analyzed by SDS-PAGE. The fluorescence in the lanes of the gel was detected by a Typhoon 9400 imager (GE Healthcare) and the gel was subsequently stained with Coomassie Blue to detect protein bands.

2.4 Labeling of Rhodopsin with Nanogold

Nanogold labeling of rhodopsin was also performed on ROS membranes using monomaleimido nanogold (Nanoprobes, Yaphank, NY) using manufacturer recommended conditions and concentrations. A 9:1 (M/M) ratio of monomaleimido nanogold to rhodopsin was used, with 2.5mg of rho in ROS. The mixture was incubated at 28°C for 16 h without shaking. The labeled rhodopsin was purified as described in Method 2.3. The labeling stoichiometry was determined by comparing the characteristic absorbance of nanogold at 420nm

with rhodopsin absorbance at 500nm determined by UV-vis difference spectroscopy and was found to be 0.8-0.9 (M/M) Nanogold/rhodopsin.

2.5 Isolation and Purification of Holotransducin

Frozen, dark-adapted bovine retinae (200 retinae in vials) were thawed in a room temperature water bath for 30 min. 100mL cold ISO buffer was added with protease inhibitors and stirred on an ice-bath for 30 min. The slurry was filtered through a metal filter in batches. The volume was increased to 200mL with ISO buffer. The solution was layered onto a 37% (w/w) sucrose cushion in centrifuge tubes for a Beckman SW-28 rotor. Each tube contained 13mL of 37% sucrose and 25mL retina slurry. The tubes were centrifuged in a SW-28 rotor at 22k rpm, 25 min, accel/decel 6/6 at 4°C. The tubes were opened in the dark room and black bands at the interface of the sucrose and slurry were collected with an 18G needle and 10mL syringes. The volume of the collected bands was increased to 250mL using cold ISO buffer. The sucrose cushion step was repeated and the band at the same location of the tube was collected. Cold ISO buffer was added to increase the volume of the collected bands to 200mL. The solution was distributed in Ti-45 centrifuge tubes. The solution was centrifuged for 28k rpm, 20 min, 4°C. The reddish-orange pellet was resuspended in 200mL total ISO buffer using a dounce homogenizer. The slurry was transferred to a beaker kept on ice and illuminated from below with >495nm light with constant stirring for 20

min. The illuminated slurry was distributed into Ti-45 tubes (50mL per tube) and centrifuged at 30k, 20 min, 4°C. The pellet was then resuspended in HYPO buffer and homogenized using the dounce homogenizer. The centrifugation and homogenization steps were repeated with increasing centrifugation speeds each time- 32k, 36k, 40k for 20 min, 4°C. Holotransducin (Gt) was extracted from the ROS membranes by adding 200 μM GTP containing HYPO buffer and incubating on ice for 10 min. The slurry was centrifuged at 42k, 20 min, 4°C and the supernatant was collected. The total volume of the extractions was kept under 150mL. The pooled GTP extractions were centrifuged at 42k, 20 min, 4°C to remove any residual membranes. The extract was then loaded on a hexylagarose column (25mL hexylagarose packed in a GE Healthcare XK 16/20 column) at 0.25mL/min at 4°C equilibrated with HYPO buffer. The hexylagarose column was washed sequentially with HYPO buffer, 75 mM NaCl containing HYPO buffer. The Gt was eluted with a step of 300 mM NaCl in HYPO. The peak fractions were pooled and dialyzed against Gt storage buffer (20 mM Tris pH 7.1, 2 mM $MgSO_4$, 1 mM DTT, 5 μM GDP, 10% glycerol). The dialyzed product was distributed as 200μL aliquots, flash-frozen in liquid N_2 and stored at –80°C till further use. A concentration of 15 μM Gt, and approximately 7-9mg Gt was obtained from 200 retinae using this protocol.

2.6 Isolation of βγ subunits from Holotransducin

Holotransducin (Gt) stock containing 1 mg of Gt was thawed and diluted 1:4 in buffer BG1. The sample was applied to a 1mL Blue Sepharose column (GE Healthcare) using an Akta Exlorer 10 FLPC system. The column was washed with 5 column volumes using buffer BG1 and eluted with a linear gradient of buffer BG1 containing 2 M NaCl. The βγ subunits elute first, followed by the Gtα subunit. The proteins were identified on the basis of molecular weight using SDS-PAGE.

2.7 Site-directed Mutagenesis of $G_{i1}\alpha$ DNA

Multiple site-directed mutagenesis reactions were performed on the pET-28a(+) $G_{i1}\alpha$ DNA using the components and parameters specified in the QuikChange Multi Site-Directed Mutagenesis Kit (Stratagene, La Jolla, CA). Six cysteine residues were chosen to be modified such that four single-cysteine containing $G_{i1}\alpha$ DNA would be produced, each construct containing a Cys at a distinct, known position in the sequence- C66, C214, C305, C325. The following amino-acid mutations and corresponding DNA primers were used for the mutagenesis, with the specific codon change underlined:

(1) C3S- ggctagcatgggctccacactgagcgctgaggac

(2) C66A- gctggctactcagaggaagaggctaagcagtacaaagcagtg

(3) C214S- cggaagaagtggattcacagctttgaaggcgtgactgcc

(4) C305S- ggcggctgcgtatatccagagccagtttgaagacctc

(5) C325A- cacccacttcactgccgccacggatacgaagaatgtg

(6) C351I- gaataacctaaaagacattggtctcttctaagaattcgagctcc

100ng of template DNA was mixed with 100ng of each primer. Only anti-sense primers were added. The 10x reaction buffer, dNTP mix and QuikChange Multi Enzyme blend were mixed in de-ionized water was added to make a final reaction volume of 25μL. The thermal cycler was programmed to run the following temperature and time cycles- (1) 1x 95°C, 1 min; (2) 30x 95°C, 1 min; 55°C, 1 min; 68°C 13 min; (3) 1x 4°C, overnight. At the end of the PCR reaction, the mixture was treated with 1μL of Dpn-I restriction endonuclease and incubated at 37°C for 1 h. The Dpn-I treated product was transformed into XL-10 Gold *E. coli* cells according to the manufacturer's protocol. The cells were plated on an LB-agar plate containing 50μg/mL Kanamycin (*Kan*) and incubated overnight at 37°C. 8-12 single colonies were picked and re-streaked on a fresh *Kan* plate and sent for sequencing to Genewiz (NJ). The Multi-site QuikChange reaction was repeated twice in order to obtain all the desired Cys mutations of the DNA.

2.8 Purification of Recombinant G_i proteins

2.8.1 Hi-yield Heterologous Expression of $G_{i1}\alpha$

BL21(DE3) *E. coli* cells were transformed with pET28a(+) $G_{i1}\alpha$ construct with C66 as the accessible cysteine (see section 2.6). A single colony was isolated from LB-*Kan* agar plates and introduced into 250mL LB-*Kan* media, and the culture was grown overnight at 37°C with shaking at 250rpm in an incubator. The starter culture was diluted 1:100 into 1.6 L of sterilized LB-*Kan* media, incubated at 37°C with shaking at 180rpm and induced with 0.5mM isopropyl-β-D-thiogalactopyranoside (IPTG) at OD_{600} of 0.5-0.6. The temperature was decreased to 30°C and the cells were harvested after for 16 hours. The cell pellet was resuspended in storage buffer (40 mM Tris pH 8, 0.3 M NaCl, 2 mM PMSF, 5 mM 2-mercaptoethanol, 1x Aprotinin and Complete EDTA-free protease inhibitor tablets) and stored at -80^{o}C until further use.

2.8.2 Site-specific Labeling and Purification of C66 $G_{i1}\alpha$

E. coli cells were thawed and lysed using a French Press. The lysate was centrifuged at 30,000xg, 45 min, 4°C. The supernatant was clarified by passing through a 0.45μm syringe filter. 2mL of Ni-Sepharose 6 FF slurry (GE Healthcare) equilibrated with 20 mM Tris pH 8, 150 mM NaCl, 2 mM 2-mercaptoethanol was added to the reaction mixture alongwith

20 mM imidazole and incubated for 2-3 h at 4°C. The solution was centrifuged and the resin was washed with 10 volumes of buffer G1 containing 20 mM imidazole. The resin was transferred to a 2mL eppendorf tube and 0.3 mM Alexa-546 maleimide was added in 1mL of slurry. The tube was flushed with Ar, wrapped in foil and kept nutating overnight at 4°C. The slurry was transferred to a 15mL tube and was washed thrice with buffer G1 containing 1 mM DTT. The protein was eluted thrice with 300 mM imidazole. The eluate was concentrated to approximately 2.5mL using a Centricon centrifugal concentrator with 10 kD MWCO. 0.5mL of GST-tagged PreScission protease was added, and the solution was dialyzed overnight at 4°C in a 3mL Slide-A-Lyzer dialysis cassette (Pierce) against 1000-fold excess of buffer G2. The dialyzed mixture was loaded on a 1mL Ni Sepharose 6 FF column (GE Healthcare) and the flowthrough collected, which now contained the cleaved, labeled $G_{i1}\alpha$. The Ni column flowthrough was applied to a GST-Sepharose column and the flowthrough collected. GST-tagged PreScission protease was removed from $G_{i1}\alpha$ at this stage. The GST column flowthrough was finally applied to a Superdex 200 10/300 gel-filtration column, and the fractions analyzed by SDS-PAGE. Using the above protocol, a stoichiometry of 1:10 label to $G_{i1}\alpha$ was obtained.

2.8.3 Expression and Purification of N-myristoylated $G_{i1}\alpha$

DNA plasmids coding for $G_{i1}\alpha$ (pQE60-$G_{i1}\alpha$) and yeast N-myristoyltransferase 1 (NMT1) enzyme (pBB131-NMT1) were a kind gift of Dr.

Maurine Linder and were used to express N-myristoylated $G_{i1}\alpha$ (Duronio, Jackson-Machelski *et al.* 1990). Yeast NMT1 has been shown to co-translationally myristoylate G-protein α-subunits, including $G_{i1}\alpha$ (Greentree and Linder 2004). The two plasmids were incorporated into BL21(DE3) strain of *E. coli* by heat-shock transformation. pQE60-$G_{i1}\alpha$ had the *Amp* resistance marker and pBB131-NMT1 had the *Kan* resistance marker; therefore both Ampicilin and Kanamycin were used at 50μg/mL each in the LB-agar plates and media. The starter cultures and media were prepared similar to Method 2.7.1. The cells were grown in LB-*Kan-Amp* for approx. 3 h at 37°C until the OD_{600} reached 0.6–0.8. The culture was induced with 0.25 mM IPTG and grown at 30°C, 16 h, with 180rpm shaking. The cells were harvested and stored in 40 mM Tris pH 8, 1 mM PMSF, 1x protease inhibitor cocktail mix (note: no NaCl was used since NaCl would interfere with subsequent purification steps) and frozen in liquid N_2.

The cell pellet was thawed and lysed using a French Press. 0.5 mM DNase-I and 5 mM $MgSO_4$ was added and the mixture incubated for 30 min at 4°C. The solution was centrifuged for 30 min, 30,000xg, 4°C. The supernatant was added to 15mL DEAE resin equilibrated with buffer GM1. The slurry was incubated for 30 min at 4°C. The slurry was then poured onto a 0.22μm filter attached to a Buchner funnel and vacuum line and washed with 100-200mL of buffer GM1 under vacuum. The protein was eluted thrice with 40mL buffer GM1 containing 300 mM NaCl under vacuum and collected. Ammonium sulfate was added from a 3.6 M stock to make 1.2 M in the solution containing the DEAE eluate. This was loaded on a 25mL Phenyl Sepharose (PS) column (GE

Healthcare) pre-equilibrated with buffer GM2 using an Akta Explorer 10 FPLC system. The bound proteins were eluted by a decreasing linear gradient of ammonium sulfate (buffer GM2) and using buffer GM3 as the elution buffer. The peaks were assayed for $G_{i1}\alpha$ presence by using small aliquots and observing Trp fluorescence increase upon addition of aluminium fluoride (Phillips and Cerione 1988) in a SPEX fluorolog instrument. The final eluted peak is assumed to be myristoylated $G_{i1}\alpha$ based on its higher hydrophobicity and AlF_4^- mediated increase in Trp fluorescence signal. The peak was applied to a desalting column equilibrated with buffer GM1 containg 25 μM GDP. The desalted product was applied to a 1mL MonoQ column equilibrated with buffer GM1 and eluted with a linear gradient of NaCl. The eluted peaks were assayed for GDP binding by AlF_4^- and the relevant peak was collected and applied to a Superdex 200 gel-filtration column. The peaks eluted from the column were analyzed using SDS-PAGE and stored at –80°C until use.

2.9 Amino Acid Alignment of Zebrafish and Human Apo A-I

Amino acid sequences of *Danio rerio* apolipoprotein A-I (NCBI accession number: NP_571203) and *Homo sapiens* apolipoprotein A-I preproprotein (NCBI accession number: NP_000030) were downloaded from NCBI in FASTA format for analysis. The first 21 amino acids from the N-terminus of *Danio rerio* apo A-I sequence and the first 24 amino acids from the N-terminus of *Homo sapiens* apo

A-I preproprotein sequence were discarded from the analysis (and subsequent constructs) as putative hydrophobic or signal sequences. The sequences were aligned using ClustalW (http://www.ebi.ac.uk/clustalw/) and the amino acids were color coded to highlight different levels of similarity.

2.10 Determination of Salt-Bridging Score in Apo A-I

Salt-bridging analysis, and helical net representations were done computationally using the ALIGN and WHEEL software programs (Jones, Anantharamaiah *et al.* 1992; Segrest, Jones *et al.* 1999) kindly provided to us by Jere Segrest from the University of Alabama Medical Center (Birmingham, AL). The software was installed, compiled and run on a SGI Octane machine (Silicon Graphics Inc., Sunnyvale, CA).

ALIGN uses an algorithm to sum a weighted score of salt-bridges and charge appositions for each helix-helix docking position of the three possible interfacial orientations of apo A-I. Salt-bridges and charge appositions are determined in the software by taking a helical net representation of the protein helix (Jones, Anantharamaiah *et al.* 1992) arranged as an α11/3 helix monomer and inverting and superimposing its L or R interface onto the L or R interface of a second monomer beginning with a complete overlap between them. Interactions were controlled by distance between residues down the helix axis, by radial distance between residues and by radial distance of their average position from

the polar-nonpolar interface. Salt-bridges are assigned a score of -1, and like charge appositions a score of +1, weighted by a sliding scale reflecting the average position of the residue relative to the interface of the polar-nonpolar faces. The 2 helical nets were translated relative to each other, one residue at a time, in a closed loop fashion.

Helical net representations were obtained using the HELNET program which was part of the WHEEL software suite. This program creates a diagram of the α helix seen as a cylinder cut along the center of the polar face and flattened. The center of the hydrophobic face (determined by the hydrophobic moment) lies in the center of the figure and is oriented to rise out of the page.

2.11 Cloning of apo A-I DNA Plasmids

Danio rerio apolipoprotein A-I cDNA was generated by reverse transcriptase PCR from 1μg of *D. rerio* total RNA using the primers 5'-CAGGCTGATGCCCCGAC-3' corresponding to N-terminus of the translated protein and 5'-TTATGCCTGGATGGCCTTGG-3' corresponding to the C-terminus. Restriction sequences for NheI and HindIII were incorporated in the primer sequence upstream of the apolipoprotein cDNA sequences. RT-PCR was performed using a one-step RT-PCR kit (cMaster RT plus PCR system, Eppendorf). The cDNA obtained was cloned into the TOPO cloning vector (Invitrogen) and the sequence confirmed. The cDNA was then cut by NheI and

HindIII restriction endonucleases and ligated into pET28a(+) vector (Stratagene) to give the vector pE28-ZAP1. To incorporate a site-specific cysteine, a single Gln residue near the N-terminus was mutated to Cys (Q26C) by site-directed mutagenesis of pE28-ZAP1 to yield pE28-ZAP1Q26C.

Human apo A-I clone was obtained from ATCC (MGC-12499) and cloned into a pET16a vector (Stratagene) which was altered to have a N-terminal hexa-histidine purification tag to give the vector pE16-HAP1. All nucleotide sequences were confirmed by DNA sequencing (Genewiz, South Plainfield, NJ).

2.12 Purification of His-tagged Apo A-I

The vector was transformed into BL21(DE3) Rosetta2 strain of *E. coli* and colonies were streak-purified on Kanamycin and Chloramphenicol containing LB-agar plates. A single colony was grown in 250mL LB media containing 50μg/mL of both kanamycin and chloramphenicol overnight at 37^{o}C with shaking and called the starter culture. The starter culture was diluted 1:100 into 1.6 L of sterilized TB media, incubated at 37^{o}C with shaking at 180rpm and induced with 1 mM isopropyl-β-D-thiogalactopyranoside (IPTG) at OD_{600} of 0.5–0.6. The cells were harvested after for 3-4 hours. The cell pellet was resuspended in storage buffer (40 mM Tris pH 8, 0.3 M NaCl, 2 mM PMSF, 5 mM 2-mercaptoethanol, 1x Aprotinin and Complete EDTA-free protease inhibitor tablets) and stored at –80^{o}C until further use.

The cell pellet was thawed and the cells disrupted by a French press. Solid guanidinum chloride was added to make the 6M concentration in the cell lysate. The lysate was incubated at room temperature for 30 minutes, then centrifuged at >25,000xg for 1 hour. The supernatant was filtered through a 0.45μm filter and loaded onto a Ni-Sepharose 6 FF column (GE Healthcare) pre-equilibrated with Buffer T containing 6 M Gn.HCl, 25 mM imidazole at pH 8. The column was washed sequentially with 2CV 6 M Gn.HCl containing buffer, 2CV 2 M Gn.HCl buffer and finally 5CV of Gn.HCl free Buffer T containing 25 mM imidazole. The protein was eluted by an imidazole gradient and the elution followed by monitoring OD at 280nm on an Akta Explorer 10 FPLC system. Maximum elution occurred at 250–300 mM imidazole. Gel-filtration chromatography was performed by pooling the zap1 containing fractions and running on a Superdex 200 26/60 column (GE Healthcare) and eluting with buffer T with 1 mM TCEP. The peaks were assayed for purity by SDS-PAGE. The pure protein was termed 6xHis-zap1.

2.13 Site-specific Labeling of 6xHis-zap1Q26C

A novel on-column approach was used to facilely label the zapIQ26C mutant with Alexa-488 maleimide. A 1mL Ni-Sepharose 6 FF column was used for labeling the Cys mutant. The fluorophore was made upto 0.2 mM in Buffer T containing 2 M Gn.HCl at pH 7.4 from a 22 mM fluorophore stock in DMSO.

After the binding zapIQ26C to the column and washing with Buffer T with 6 M Gn.HCl at pH 7.4, the fluorophore was introduced with a syringe and the flowthrough was passed over the column again. The column was then washed with 4CV of Buffer T containing 2 M Gn.HCl and finally 5CV of Gn.HCl free buffer containing 25 mM imidazole. The protein was eluted by introducing a 300 mM imidazole solution in buffer T pH 7.4 by a syringe. The collected fraction was subjected to gel-filtration on a Superdex 200 10/30 column and eluted with buffer T with 1 mM TCEP. The peaks were assayed for purity and the labeling ratio was determined by comparing OD488 and OD280. A 1:1 ratio of Alexa-488 to zap1 was obtained under the above conditions.

2.14 Preparation of Labeled Lipids

POPC was weighed from lyophilized stock and dissolved in 1% sodium cholate containing buffer H1 to make a 1% POPC solution. The solution was subjected to several freeze cycles in liquid nitrogen followed by vortexing at room temperature to get a clear solution. In order to make a labeled lipid stock, lissamine rhodamine B-sulfonyl labeled DOPE was dried from a 2mg/mL $CHCl_3$ stock vial in a glass round bottom flask under Ar gas. The flask was put under high vacuum overnight to remove traces of $CHCl_3$. The flask was weighed and the amount of dry labeled DOPE was calculated. The dried DOPE was dissolved in 1% cholate containing buffer H1 to make a 1mg/mL solution. A part of the POPC

stock was doped at 1% (w/w) of lissamine rhodamine B sulfonyl and this was taken to be the labeled lipid stock.

2.15 Self-assembly of NABBs and Rhodopsin-NABBs

The NABB formation with or without rhodopsin incorporated is a self-assembly process triggered on detergent removal after mixing and incubating the NABB components. A molar ratio of 150 POPC : 2 zap1 in 1.5% (w/w) sodium cholate and 1.5% OG containing buffer T was taken to form an 'empty' NABB. For each rhodopsin to be incorporated, 34 POPC were subtracted from the initial reaction mixture based on previous reports of area occupied by a rhodopsin molecule in a POPC bilayer (Huber, Botelho *et al.* 2004). Detergent removal was accomplished either by dialyzing the samples using Slide-A-Lyzers (Pierce Biotechnology, Rockford IL) of appropriate volume against 1000x excess volume of detergent free buffer for 36 hours with 2-3 buffer exchanges or by loading the reaction mixtures onto pre-equilibrated Extracti Gel D (Pierce Biotechnology, Rockford IL) columns typically of 1mL volume, made by loading Extracti Gel D slurry into cleaned Sep-Pak columns (Waters). In the case of Extracti Gel D reconstitutions, typically 200μL of the detergent containing initial reaction mixture was layered on top of the packed 1.5mL resin. The solution was allowed to completely enter the column and then eluted by adding 200μL of detergent free buffer on top and collecting equal volume of eluate fractions in 1.5mL eppendorf

tubes till 1mL of the detergent free buffer has been added to the column. The NABBs eluted over 2-3 fractions, as determined by UV-vis spectroscopy. Removal of bile-salt based detergents by both dialysis and the rapid extracti gel D reconstitution was quantitated by using a 3-α-steroid dehydrogenase enzyme assay using a total bile-acid assay kit (Diazyme, San Diego, CA) calibrated with either cholate or CHAPS and POPC. No significant traces of detergents were found after the reconstitutions. Once formed, the rho-NABBs were purified by gel-filtration chromatography on a Superose 6 10/30 column using an Akta Explorer 10 FPLC system (GE Healthcare, Piscataway, NJ) used within 1-2 days for the various assays. All of the above steps were carried out under dim red light to keep rhodopsin in its dark state.

Direct incorporation of rhodopsin from ROS into NABBs was done taking a molar stoichiometry of 1 rho per 100 NABBs. Typically, ROS containing 0.5 μM rhodopsin was taken in a 200 μL aliquot containing 100 μM 6xHis-zap1, 7.5 mM POPC, 1% DM, Buffer H2 with 2 mM $MgCl_2$ and 1 mM $CaCl_2$. The mixture was vortexed, centrifuged and loaded onto pre-equilibrated 1.5 mL Extracti Gel D columns, and eluted using detergent free buffer.

2.16 FRET Measurements between Rhodopsins

Fluorescence resonance energy transfer (FRET) measurements were made in a SPEX Fluorolog tau-3 spectrofluorimeter, equipped with a 450 W Xenon arc-

lamp and single grating excitation monochromator, set to 0.26nm bandpass and the single grating emission monochromator, set to 5nm bandpass. The signal was integrated for 2 seconds. Data was recorded for 1 h in 30 seconds intervals to account for any changes in the signal due to bleaching of rhodopsin from dark to light state by the excitation beam. The excitation shutter was closed in between acquisitions to minimize photobleaching. The temperature of the cuvette holder was maintained at 20°C by a circulating water bath. The concentration of rhodopsin in NABBs or vesicles was kept at 10 nM in the cuvette with 250μL buffer H1 for all experiments. The experiment was started after 10 min incubation of the rho sample in the cuvette at 20°C. The excitation and emission wavelength pairs (in nm) used on the instrument were- (1) Donor (Alexa-546) channel: Ex= 558, Em= 570; (2) FRET (Alexa-546 to Alexa-647) channel: Ex= 558, Em= 670; (3) Acceptor (Alexa-647) channel: Ex= 655, Em= 670. After 1 h of data acquisition, dodecyl maltoside (DM) was added from a 20% stock to make 1.5% in the cuvette and the solution was mixed. The data acquisition was continued. Finally, hydroxylamine was added from a 3.5 M stock to obtain 50mM in the cuvette, and the sample bleached using >495nm light and the spectrum was taken of the sample in a detergent solubilized, bleached state. The detergent solubilized rho reading was considered as the internal control for the respective samples and the spectra were normalized using this control. The data right before detergent addition was taken for analyzing the FRET index.

2.17 Decoration of Rhodopsin in NABBs by Fab Fragments

Fab fragments from the monoclonal antibody 1D4 were generated by proteolytic cleavage of 1D4 by Papain, followed by gel-filtration chromatography on a Superdex 200 10/300 column. Purity of the Fab fraction was checked by SDS-PAGE and concentration determined by absorbance at 280nm. Fab fragments were incubated at equimolar ratio to the rhodopsin in NABBs with gentle nutation in the presence of Concanavalin A–Sepaharose beads (Sigma) overnight at 4°C. The beads were washed three times with buffer and then the Fab-rho-NABB complex was eluted thrice using 100mM α-methyl mannoside containing elution buffer. The elutions were concentrated using an Amicon-15 centrifugation filtration device with a 50kD MWCO and the buffer was exchanged simultaneously with α-methyl mannoside free buffer. The complex was then subjected to gel-filtration chromatography over a Superose 6 10/30 column (GE Healthcare) and the peak fractions were used for EM analysis.

2.18 Negative-stain Transmission Electron Microscopy

5μL of freshly prepared NABB sample at a protein concentration of approximately 5-10 μg/mL was applied on a 400 mesh carbon coated copper grid which had been glow discharged for 10-20 seconds prior to sample application. The NABB solution was blotted after 1 minute and an equal volume of 1% uranyl

acetate was added immediately. The stain was gently wicked away and the staining repeated again. The grids were then imaged under 80keV using a Jeol 1230 transmission electron microscope equipped with a 1Kx1K CCD camera. Images were acquired typically at 1-2 μm underfocus to obtain optimal contrast. Nanogold images were acquired at regions of sparse stain and at lower defocus (200-500nm) in order to achieve highest density and contrast of the gold clusters (Hainfeld, Powell *et al.* 2002).

2.19 Circular Dichroism (CD) Spectroscopy and Isothermal Titration Calorimetry (ITC)

CD spectra were recorded at 25°C in an AVIV 202 circular dichroism spectropolarimeter. Typically, 22 μL of apo A-I sample at 1.1 mg/mL was incubated with 100 μL of POPC at 1.5 mg/mL in the form of Small Unilamellar Vesicles formed by sonication. Tris salt buffer (50 mM Tris pH 7.6, 150 mM NaCl) was added to a final volume of 400 μL. The sample was vortexed immediately and loading into a 0.1 cm path length cuvette and scanned from 250nm to 190nm with 0.5nm resolution and 1nm bandwidth. The temperature was kept constant with a circulating water bath. Raw ellipticity values were converted to Molar Residue Ellipticity for comparison of spectra between peptides and proteins of varying lengths and concentrations. Ellipticity values in millidegrees

from the AVIV CD software was converted to Molar Residue Ellipticity using the equation:

$$\text{Molar Residue Ellipticity } [\Theta] = \frac{\text{millidegrees}}{\#a.acids \times conc(M) \times pathlength(cm) \times 10}$$

The fraction alpha helicity was calculated from Molar Residue Ellipticity at 222nm according the following equation (Wieprecht, Beyermann *et al.* 2002):

$$f_h = \frac{[\Theta]obs - [\Theta]coil}{[\Theta]helix - [\Theta]coil}$$

[Θ] values for the alpha helical and coil parts are derived from:

$[\Theta]helix = -40000(1 - 2.5/n) + 100t$, $[\Theta]coil = 640 - 45t$,

where n is the number of amino acids in the protein (n for zap1 is 266 and for hΔap1 it is 222) and t is the temperature in °C.

Isothermal Titration Calorimetry experiments were performed in the VP-ITC high-sensitivity titration calorimeter (MicroCal, MA). Typically, 20 consecutive injections of 10 μL aliquots of the apolipoproteins from a stock concentration of 60 μM were made into 2 mM POPC Small Unilamellar Vesicles in the sample cell. The protein and POPC SUVs were dialyzed against the same buffer prior to the experiment and both lipid and protein solutions were degassed under vacuum immediately before use. Injections were made at intervals of 15 min, the duration of each injection was 2 s/μL and a constant stirring speed of 400rpm was maintained throughout the experiment to ensure proper mixing. The

ITC cell temperature was kept at 30°C. Data were analyzed using the Origin software provided by MicroCal Inc.

The experimental data were fitted to a curve corresponding to a Langmuir adsorption model of a single class of binding sites to obtain the equilibrium association constant (Ka), the enthalpy change (ΔH^o) and the stoichiometry parameter (*N*, the number of protein molecules bound per lipid molecule). The areas under the negative peaks corresponded to the heat released during the reaction after the addition of the protein to the SUVs. The values of Ka and ΔH^o obtained from curve fitting were used to calculate the standard free energy change (ΔG^o) and the standard entropy change (ΔS^o) for the binding using the equation:

$$\Delta G^\circ = -RT \ln K_a = \Delta H^\circ - T\Delta S^\circ$$

We use a modified standard state with respect to the experimental temperature of 30°C.

2.20 Thermal Stability Assay of Rhodopsin

Rho-NABBs were formed by dialysis, followed by Ni affinity purification in the dark. Aliquots of 1 μM rhodopsin in NABBs or ROS or detergent containing buffer H1 were incubated in 0.6mL eppendorf tubes at various temperatures in a thermomixer without shaking. After 15 minutes of incubation, each aliquot was kept on ice till it was used for a UV-visible scan in a Perkin-Elmer Lambda 800 UV-visible spectrophotometer at room temperature. The

sample was then photobleached under yellow light (>495nm wavelength) for 30 seconds in the presence of 50 mM hydroxylamine. The intact rhodopsin content of the sample was estimated by calculating the difference in absorption intensity between the dark and light spectra at 500nm. The absorption was expressed as the fraction of absorption of a sample stored at 4^{o}C and plotted as a function of temperature.

2.21 Rhodopsin Meta-II Decay Assay

Decay of rhodopsin Meta-II state in NABBs was followed by tryptophan fluorescence. Rhodopsin concentration was adjusted to 10nM in 10 mM HEPES-MES-KOH buffer pH 6, 100 mM KCl, 2 mM $MgCl_2$ in a magnetically stirred cuvette. The temperature was maintained at 20°C by a circulating water bath attached to the cuvette holder. Tryptophan fluorescence was recorded in a SPEX Fluorolog tau-3 spectrofluorimeter, equipped with a 450 W Xenon arc-lamp and single grating excitation monochromator, set to a center wavelength of 295nm with 0.2nm bandpass. A UV-bandpass filter (Hoya U-340, Edmund Optics, Inc., Barrington, NJ) was used in addition to the single grating emission monochromator, set to 330nm and 10nm bandpass. The signal of the photon-counting photomultiplier was integrated for 2 seconds. Data was recorded for two hours in 30 seconds intervals with the excitation shutter closed in between acquisitions to minimize photobleaching, unless stated otherwise. The rhodopsin

sample in the cuvette was bleached for 15 sec using a fiber-optics 150 W illuminator at full intensity with a yellow filter (model A-200, Dolan-Jenner Industries, Inc., Boxborough, MA) after obtaining a dark baseline for 3 minutes. The decay of the photolyzed state was followed for 2 hours.

2.22 Regeneration of Opsin in NABBs

Opsin-NABBs were generated by photobleaching 1 μM of 1 rho-NABB in buffer H2 pH 6 for 1 minute and incubating the photobleached sample at room temperature for more than 2 hours. A UV-vis scan was done every 10 minutes to ensure the lack of any significant absorbance at 480-550nm region. The sample was compared with a control containing 50 mM NH_2OH. 11-cis-retinal was solubilized from a 2 mM ethanolic stock upto 100 μM in approximately 1μM empty NABBs and vortexed vigorously to ensure proper mixing. Concentration of 11-cis-retinal was determined by its absorption peak at 378nm and using a molar extinction coefficient of 24940 M^{-1} cm^{-1}. Under dim light, 11-cis-retinal loaded NABBs were gently added by a microcapillary pipette tip to a final concentration of 0.5 μM 11-cis-retinal to a stirred microcuvette containing 700μL of 0.5 μM opsin-NABBs. Absorbance was monitored at 520nm, with a slit width of 0.5nm, integration time of 1 sec and time interval of 3 seconds. After saturation of the absorbance signal, 50 mM of NH_2OH was gently added from a 3.5 M NH_2OH stock. Finally, the sample was bleached using hi yellow light.

2.23 Transducin Activation Assay using Intrinsic Trp Fluorescence

1 rho-NABB sample was purified by 1D4 affinity purification of the dialysis product of a starting ratio of 0.1 rho/NABB to remove 'empty' NABBs from interfering in the assay. Following 1D4 affinity, both 1 rho-NABB and 2 rho-NABB samples were subjected to FPLC purification in the dark. Activation of holotransducin by rhodopsin incorporated in NABBs was analyzed by the tryptophan fluorescence assay (Fahmy and Sakmar 1993). Typically, 10 nM of rhodopsin-NABBs was added to 100 nM holotransducin in 10 mM HEPES-MES-KOH buffer pH6.9, 100 mM KCl, 2 mM $MgCl_2$ in a continuously stirred cuvette thermostatted at 10°C in a SPEX Fluorolog-II spectrofluorimeter. The sample was excited at 300nm with 2nm slit width and emission was recorded at 340nm with a 12nm slit width. GTP-γS was added to a final concentration of 5 μM in the cuvette. The cuvette was then illuminated by 543nm light from a HeNe laser and the spectra was collected under constant illumination to photoactivate rhodopsin. The curve obtained was analyzed by fitting an exponential corresponding to a pseudo-first order kinetics.

2.24 Isolation of Heterologously Expressed CCR5 Receptor and Incorporation in NABBs

HEK-293 cells stably expressing CCR5 were harvested and the cell pellet stored in PBS buffer containing protease inhibitors at –80°C. Cell pellets corresponding to 2 x 10 cm plates were thawed on ice and lysed using 500mL of buffer N1. The solution was sonicated using a probe-tip sonicator for 6 x 1 s pulses with 10 s cooling on ice. The tube was then incubated at 4°C with gentle mixing for 30 min. The tube was centrifuged at 20,000xg for 20 min at 4°C. The supernatant was collected and applied to 50mL of 1D4-sepharose slurry loaded with 2mg/mL of 1D4 and the mixture incubated at 4°C with gentle mixing for 30 min. The resin was centrifuged and washed with 500mL of buffer P2. The 1D4 bound protein was eluted by adding 50mL of buffer P2 containing 1D5-nonapeptide. Zap1 was added to the eluate at a final concentration of 80 μM. The mixture was vortexed, incubated on ice for 30 min and applied to a pre-equilibrated 500mL Extracti Gel–D column at 4°C. Elution was carried out under gravity flow by addition of detergent free buffer to the column and collecting 50mL fractions. The fractions were analyzed for protein elution by monitoring absorbance at 280nm.

The protein containing fractions were pooled and applied to a Superose 6 PC 3.2/30 gel-filtration column. The eluted peaks corresponding to the NABB elution were applied to 50μL of 1D4-sepharose. The resin was washed with buffer

P2 and eluted with 1D5 containing buffer P2. Aliquots from different stages of this protocol were used to assay for CCR5 using ELISA or western blots.

2.25 Sandwich ELISA to detect GPCR in NABBs

The primary (capture) antibody was diluted to 1μg/mL in 1xPBS pH 7.2 and 100μL was added to each well of the microplate (Costar clear-bottom, black 96-well). The plate was kept overnight at 4°C. The wells were washed twice with PBS containing 0.05% Tween-20. The wells were washed once with PBS and 200μL of 10mg/mL (1%) fatty-acid free BSA in PBS. The plate was either incubated at room temperature for 2 h or overnight at 4°C. The GPCR-NABBs were added to the respective wells in a final volume of 100μL. The GPCR-NABB was diluted in PBS containing 1mg/mL (0.1%) BSA. The microplate was incubated at 4°C overnight to ensure complete binding of epitope on the GPCR-NABB to the capture antibody. The analyte was then washed out thrice with 0.1% BSA-PBS using 200μL per wash. HRP-conjugated secondary (detection) antibody was added at 0.5-1.0μg/mL in each well (depending on the antibody affinity to the second epitope on the GPCR-NABB). The plate was incubated at room temperature for 2 h. The wells were washed 3-4 times with 0.1% BSA-PBS. A fresh working solution of Amplex Red and H_2O_2 was prepared from DMSO stock of Amplex Red and 3% H_2O_2 according to the manufacturer recommended protocol (Invitrogen, CA). 50μL of the Amplex Red working solution was

dispensed in each well and the plate was incubated for 30 min at room temperature, protected from light. The fluorescence in the wells were measured using a Cytofluor-II spectrofluorimeter with excitation at 530nm and emission at 590nm.

2.26 High-throughput G-protein activation assay

A black, C-bottom 96-well plate was used for the high-throughput G-protein activation assay. 25μL of purified G protein or its subunits were added to the microplate wells from 150 mM protein stock. The proteins added were either $G_{i1}\alpha$ subunit, $G_{i1}\alpha$ with transducin βγ subunits, or holotransducin (Gt), with 25μL of buffer G1 without GDP. CCR5-NABBs was incubated with 50 nM RANTES on ice for 30 min. 100μL of CCR5-NABB solution with and without RANTES were added to the respective wells and the microplate incubated at room temperature for 15 min. 60μL of BODIPY-FL-GTPγS was added from a 1 μM stock to all wells using a multi-channel pipettor. The plate was shaken for 30 sec, covered and incubated at room temperature for 5 min. The fluorescence in the wells was recorded using a Cytofluor II microplate reader with excitation wavelength= 485nm and 20nm bandpass, emission wavelength= 530nm and 25nm bandpass. The gain was set to 95 and 15 reads were integrated for each well. The fluorescence values from the wells containing BODIPY-FL-GTPγS and no G protein was subtracted from the rest of the data as background. The

fluorescence values from wells containing the CCR5-NABBs with no RANTES was subtracted from RANTES containing wells to give the RANTES specific response.

3.0

Formation and Characterization of Nanoscale Apolipoprotein Bound Bilayer (NABB) Particles by Zebrafish Apo A-I (Zap1)

3.1 Introduction

Apolipoproteins have been classified as 'protein detergents' (Segrest, Garber *et al.* 1994) that stabilize the size and structure of lipoprotein particles. The main function of apolipoproteins is considered to be lipid transport in the intravascular and extravascular regions in all organisms where these apolipoproteins are present (Li, Tanimura *et al.* 1988). Apo A-I is the main protein in high density lipoprotein (HDL) particles (density 1.06-1.21 g/mL) and involved in reverse cholesterol transport in the body. The structure and mechanism of action of human apo A-I has been a topic of intense investigation since human apo A-I has been implicated to play a protective role against

---

Material in this chapter has been previously published in: Banerjee S, Huber T, Sakmar TP. (2008) Rapid Incorporation of Functional Rhodopsin into Nanoscale Apolipoprotein Bound Bilayer (NABB) Particles. *J. Mol. Biol.* **377**(4): 1067-81.

coronary heart disease in humans (Bhat, Sorci-Thomas *et al.* 2005). Human apo A-I is a 243 amino acid protein that contains a putative globular N-terminal domain (residues 1-43) and a lipid-binding C-terminal domain (residues 44-243) (Segrest, Jones *et al.* 1992). Analysis of the human apo A-I gene and protein sequence first gave the idea that apo A-I contains eight 22-mer and two 11-mer tandem amino acid sequence repeats punctuated by prolines, and encoded by exon 4 of the apo A-I gene (McLachlan 1977; Karathanasis, Zannis *et al.* 1983).

The 4Å solution X-ray crystal structure of human apo A-I (44-243 amino acids) (Borhani, Rogers *et al.* 1997) showed an almost continuous α-helix punctuated by small or large proline induced kinks (**Fig. 1-6 A**). Apo A-I appears as four monomers in a unit cell, forming two antiparallel dimers. The dimers form central helix 5-5 and C-terminal helix 10-10 overlaps. A detailed molecular 'double-belt' model of apo A-I was subsequently proposed by considering lipid bilayer constraints on the arrangement of the protein (Segrest, Jones *et al.* 1999). The double-belt orientation of apo A-I (**Fig. 1-7**) has since been generally accepted and has proved consistent with recent analyses of HDL structure (Li, Lyles *et al.* 2000; Li, Chen *et al.* 2004; Silva, Hilliard *et al.* 2005; Li, Kijac *et al.* 2006).

The common lipid-associating structural motif in all exchangeable apolipoproteins is the amphipathic α-helix and any differences in lipid-binding properties of the apolipoproteins of similar number of amino acids can therefore be extrapolated to differences in the properties of the amino acids constituting the α-helices as well as the relative arrangement of the α-helices.

Formation and structural stability of HDL particles is critically dependent on the following parameters (Catte, Patterson *et al.* 2006):

1. Amphiphatic properties of apo A-I helices.
2. Flat planar discoidal (bilayer) geometry of HDL particles.
3. Helical curvature of the apolipoprotein dictated by the low dielectric constant of the lipid tails and high dielectric constant of the solvent.
4. Critical role of salt-bridges between the apolipoprotein helices to form a 'dimer' of apolipoprotein around the circumference of the bilayer disc.

The salt-bridging pattern between pairs of identical apo A-I helices from different species has been estimated by computationally docking one molecule of apo A-I over the second one in a certain interfacial orientation (Segrest, Jones *et al.* 1999). Strikingly, the general pattern of inter-helical salt-bridging in apo A-I is conserved in birds, mammals and fish. The salt-bridging pattern for zebrafish apo A-I shows a regular appearance of minima throughout the length of the helix, compared with human apo A-I where the minima are less regular and often compensated by charge appositions (**Fig. 1-7 E**). We hypothesized that this difference in salt-bridging pattern between zebrafish and human apo A-I may indicate that zebrafish apo A-I may adopt a higher number of stable inter-helical orientations compared with human apo A-I – a property that may enable us to utilize zebrafish apo A-I for forming discoidal lipoprotein particles rapidly and with stability even upon dilution. Although there have been scarce reports on the

properties of fish apo A-I, it has mainly been implicated in a direct functional role of maintaining trans-epithelial resistance in rainbow trout gills (Smith, Wood *et al.* 2005).

Figure 3-1. Sequence Comparison of Zebrafish apo A-I with Human apo A-I

Amino acid sequence comparison of mature zebrafish apolipoprotein A-I with human apolipoprotein A-I. (Top) Amino acid sequence alignment of *D. rerio* (Z) apo A-I, aligned with *H. sapiens* (H) apo A-I was performed using ClustalW 1.8 program (http://www.ebi.ac.uk/clustalw/). Invariant amino acid residues are shown in red and chemically similar residues are shown in green. Residue on zebrafish apo A-I that was chosen for a single point mutation to Cys in zap1Q26C is marked with *. N-terminal deletion for human Δ1–43 apo A-I is also marked. (Bottom) Domain structure of hexa-histidine tagged zebrafish apo A-I construct (zap1) and human Δ1–43 apo A-I (hΔap1) cloned and purified as described (Materials and Methods).

Figure 3-1

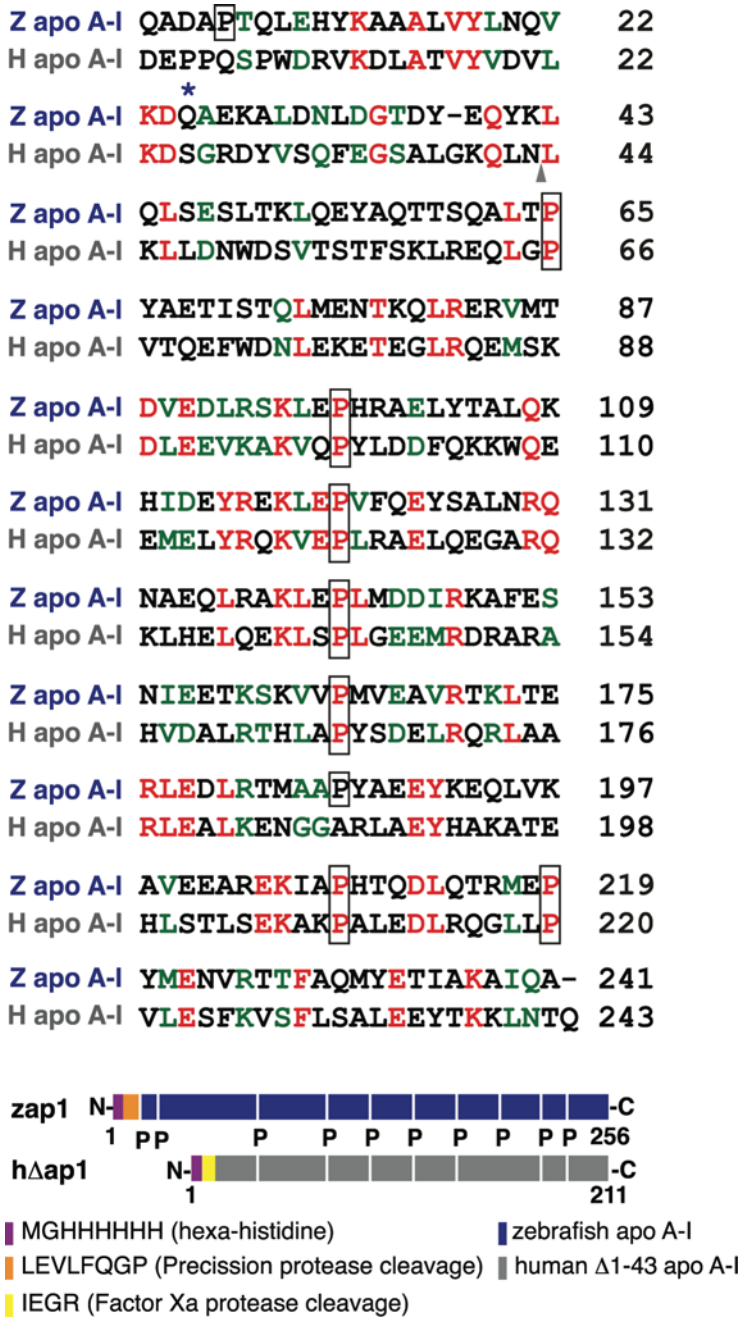
Z apo A-I QADAPTQLEHYKAAALVYLNQV 22
H apo A-I DEPPQSPWDRVKDLATVYVDVL 22
Z apo A-I KDQAEKALDNLDGTDY-EQYKL 43
H apo A-I KDSGRDYVSQFEGSALGKQLNL 44
Z apo A-I QLSESLTKLQEYAQTTSQALTP 65
H apo A-I KLLDNWDSVTSTFSKLREQLGP 66
Z apo A-I YAETISTQLMENTKQLRERVMT 87
H apo A-I VTQEFWDNLEKETEGLRQEMSK 88
Z apo A-I DVEDLRSKLEPHRAELYTALQK 109
H apo A-I DLEEVKAKVQPYLDDFQKKWQE 110
Z apo A-I HIDEYREKLEPVFQEYSALNRQ 131
H apo A-I EMELYRQKVEPLRAELQEGARQ 132
Z apo A-I NAEQLRAKLEPLMDDIRKAFES 153
H apo A-I KLHELQEKLSPLGEEMRDRARA 154
Z apo A-I NIEETKSKVVPMVEAVRTKLTE 175
H apo A-I HVDALRTHLAPYSDELRQRLAA 176
Z apo A-I RLEDLRTMAAPYAEEYKEQLVK 197
H apo A-I RLEALKENGGARLAEYHAKATE 198
Z apo A-I AVEEAREKIAPHTQDLQTRMEP 219
H apo A-I HLSTLSEKAKPALEDLRQGLLP 220
Z apo A-I YMENVRTTFAQMYETIAKAIQA- 241
H apo A-I VLESFKVSFLSALEEYTKKLNTQ 243
zap1
N-
-C
1
PP
P
P
P
P
P
P
P
256
hΔap1
N-
-C
1
211
MGHHHHHH (hexa-histidine)
zebrafish apo A-I
LEVLFQGP (Precission protease cleavage)
human Δ1-43 apo A-I
IEGR (Factor Xa protease cleavage)

3.2 Results

3.2.1 Amino Acid Sequence Comparison between Human Apo A-I and Zebrafish Apo A-I

In a discoidal High Density Lipoprotein (HDL) particle, two molecules of human apo A-I are hypothesized to form a 'double-belt' around the discoidal lipid particle that run circumferentially anti-parallel to each other (Segrest, Jones *et al.* 1999). The amphipathic helices are punctuated by periodic proline residues, which are believed to kink the helices to facilitate forming of the circumferential belt with the helix axis perpendicular to the lipid acyl chains. An apolipoprotein that binds to lipids in a manner similar to human apo A-I to form discoidal lipid particles would share a similar distribution of amino acids. To test the conservation of amino acid patterns between the two apolipoproteins, an amino acid sequence alignment was performed (**Fig. 3-1**). Invariant proline residues occur every 22 or 11 amino acids, suggesting that the length of zebrafish apo A-I may be divided into tandem 22/11-mer helices which interact with the lipid side chains and are punctuated by proline 'hinges', similar to the hypothesized lipid-binding mechanism of human apo A-I. The alignment also shows a general conservation of the chemical type of the amino acid residue in zebrafish apo A-I at the corresponding positions of the human apo A-I. The sequence similarity points to a similar lipid binding mechanism and amphipathicity of zebrafish apo A-I compared with human apo A-I. Hydropathy analysis shows the C-terminal

residues may not be as important for lipid binding in zebrafish apo A-I compared with human apo A-I. N-terminal tails of both zebrafish and human apo A-I show a conserved pattern of high hydrophobicity, indicating a possible role of the N-terminal residues of zebrafish apo A-I in lipid binding.

Human apo A-I is known to form various HDL subclasses distinguished on the basis of the diameters of the discoidal complexes (Jonas, Kezdy *et al.* 1989; Jonas, Steinmetz *et al.* 1993). The amino acid sequence of apo A-I is considered to be the primary determinant of HDL subclass formation. Most species, for example mice, generate monodisperse HDL particles, whereas primates and humans make distinct HDL subclasses. The two major subclasses being HDL_2 (larger and more buoyant) and HDL_3 (smaller) (Reschly, Sorci-Thomas *et al.* 2002). A major difference between the amino acid sequences of apo A-I in humans and non-primates is the lack of a Pro residue between putative helices 7 and 8 in human apo A-I (Frank and Marcel 2000). A report comparing the effects of replacing the non-proline containing sequence between helices 7 and 8 in human apo A-I with a proline containing sequence led to preferential formation of HDL_2 (smaller discs) by the chimeric human apo A-I (Carnemolla, Ren *et al.* 2008). Notably, zebrafish apo A-I contains a proline at position 186 (**Fig. 3-1**) which is the region between putative helices 7 and 8, with no corresponding proline at the same position in human apo A-I. The presence of Pro186 in zebrafish apo A-I may be a possible reason for the monodisperse nature of discoidal liproprotein particles formed by zebrafish apo A-I NABBs, compared with human apo A-I.

3.2.2 Salt Bridging between Apo A-I Helices

We analyzed the distribution of amino acids on zebrafish apo A-I using the HELNET program (**Fig. 3-2 A, B**). This program creates a diagram of the α helix seen as a cylinder cut along the center of the polar face and flattened. A continuous α helical net display of the putative tandem helices formed by the C-terminal 200 amino acids was plotted using either a pitch of 3.6 residues (18/5) per turn (**Fig. 3-2 A**) , or a 'tighter' pitch of 3.6667 residues (11/3) per turn (**Fig. 3-2 B**). As seen in the amino-acid distribution in the 18/5 helix, if the helix were closed as a cylinder, the hydrophobic face would twist around the resulting torus, instead of lying at the center of the helix as required by the double-belt model (Segrest, Jones *et al.* 1999). If the amino-acids are arranged according to a 11/3 helix, a comparatively straight (planar) hydrophobic face is formed. Further, we saw a marked separation of positively charged residues and negatively charged residues on respective edges of the helical net in the 11/3 helix (**Fig. 3-2 B**). Such a separation may be critical to the formation of effective and long-range salt-bridges between two anti-parallel arrangements of the zap1 helices in a discoidal lipoprotein particle. However, the HELNET program does not account for the special role of proline residues in the sequence, the presence of which may break the pattern of amino-acids.

Figure 3-2. Helical Net Analysis and Salt Bridging Scores between Zebrafish Apo A-I Helices

(A) Arrangement of hydrophobic (black), positively charged (blue) and negatively charged (red) amino acids in zebrafish apo A-I (Zap1) when Zap1 adopts a regular α 18/5 helix. Zap1 was plotted with an idealized pitch of 3.6 residues/turn using the HELNET program. **(B)** HELNET plot of zap1 with the amino acid residues arranged in an α–11/3 helix with 3.6667 resuidues per turn of the helix. A difference in the distribution of hydrophobic and charged amino acids can be seen in these two types of helical arrangements. Clustering of charged amino acids towards the edges of the helix and hydrophobic amino acids towards the center is observed in the α–11/3 helix configuration **(C)** Weighted salt bridging scores of two zap1 molecules arranged in an α–11/3 helix. Salt bridging scores using all possible ring pair interfaces between the 2 zap1 molecules are shown. Antiparallel arrangements- left to left (LL) and right to right (RR). Parallel arrangements- left to right (LR) and right to left (RL). For each residue step (x axis) representing one docking position, each weighted score is shown (y axis). The weighted number of salt bridges and like charge appositions were calculated for each docking position using the ALIGN program. The net salt bridging score is favorable only in the LL (antiparallel) arrangement of the helices.

Figure 3-2

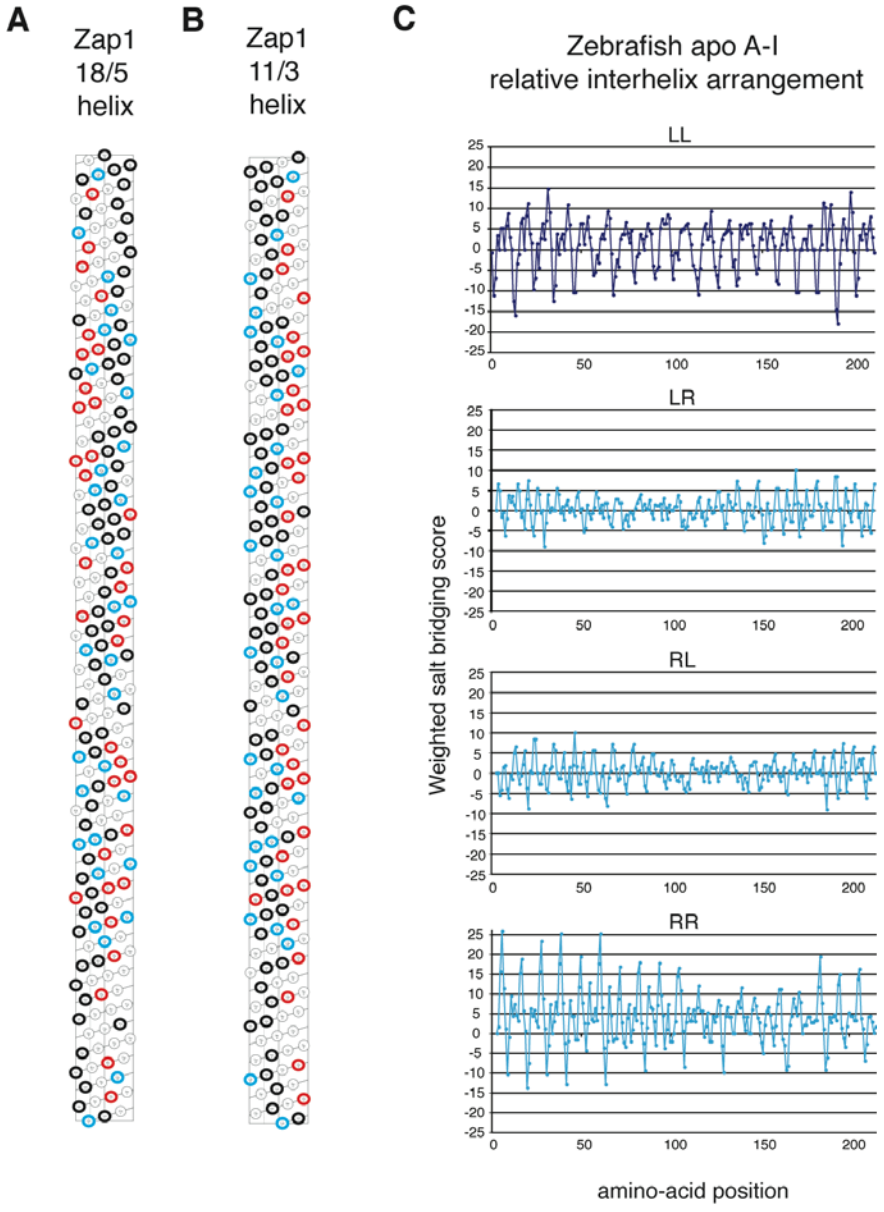
A
Zap1
18/5
helix
B
Zap1
11/3
helix
C
Zebrafish apo A-I
relative interhelix arrangement
LL
LR
RL
RR
Weighted salt bridging score
amino-acid position

Salt bridging between the apo A-I helices is reported to play a crucial role in determining the specificity of the helix-helix registry in a HDL particle (Segrest, Jones *et al.* 1999; Klon, Jones *et al.* 2000; Klon, Segrest *et al.* 2002). Molecular dynamics simulations of model peptides with POPC bilayer has shown that interhelical energetics is dominated by salt bridges (Sheldahl and Harvey 1999). We used the ALIGN program (Segrest, Jones *et al.* 1999) to compare the weighted salt-bridging score between helices in mature zebrafish apo A-I and human apo A-I proteins (**Fig. 3-2**). A lower score indicates more favorable salt bridging (attractive forces) between helices at that position. We noticed that both apolipoproteins have a net favorable salt bridging score when the two apo A-I helices are in antiparallel orientation with respect to each other (**Fig. 3-2**). We also noticed that zebrafish apo A-I exhibited a more regular pattern of negative peaks (favorable salt bridges) in the score throughout the length of its helix compared with human apo A-I. This may point to a mechanism in zebrafish apo A-I where multiple possible helical registries are possible, as opposed to one particular more favorable registry as with human apo A-I. It is likely that by not constraining the relative orientations (helix registers) of the apo A-I helices, zebrafish apo A-I may be able to form discoidal lipid particles rapidly. The particles formed by zebrafish apo A-I may also be more resistant to dilution compared with human apo A-I since the zebrafish apo A-I helices will be able to dock in multiple orientations in an equilibrium between lipid-bound and lipid-free states at high dilutions.

Figure 3-3. Vector Map and Purification of Zebrafish Apo A-I

(A) Vector map showing the salient features of the pE28-ZAP1 DNA derived from the pET28a(+) vector. Restriction endonuclease sites utilized for preparing and checking the vector are shown. **(B)** Ni-affinity purification of zap1 was performed and His-tagged protein eluted with an imidazole gradient. **(C)** Gel-filtration chromatography using a Superdex 200 26/60 column showed that the zap1 formed tetramers in the gel-filtration buffer. The tetramer peak was pooled to obtain pure zap1 (>95%) as shown in the inset. The presence of truncated protein (*trunc.*) contaminates the monomer peak, but not the tetramer. The inset shows Coomassie Blue stained fractions of lysate and the tetramer peak from the Superdex 200 column. The rightmost lane shows fluorescent detection of Alexa-488 modified zap1Q26C protein cloned and labeled as outlined in Method 2.11 and 2.12, and purified under similar conditions.

Figure 3-3

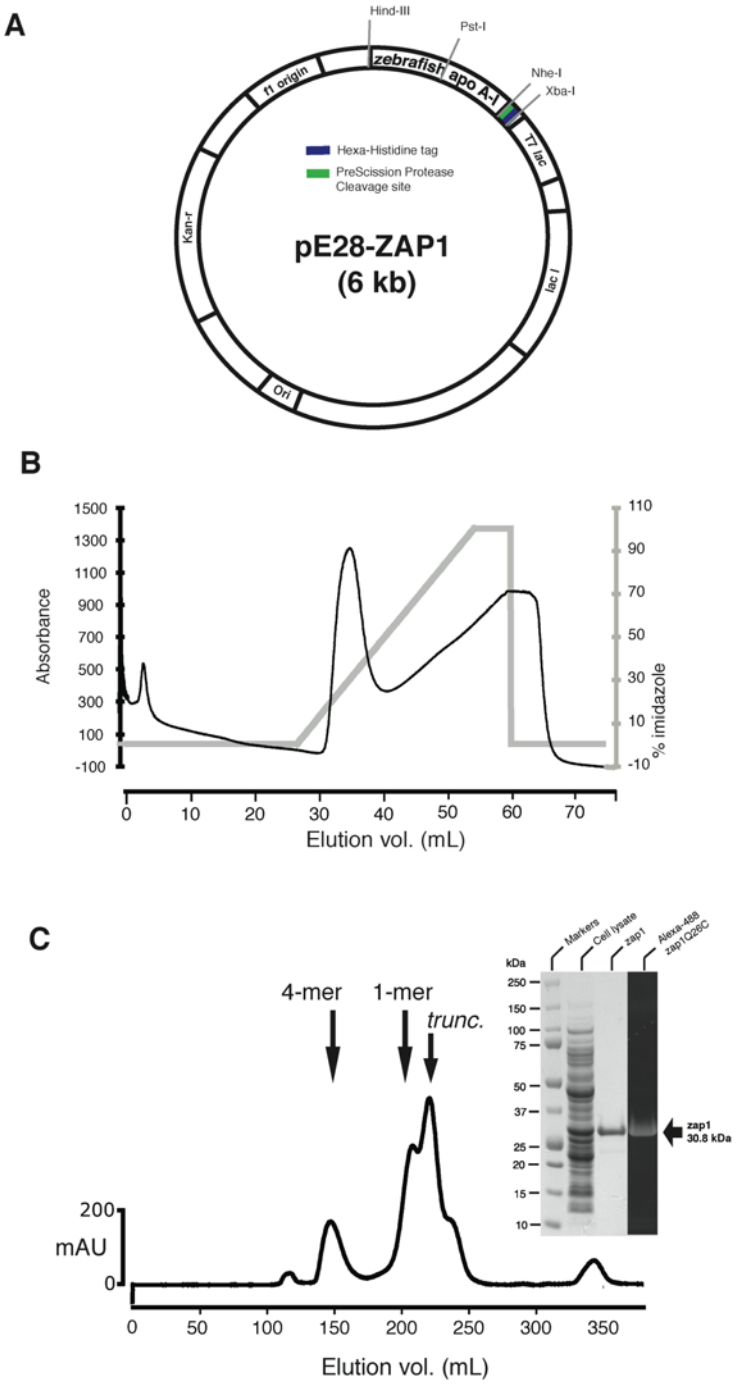
A
Hind-III
Pst-I
Nhe-I
Xba-I
zebrafish apo A-I
f1 origin
T7 lac
lac I
Ori
Kan-r
Hexa-Histidine tag
PreScission Protease Cleavage site
pE28-ZAP1
(6 kb)
B
Absorbance
% imidazole
Elution vol. (mL)
C
4-mer
1-mer
trunc.
Markers
Cell lysate
zap1
Alexa-488 zap1C250C
kDa
zap1
30.8 kDa
mAU
Elution vol. (mL)

3.2.3 Purification and Site-specific Fluorescent Labeling of Zebrafish apolipoprotein A-I (zap1)

We used reverse-transcriptase PCR to generate zebrafish apo A-I cDNA, which was inserted in a high-fidelity protein expression vector pET28a(+) (Novagen, San Diego, CA). The resulting vector- pE28ZAP1 (**Fig. 3-3 A)** had the zap1 sequence transcribed by the T7 RNA polymerase, under control of the lacI promoter which was de-repressed by the addition of isopropyl-β-D-thiogalactoside (IPTG) (Glick and Pasternak 1994). The vector carried a Kanamycin resistance marker which was used for selecting colonies containing the vector on a LB-Agar plate (or other media) supplemented with 50μg/mL Kanamycin. The vector also carried a hexa-histidine coding region upstream of the zap1 sequence, followed by a PreScission protease cleavage site. We also prepared a bacterial expression vector coding for human apo A-I using pET16b vector (Novagen). Human apo A-I cDNA was obtained from ATCC, excised and inserted into pET16b vector using appropriate restriction endonucleases. The resulting vector- pE16HAP1 contained the human apo A-I sequence transcribed by T7 RNA polymerase, under control of the lacI promoter. The vector carried an Ampicillin resistance marker, and a hexa-histidine coding sequence upstream of the hap1 sequence, followed by a Factor Xa protease cleavage site. Subsequent site-directed mutagenesis reactions were performed on these DNA constructs.

After *E. coli* expression and cell lysis, the hexa-histidine tag was used to affinity purify zap1 on a Ni column, using an imidazole gradient (**Fig. 3-3 B**). Gel-filtration chromatography of Ni-affinity purified hexa-histidine tagged zebrafish apo A-I (zap1) yielded protein at greater than 95% purity as judged by densitometry of the SDS-PAGE lane (**Fig. 3-3 C**). The tendency of apo A-I to form higher order oligomers was exploited in the gel-filtration step; the highest purity of zap1 on SDS-PAGE was the fraction corresponding to the size of a zap1 tetramer. A large amount of protein in the subsequent fractions was truncated as judged by SDS-PAGE. The truncation may either be due to aborted protein synthesis of zap1 in *E.coli* or proteolysis of the full-length protein in the bacteria. The ability of the truncated products to be co-purified on the Ni-affinity column alongwith the full-length zap1 under denaturating conditions indicates that the truncation occurred from the C-terminus (the hexa-histidine tag is present on the N-terminus).

A putative solvent-accessible glutamine residue near the N-terminus was chosen for point mutation to cysteine (shown by * in **Fig. 3-1**) to enable coupling to maleimide-linked fluorophores. For labeling the Cys mutant, a protocol reported for an on-column labeling procedure (Bergendahl, Anthony *et al.* 2002) was followed with slight modifications.

Figure 3-4. Native Polyacrylamide Gradient Gel Electrophoresis of NABBs

NABBs were prepared using LRB-DOPE doped POPC and zap1 in 75 POPC : 1 zap1 ratio. *(Top panel)* Gray curve— Densitometric scan of the fluorescence distribution in the gel lane after detection of rhodamine fluorescence (corresponding to doped lipids). Black curve— Densitometric scan of protein distribution made after Coomassie Blue staining of the same lane. The Stokes' diameter was calculated from the migration of standard proteins with known hydrodynamic radii in adjacent lanes: Thyroglobulin 17nm, Ferritin 12.2nm, Catalase 9.2nm, Bovine Serum Albumin 7.1nm. *(Bottom panel)* Lane showing protein distribution detected by Coomassie blue staining and lipid distribution detected by rhodamine fluorescence of the same lane. The gel was run to equilibrium in Tris-Borate-EDTA pH 8.5 for 24 h at 16°C.

Figure 3-4

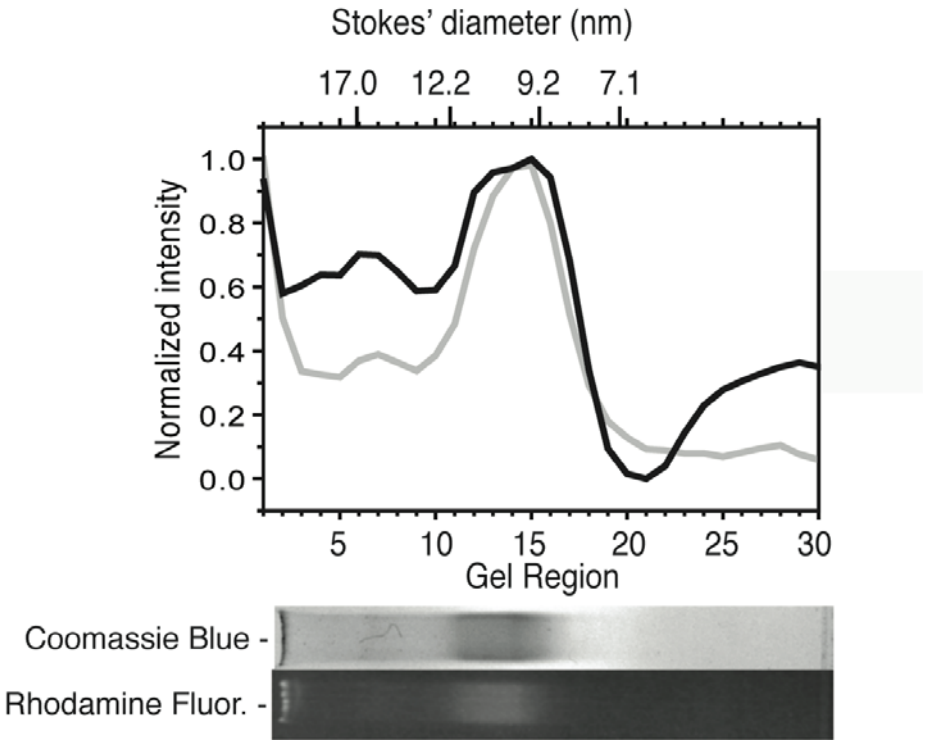
Stokes' diameter (nm)
17.0
12.2
9.2
7.1
Normalized intensity
1.0
0.8
0.6
0.4
0.2
0.0
5
10
15
20
25
30
Gel Region
Coomassie Blue -
Rhodamine Fluor. -

3.2.4 Characterization of Lipoprotein Particles formed by Zebrafish Apo A-I

The products of the interaction of zebrafish apo A-I (zap1) and POPC upon detergent removal were characterized by native polyacrylamide gradient gel electrophoresis, and gel-filtration chromatography followed by electron microscopy imaging. The native gradient gels were analyzed at equilibrium by running the gels for 24 h at 16°C (**Fig. 3-4**). Under these conditions, the particles migrate due to a combined influence of the net charge on the particle (primarily due to zap1, since POPC is a zwitterionic lipid) and sieving effects of the cross-linked agarose gel.

To observe the effect of different POPC ratios on the hydrodynamic radius of NABBs, different POPC to zap1 ratios were used to reconstitute NABBs by extensive dialysis to remove detergent. The NABB samples were then analyzed by gel-filtration chromatography on a calibrated Superose 6 10/30 column. Three POPC to zap1 ratios are shown in **Fig. 3-5**. We detected evidence of three particle populations with maximal Stokes diameters of 10nm, 11.6nm, and 12.5nm in addition to a void volume fraction containing vesicles. Upon increasing the POPC:zap1 ratio to 100:1, we also detect a significant population of 17nm diameter discs.

Figure 3-5. Gel-filtration, EM imaging and Histogram of Diameters of Lipoprotein Particles formed by zebrafish apo A-I

(A) Formation of discoidal lipoprotein particles by zebrafish apo A-I with POPC. Size-exclusion chromatography of lipoprotein particles formed between zebrafish apo A-I and POPC upon detergent removal by dialysis at different molar ratios of POPC to zap1— 25:1, 75:1, and 200:1. The Stokes' Radii determined by calibration of the Superose 6 10/30 column were: *a*-12.5nm, *b*-11.6nm, *c*-10.0nm, *v*-void volume. Representative negative stain EM images of the main peak fractions (shaded area) are shown as insets. The scale bar in all cases is 50nm. **(B)** A histogram of the size distribution of particles formed by zebrafish apo A-I and POPC at a POPC to zap1 ratio of 75:1 from EM imaging.

Figure 3-5

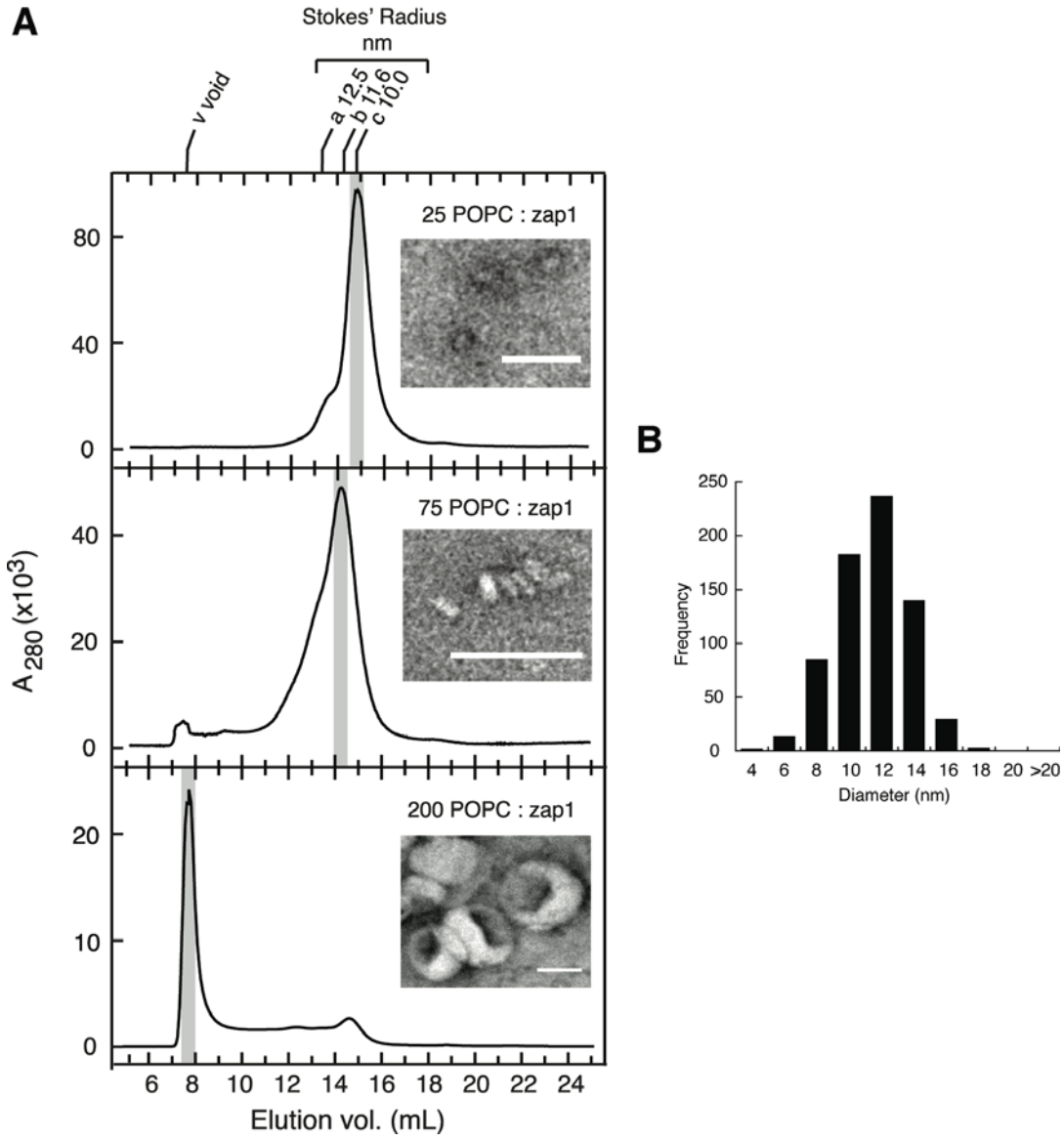
A
Stokes' Radius
nm
v void
a 12.5
b 11.6
c 10.0
25 POPC : zap1
75 POPC : zap1
200 POPC : zap1
A280 (x10^3)
Elution vol. (mL)
B
Frequency
Diameter (nm)

In comparison, Rogers *et al*. (Rogers, Brouillette *et al.* 1997) have reported that human apo A-I forms particles of diameters 8.5nm (78%), 12.0nm (21%) and 15.5nm (1%) with POPC, whereas human Δ1-43 apo A-I gives particles of diameters 8.5nm (47%), 12.5nm (18%) and 16.5nm (35%). These results are consistent with our experience. Compared with zap1 and POPC which tends to form a homogeneous disc population, hΔap1 forms discs with a broad and heterogeneous size distribution. A smaller diameter of NABBs in very low POPC: zap1 ratios could either be explained by correspondingly smaller number of amino acids contacting the lipid which is limiting, resulting in a 'buckling' of the planar disc structure (Catte, Patterson *et al.* 2006). When the lipid: zap1 ratio is in large excess of the optimized ratio for disc formation, the dominant product is vesicles. We confirmed discoidal morphology of the NABBs by negative stain EM and observed typical rouleaux (stack) formations of NABBs as well as well-defined separated NABBs with average diameters of 10–13nm and thickness of about 5nm as the main structures when the molar ratio was 75 POPC:zap1.

Sizing of the particles was done from the images using the magnification parameters of the image in the ImageJ software image analysis program. Measurements of diameter were done on free-standing particles with a circular profile and plotted as a histogram (**Fig. 3-5 B**).

Figure 3-6. Circular Dichroism (CD) and Isothermal Titration Calorimetry (ITC) of zap1 Interaction with POPC Small Unilamellar Vesicles (SUVs)

(A) Far UV CD spectra are shown for 6×His zebrafish apo A-I (zap1) in buffer (empty circles) or in buffer containing POPC SUVs (filled circles). Spectra are also shown for 6×His human Δ1–43 apo A-I (hΔap1) in buffer (empty triangles) or in buffer with POPC small unilamellar vesicles (filled triangles). **(B)** ITC time trace of zap1 injected into dispersion of POPC SUVs. The heat of injection (lower panel) is plotted by integrating the area under each injection peak (upper panel). The last few injections were taken as the heat of dilution and subtracted from the entire run.

Figure 3-6

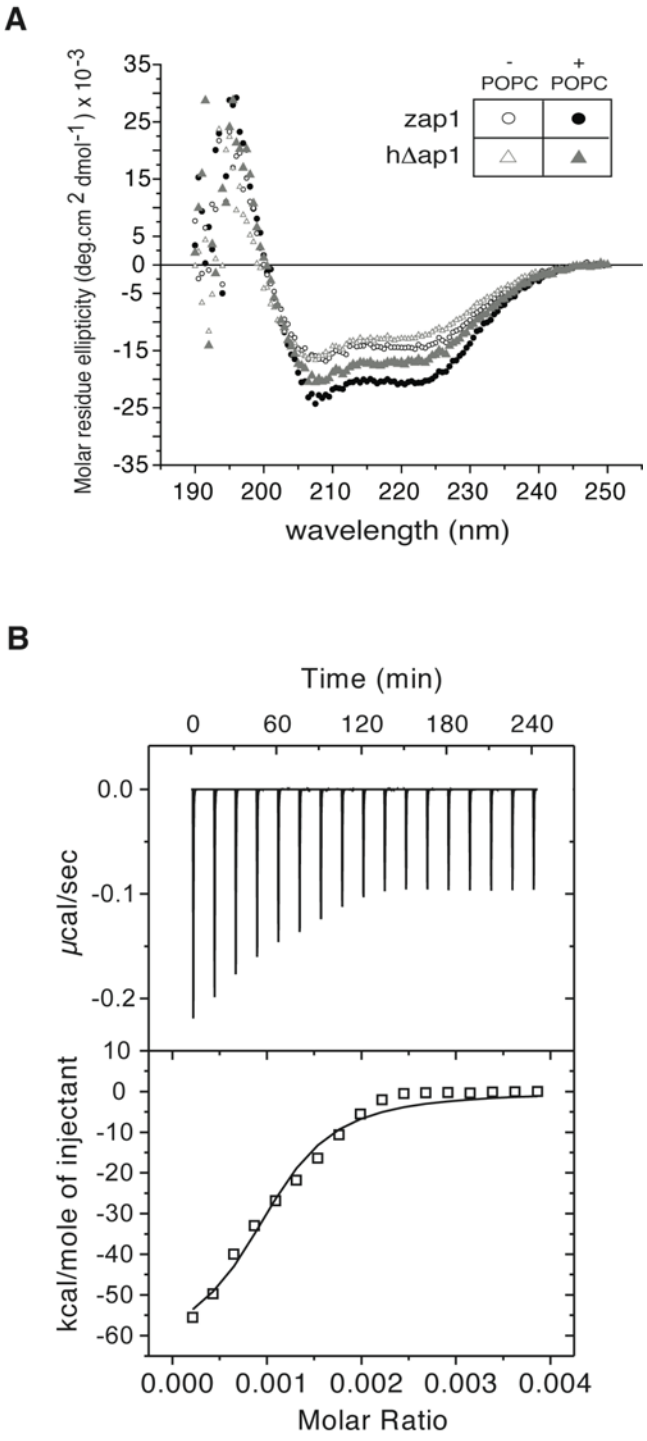
A
Molar residue ellipticity (deg.cm 2 dmol-1) x 10-3
35
25
15
5
0
-5
-15
-25
-35
190
200
210
220
230
240
250
wavelength (nm)
-
POPC
+
POPC
zap1
hΔap1
B
Time (min)
0
60
120
180
240
0.0
-0.1
-0.2
µcal/sec
10
0
-10
-20
-30
-40
-50
-60
kcal/mole of injectant
0.000
0.001
0.002
0.003
0.004
Molar Ratio

Table 1. Interaction of Apo A-I with POPC Vesicles

CD parameters for zap1 and hΔap1*			
Sample	**$[\theta]_{222} \times 10^3$**	**f_h**	**Residues**
zap1 in buffer	~14.4±0.3	0.38	102
zap1 + POPC	~20.7±0.3	0.55	147
hΔap1 in buffer	~12.9±0.4	0.33	76
hΔap1 + POPC	~17.0±0.1	0.45	101

ITC parameters of POPC interaction with zap1 and hΔap1					
Sample	**K_a (M^{-1}) $\times 10^{-6}$**	***N* (mmol apo/mol POPC)**	**$\Delta H°$ (kcal/mol)**	**$\Delta G°$[a] (kcal/mol)**	**$T\Delta S°$[b] (kcal/mol)**
zap1 + POPC	4.09±0.80	1.91±0.05	−59.7±1.1	−11.6	−48.0
hΔap1 + POPC	0.55±0.95	1.70±0.14	−98.5±1.1	−10.4	−88.1

* Experiments were performed at 25°C.

** Experiments were performed at 30°C. Each value represents the average of at least three experiments. The $\Delta H°$ and $\Delta S°$ values are per mole of apo A-I**.**

[a] $\Delta G° = -RT\ln(55.5\text{M} \cdot K_a)$ (Rogers, Brouillette *et al.* 1997; Seelig 2004)

[b] $T\Delta S° = \Delta H° - \Delta G°$

3.2.5 Interaction of Zebrafish Apo A-I with Lipid Vesicles

We compared the lipid-mediated helicity change and thermodynamics of zap1 with that of an N-terminal 1–43 amino acid truncated human apolipoprotein A-I (hΔap1) construct that has been hypothesized to form a model antiparallel double-belt orientation around a HDL particle (Borhani, Rogers *et al.* 1997) and has been used to incorporate membrane proteins (Bayburt, Grinkova *et al.* 2002). It is noteworthy that apo A-I interaction with POPC SUVs does not form NABBs. However, the interaction of lipid-free apo A-I with the phospholipid membrane of the SUV induces α-helical structure (White and Wimley 1999; Seelig 2004), which may be measured using circular dichroism (CD) spectroscopy and isothermal titration caloriemetry (ITC). The conditions in our CD experiments are similar to those in Arnulphi *et al.* (Arnulphi, Jin *et al.* 2004), who reported interaction of mature human apo A-I with POPC SUVs. The data for Molar Residue Ellipticity (MRE) obtained by them for human apo A-I are similar to our data using zap1. Surprisingly, the fractional helicity (f_h) obtained by us for zap1 (Table 1) using the empirical relation of Scholtz *et al.* (Scholtz, Hong *et al.* 1991) are 20-25% lower than what Arnulphi *et al.* report for human apo A-I. However, based on the similarity of the two proteins and experimental conditions, the f_h values of human apo A-I and zap1 should be identical since the MRE values are virtually identical. Rogers *et al.* (Rogers, Brouillette *et al.* 1997) and Li *et al.* (Li, Chen *et al.* 2004) have reported comparisons of human apo A-I with N-terminal 1-43 truncated human apo A-I (similar to hΔap1). The MRE values reported in

these papers are systematically higher than those of either Arnulphi *et al.* or ours. Interestingly, these two papers seemingly contradict each other in the extent of helicity of human apo A-I and hΔap1. The discrepancy between our data and the published data highlighted above are likely due to an instrumental artifact of the CD spectrometer used in these studies that appears to give systematically lower ellipticity values, not unusual for CD instruments (Konno, Meguro *et al.* 1975). Despite the difficulties in comparing data from different groups, our data in Table 1 clearly indicate that zap1 undergoes a larger increase in helicity compared with hΔap1 upon interacting with POPC SUVs. Apparently, nearly twice as many amino acid residues become α-helical in zap1 compared with hΔap1 upon interaction with POPC SUVs.

Comparing the affinity of apo A-I to POPC SUVs from our data (**Table 1**) and from Arnulphi *et al.* (Arnulphi, Jin *et al.* 2004), we found that the association constant (K_a) for zap1 is more than 7-fold greater than that of hΔap1, but approximately equal to that of human apo A-I. On the other hand, the stoichiometry of binding of zap1 and hΔap1 to POPC are similar but 3-times higher than reported for human apo A-I. The reaction enthalphy ($\Delta H°$) shows that zap1 has only about 60% of the favorable reaction enthalpy compared with hΔap1 and human apo A-I. It is interesting to note that while zap1 shows significantly reduced values of enthalpic and entropic contributions to the free energy change compared with hΔap1, enthalpy-entropy compensation results in similar $\Delta G°$ values for both apolipoproteins. In both cases the interaction with POPC is enthalpy driven.

3.3 Discussion

3.3.1 Biological Role of Apo A-I

The main role of apolipoprotein A-I in most organisms where it is found is in the reverse cholesterol transport (RCT) pathway. In RCT, lipids and free and esterfied cholesterol are carried from peripheral tissues to the liver by High Density Lipoprotein (HDL) particles. These HDL particles are formed by lipids and apo A-I, with 1–4 apo A-I molecules per HDL (Fielding P.E. and C.J. 2002), together with other apolipoproteins that specify the metabolism and delivery of these lipids. Newly formed HDL have high density primarily due to apo A-I and little lipid. Their density decreases as they take up lipid in the circulation. The classical subfractions of HDL are– HDL_3 (density 1.12-1.219 g/mL), HDL_2 (1.063-1.12 g/mL), HDL_1 (density < 1.063 g/mL).

In humans, apo A-I is synthesized by the liver and small intestine. HDL-containing apo A-I is formed in the extracellular space. Lipid-poor apo A-I associates with cell-derived phospholipids and cholesterol. The association of apo A-I and phospholipids is thermodynamically favorable; phospholipid-free mature human apo A-I has not been detected in biological fluids.

3.3.2 Evolution of Apo A-I

Apolipoproteins are lipid binding proteins comprising of amphipathic helices. Apo A-I is conserved throughout evolution from insects (called apolipophorins) to humans with its primary function being lipid binding and transport. The majority of the structural and functional aspects of apo A-I had been elucidated due to extensive studies on human apo A-I. Apo A-I is synthesized *in-vivo* in the liver and small intestine as a 267 amino acid pre-proapoA-I. The proapoA-I is secreted into the plasma after an intracellular peptidase cleaves the 18 amino acid signal sequence from pre-proapoA-I (McGuire, Davidson *et al.* 1996). The propeptide sequence of 6 amino acids is removed by an unknown protease, releasing the mature apo A-I protein. Inspection of the amino acid sequence of pre-proapo A-I and apo A-I reveals that a large part of the protein evolved by duplication of a primordial sequence encoding a 22 amino acid sequence (22-mer). This primordial sequence seems to have evolved by a duplication of an 11-mer sequence (Boguski, Elshourbagy *et al.* 1985).

Synthetic amphipathic helical segments whose primary sequence is unrelated to that of native apo A-I can be effective mimics of natural apo A-I in binding to phospholipids, promoting cholesterol efflux from cells, and activating the formation of cholesteryl esters by the LCAT reaction (Nion, Demoor *et al.* 1998; Wool, Reardon *et al.* 2008). Some repeats in native human apo A-I have been reported to be of more significance than others for the function of HDL

particles (Sorci-Thomas, Curtiss *et al.* 1997). The reports indicate that apo A-I may retain significant tertiary structure

3.3.3 Hi-yield Expression and Purification Strategy for Apo A-I

Hi-yield heterologous expression of apo A-I was optimized by adapting strategies previously reported for human apo A-I expression and purification towards zebrafish apo A-I (McGuire, Davidson *et al.* 1996; Rogers, Roberts *et al.* 1998; Bayburt, Grinkova *et al.* 2002). A hexa-histidine tag was introduced upstream of the N-terminus of zap1 in the bacterial expression plasmid. The zap1 cDNA contained some rare codons for *E.coli* due to which an engineererd *E. coli* strain was chosen which contains an additional plasmid coding for rare *E. coli* amino acids (BL21DE3 Rosetta2) instead of codon optimizing the DNA. The bacterial strain chosen was also deficient in proteases, since apo A-I being a flexible protein, could be susceptible to proteolysis in the bacterial cell. Evidence of truncated proteins was observed however, and may be attributed to aborted protein translation in *E.coli*. Enriched bacterial culture media, called Terrific Broth, was used to maximize bacterial growth. The bacterial cells were lysed in the presence of a chaotrope (6M guanidine hydrochloride) or detergent (1% Triton X-100) in order to solubilize the hydrophobic stretches of apo A-I by delipidation for further purification.

In a solution of 6M guanidine hydrochloride or 1% Triton X-100, the apo A-I is mostly unfolded. The apo A-I is refolded on the Ni column by washing the

column with decreasing concentration of guanidine hydrochloride or Triton X-100. On-column labeling of zap1Q26C may be performed in a partially unfolded state of the protein by flowing the maleimide-functionalized fluorophore at approximately 1mM concentration in the wash buffer without any reducing agent. If Triton X-100 is used for solubilization, then a washing step with 2mM sodium cholate is recommended to separate any charged impurities. The final washes of the Ni column are chaotrope or detergent free. The protein is eluted using an imidazole gradient. Gel-filtration chromatography is carried out to obtain fractions with ful-length zap1 at different purities (**Fig. 1-3 C**). We have observed both zebrafish and human apo A-I to have a strong tendency to form non-covalent dimers and tetramers when free of chaotropes or detergents. Full-length apo A-I of very high purity (>92%) may be isolated from the gel-filtration peaks corresponding to a tetramer. The monomer peak usually overlaps with a peak containing truncated protein in a Superdex 200 column and is thus not usable.

The pure apo A-I may be stored for extended periods of time at 4°C or in standard buffers without any loss in lipid-binding activity. The apo A-I does tend to aggregate over time, therefore it is advisable to store small aliquots at -20°C. When thawing an aliquot for use, it is advisable to centrifuge the tube and make a fresh dilution of apo A-I from the supernatant and determine the concentration (by UV absorbance) before starting an experiment.

3.3.4 Molecular Basis of *in-vitro* Discoidal Lipoprotein Formation by Apo A-I

Salt bridges are weak, ionic forces between positively and negatively charged side chains of amino acids. The contribution of a single salt bridge may be as much as –5 kcal/mol (Schulz G.E. and R.H. 1979) and is heavily dependent on the electrostatic properties of the medium. The contributions of salt bridging are more important for determining specifity between protein-protein interactions, rather than the overall stability of the protein. If the charges of oppositely charged proteins, or protein surfaces are not compensated, the energy is reduced sufficiently such that the proteins will not associate.

Most of the experimental evidence on apo A-I and HDL structure has been obtained from synthetic recombinants of human apo A-I and pure phospholipids in a range of relative molar ratios. The particles have been shown to consist of a planar phospholipids bilayer, whose edges are sealed from the aqueous medium by apo A-I. It was thought earlier that a ‘picket fence’ model- where the helical repeats of apo A-I were at right angles to the lipid bilayer, accurately reflected the structure of these particles (Brasseur, De Meutter *et al.* 1990; Phillips, Wriggers *et al.* 1997). The more recent ‘double belt’ model predicts the helical repeats to be aligned circumferentially parallel to the bilayer (Segrest, Jones *et al.* 1999; Tricerri, Agree *et al.* 2001). The double-belt model of apo A-I binding to lipids is the currently accepted model.

Figure 3-7. Intermediates in a Micelle-to-Vesicle Transition

Schematic representation of a proposed micelle-to-vesicle transition pathway adapted from Leng *et al.* (Leng, Egelhaaf *et al.* 2003). Detergent removal from mixed micelles is believed to first form disc-like intermediate micelles rapidly. These micelles grow up to a certain critical radius (r*) due to coalescence, followed by closure to form vesicles. Ripening of these vesicles is thought to occur over very long timescales. Under certain conditions, there may be a significant barrier to coalescence (depending on electrostatic interactions between disks and packing contributions), and growth and closure may be slower than stacking. This leads to the formation of lamellar phase as the end state.

In a NABB, apo A-I may replace the detergent at the edge of the disc, thereby increasing the stability of the kinetically trapped discoidal intermediate (section 3.3.4).

Figure 3-7

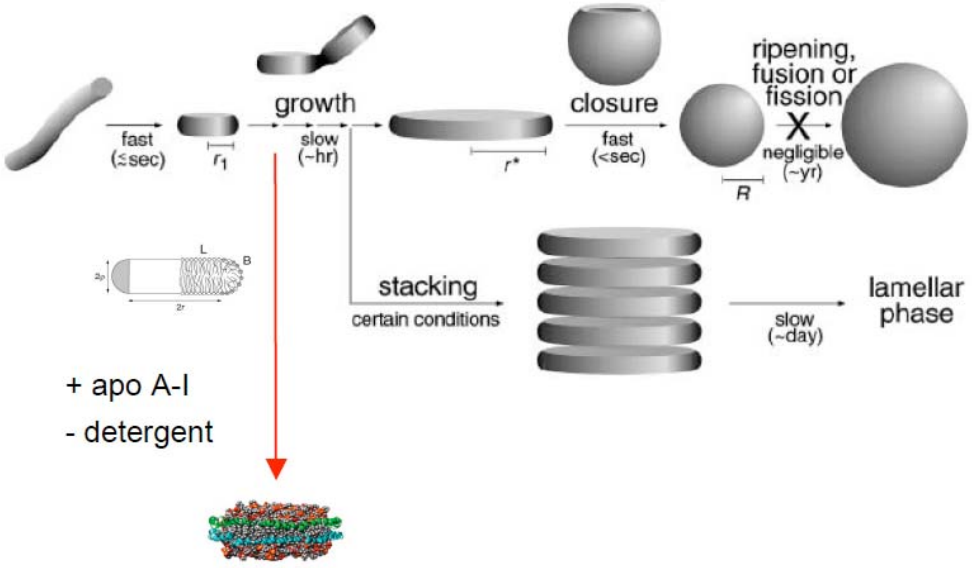
growth
fast
(≤sec)
slow
(~hr)
closure
fast
(<sec)
ripening,
fusion or
fission
negligible
(~yr)
stacking
certain conditions
slow
(~day)
lamellar
phase
+ apo A-I
- detergent

Discoidal lipid particles are hypothesized to be intermediates in a micelle-to-vesicle transition reaction of lipids upon detergent removal, as deduced from static and dynamic light scattering experiments (Leng, Egelhaaf *et al.* 2003). In the absence of apo A-I, when a detergent is removed from a mixed-micellar state of lipids and detergents, disc-like intermediate micelles are first formed rapidly (**Fig. 3-7**). These disc-like micelles grow by coalescence. Interactions between disc-like micelles are determined by the standard electrostatic potential of the system in addition to local packing contributions between the discs. Large discs then become unstable due to incomplete coverage of their perimeter by detergent which increases the energy per unit length of boundary (line tension) of the disc, finally leading to closure of the large lipid disc to form a lipid vesicle. Line tension may control the initial diameter of the disc-like micelles.

It is plausible that apo A-I present at a certain concentration replaces the surfactant stabilizing the edge of the bilayer due lipid-binding properties of its amino acids, as shown in red in Fig. 3-7. This would provide kinetic stability to the disc-like micelle formed. It should be mentioned that this proposed scheme of NABB formation is valid only when NABBs are formed by detergent removal from a mixed micellar state. Human apo A-I is able to directly solubilize vesicles around their phase transition temperature (T*m*) of the vesicle lipids (Tricerri, Toledo *et al.* 2005). The vesicles formed with dimyristoyl phosphocholine (DMPC, T*m*= 28°C) or dipalmitoyl phosphocholine (DPPC, T*m*= 40°C) are among those that are solubilized by apo A-I. The NABB formation pathway in

these cases likely involves interaction of apo A-I with lipids facilitated by interfacial packing defects in the lipids during the gel to liquid-crystalline phase change. Using lipids such as 1-palmitoyl-2-oleoyl phosphocholine (POPC, T*m*= –3°C) or 1-palmitoyl-2-oleoyl phosphoethanolamine (POPE, T*m*= 17°C) (Leekumjorn and Sum 2007), which are already in liquid crystalline phase under experimental conditions, detergent removal is the preferred method for formation of NABBs.

3.3.5 Electron Microscopy of Discoidal Lipoprotein Particles

Electron microscopy (EM) is an extremely useful tool for obtaining insight into particle size distributions and morphology under conditions where sample size is extremely small and/or dilute. Biological materials examined by EM generally have poor inherent electron scattering characteristics. A commonly used solution is using negative-staining where heavy metal salts are used that can be air-dried to give an amorphous electron-dense layer surrounding and supporting (embedding) the biological particles (Harris 1997). Negative-stain EM lends itself extremely well in examination of smaller, dense lipoproteins such as low-density lipoproteins (LDL) and high-density lipoproteins (HDL) (Forte, Nichols *et al.* 1971; Wlodawer, Segrest *et al.* 1979; Bayburt and Sligar 2003; Catte, Patterson *et al.* 2006). Negative-stains commonly used in EM are uranyl acetate, phosphotungstate, and ammonium molybdate. Uranyl acetate is favored for most applications because of its low-granularity and high contrast. The pH of this stain

is 3.5 to 4.0 and can only be used for dilute protein samples, otherwise aggregation and precipitation of the protein may occur.

We performed negative-stain EM on 400-mesh formvar carbon coated grids. The grids were glow-discharged for 20-30 sec prior to sample application to render them hydrophilic to not have the lipoprotein particles orient in any particular order. The lipoprotein particles were freshly prepared and examined in the electron microscope within 1 hour of preparing the grid. To get good contrast, a relatively low accelerating voltage of 80 kV was used in the microscope. An optimal defocus was used for imaging, one that showed minimal granularity of the background stain. Each grid was adequately sampled by taking random images within a grid square and then imaging in random grid squares to get a representative set of particles for analysis.

Aggregation of lipoprotein particles on the grid provide additional information on the physical properties of the particles. Under negative-staining techniques, discoidal lipoproteins form ‘stacks’ or rouleaux owing to their planar shape and discoidal geometry. These structures were predominantly seen at defined lipid:apo A-I ratios, indicating the optimal stoichiometry of components required to form small, discoidal particles having the thickness of a phospholipids bilayer.

4.0

Site-Specific Labeling of Rhodopsin

4.1 Introduction

Derivatization of GPCRs with fluorescent probes at a specific site and their characterization is a crucial and challenging step in elucidating the molecular mechanisms of GPCR activation. Chemical modification of an amino-acid side chain with a fluorophore of small molecular weight is a desirable strategy for labeling to detect relative conformational change between protein microdomains or monitoring oligomerization of proteins. The sulfhydryl group of cysteine side chains is the first target for such modifications because of the following reasons:

1. The cysteine content of most proteins is relatively low (< 3 mol%) allowing easy discrimination and identification of individual sulfhydryl groups.
2. A large variety of very specific reagents are commercially available, including compounds that introduce reporter groups for spectrophotometric, fluorometric, ESR, NMR, and biochemical analysis.

3. The SH group reactivity is fast without the requirement of a catayst.

Bovine rhodopsin has 10 cysteine residues at positions 110, 140, 167, 185, 187, 222, 264, 316, 322 and 323 (Hargrave, McDowell *et al.* 1984). Cys 110 and 187 form a disulfide bond, Cys 322 and 323 are palmitoylated and Cys 167, 222 and 264 are buried inside the transmembrane helices (Palczewski, Kumasaka *et al.* 2000). Previous studies have indicated that Cys 140 and Cys 316 on the cytoplasmic side are found to be reactive towards maleimide and iodoacetamide, and of these residues, Cys 316 appears to be more reactive (Findlay, Barclay *et al.* 1984; Imamoto, Kataoka *et al.* 2000). In this chapter we discuss methods used to label and characterize bovine rhodopsin at these reactive cysteine residues.

Figure 4-1. Fluorescent Derivatization of Rhodopsin

(A) Stochiometry of rhodopsin labeling by commercially available maleimide-linked fluorophores. Plot of the molar excess of dye (x axis) and the final labeling ratio of detergent solubilized, affinity purified rhodopsin (y axis) determined by UV-visible difference photobleaching spectroscopy. For most dyes, the extent of labeling increases linearly with increasing dye concentration above a certain threshold. **(B)** Detection of site-specific labeling using V8 protease digestion of labeled rhodopsin. Coomassie stained gel lanes containing unlabeled rho (lane 1), V8 digested Atto655:rho initial ratios of 9:1 (lane 3) and 3:1 (lane 4) are shown. Fluorescence detection of the gel was done prior to Coomassie staining. The fluorescence of the respective Atto655 labeled rho samples are shown in lane 5 and 6. V8 digestion of rho results in two main proteolyzed fragments- F1 and F2. Cys 316 is present in the F2 fragment. Selective modification of Cys 316 may be inferred from the fluorescence signal appearing exclusively in the F2 fragment in lane 6, compared with both F2 and F1 in lane 5.

Figure 4-1

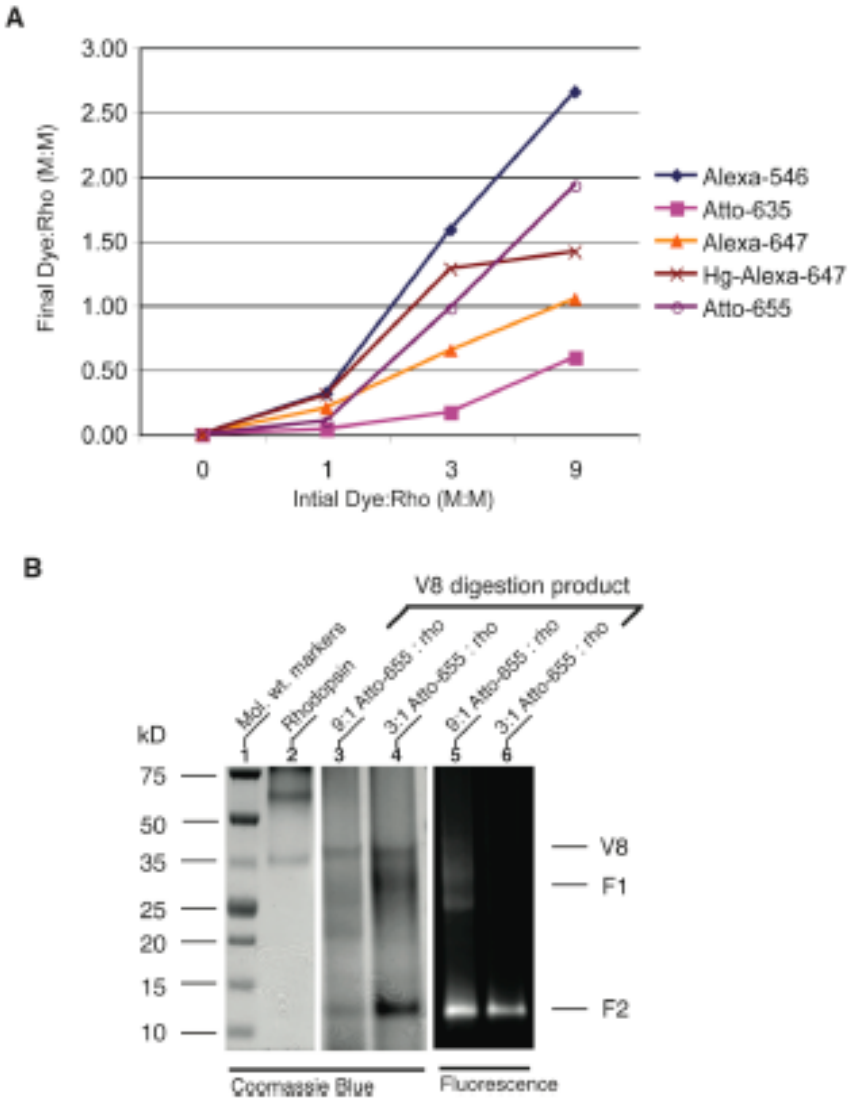
A
3.00
2.50
2.00
1.50
1.00
0.50
0.00
Final Dye:Rho (M:M)
0
1
3
9
Intial Dye:Rho (M:M)
Alexa-546
Atto-635
Alexa-647
Hg-Alexa-647
Atto-655
B
V8 digestion product
Mol. wt. markers
Rhodopsin
9:1 Atto-655 : rho
3:1 Atto-655 : rho
9:1 Atto-655 : rho
3:1 Atto-655 : rho
1
2
3
4
5
6
kD
75
50
35
25
20
15
10
V8
F1
F2
Coomassie Blue
Fluorescence

4.2 Results

4.2.1 Rhodopsin Labeling with Fluorophore Maleimides

The relation between molar excess of different dyes at the start of the rho labeling reaction and the final molar ratio of dye to rho is shown in **Fig. 4-1**. The fluorophores used exhibited differences in the optimal molar ratios required to achieve stoichiometric labeling of rho in ROS. When the dyes were used at equimolar ratios to rho, all of them resulted in sub-stoichiometric labeling of rho. Among the dyes tested, Alexa-546 led to the most efficient labeling of rho in terms of lowest dye excess required to achieve stoichiometric labeling (1:1 Dye:Rho). Atto-655 also exhibited efficient labeling of rho and appeared to be an ideal fluorophore in the long-wavelength region to label rhodopsin. Stoichiometric labeling was achieved with a 3-times molar excess of Atto-655 over rho, and two cysteines could be modified by doubling the initial dye excess (9-fold molar excess over rhodopsin) (**Fig. 4-1 A**).

Rhodopsin was labeled in ROS in order to enhance the reactivity difference between the two accessible cysteines– Cys 316 (more reactive) and Cys 140 (less reactive). We assumed that Cys 316 and Cys 140 would get sequentially modified by the maleimide dyes due to their reactivity difference. To

test this assumption, we carried out V8 protease digestion of labeled rhodopsin and analyzed the fragments for fluorescence using SDS-PAGE (**Fig. 4-1 B**). V8 protease cleaves rho mainly into 2 fragments with Cys 140 being part of the larger fragment F1 (~27 kD) and Cys 316 being a part of the smaller fragment F2 (~13 kD) (Farrens, Altenbach *et al.* 1996). As seen from the gel, the stoichiometric labeling condition for rho using Atto-655 (3:1 Atto-655:rho) predominantly modifies Cys 316.

4.2.2 Rhodopsin Labeling with Nanogold Maleimide

Nanogold® (Nanoprobes, NY) is a homogenous 1.4nm gold cluster that is designed for covalently labeling biomolecules under mild conditions and physiological buffers. The size of the gold cluster and number of gold atoms forming a cluster in the Nanogold reagent (~67 Au atoms) is between the smaller Undecagold (0.8nm, 11 Au atoms) and the larger collidal gold (10nm) reagents (Hainfeld and Powell 2000). This enables Nanogold to be visualized directly by transmission electron microscopy (TEM), while reducing the non-specific adsorption characteristics of larger, colloidal gold.

We were able to efficiently link monomaleimido nanogold to rhodopsin using methods developed for fluorophore maleimides. The main differences were a twofold higher rho concentration was used in the nanogold labeling reaction compared with fluorophores (Method 2.4), and the mixture was not shaken during incubation. After purification of rho, the labeling stoichiometry was determined

by comparing the twin absorbances of nanogold at 280nm (ε_{280}= 2.25 x 10^5 $M^{-1}cm^{-1}$) and 420nm (ε_{420}= 1.12 x 10^5 $M^{-1}cm^{-1}$) with the difference spectrum of rhodopsin. Using our labeling method, we obtained 0.8–0.9 nanogold per rho. We assumed that Cys 316 would have been modified at these labeling ratios, similar to fluorophore labeling experiments (Method 2.3). We reasoned that the larger size of the nanogold gold cluster, compared to a fluorophore molecule, may preclude its accessibility to the other Cys residues. The labeling ratio was further checked by negative stain electron microscopy using dilute NG-rho (nanogold labeled rho) samples and 1 NG-rho-NABB on the grid.

4.3 Discussion

The sulfhydryl groups of bovine rhodopsin have been reported to exhibit clearly different reactivity/accessibility upon treatment with SH reagents (De Grip and Daemen 1982). The differences depend on the following conditions-

1. Type of reagent used.
2. The microenvironment of rhodopsin.
3. Illumination condition of rhodopsin.

In this case, we chose to label rhodopsin by using only maleimide functionalized fluorophores. The fluorophores have different chemical structures which would affect the hydrophobicity of the probes as well as its size. Both these factors could control the accessibility of the probes to the cysteine residues on the cytoplasmic side. The microenvironment of rho in all cases was chosen to be the native ROS membranes. It is possible that the phospholipid headgroups of the ROS also play a part in modulating accessibility of the probes to Cys 140 which is closer to the lipid headgroups than Cys 316. Only very small, hydrophobic reagents like methylmercury iodide, used at 90-fold molar excess over rho can modify all cysteines in rhodopsin under similar conditions (Daemen, Van Breugel *et al.* 1976).

The stoichiometry profile of the maleimide probes to the cysteines in rho presented in this chapter is strictly dependent on the presence of a lipid bilayer.

When rhodopsin is solubilized in detergents, more cysteines were available for reaction with the probes (De Grip and Daemen 1982). The relative reactivity difference between Cys 140 and Cys 316 may be diminished due to the more disordered character of detergent micelles or detergent-induced changes in protein conformation. Interestingly, it has been reported that the reactivity difference between cysteines is maintained in digitonin, which forms rigid micelles where detergent-lipid exchanges are minimal (Hong and Hubbell 1973).

Since the labeling reactions are carried out on ROS, care should be taken to protect the cysteines from air oxidation, particularly since the ROS contains a large proportion of unsaturated membrane lipids. The ROS was therefore flushed with Argon to keep the sulfhydryl groups in a reduced state and remove traces of reactive oxygen species, and EDTA containing buffers were used to chelate traces of heavy metals. Maleimides start to react slowly with amino groups above pH 7, therefore the pH was kept between 6 – 7 using a buffer that is not temperature dependent (in this case, HEPES or sodium phosphate). Temperature and time of the reaction are very highly correlated in these reactions. Below 20°C, reaction rates with hydrophilic reagents decrease considerably and above 30°C, thermal stability of rhodopsin is not enough for long incubations.

5.0

Studies on Rhodopsin Monomers and Dimers Incorporated into NABBs

5.1 Introduction

G protein-coupled receptors (GPCRs) are excellent examples of allosteric proteins (Huber and Sakmar 2008). Knowledge about the functions of GPCRs and biological processes governing their regulation has been increasing at an accelerated rate. One of the aspects that can be reconciled with the allosteric nature of many GPCRs is their ability to form homo- and heterodimers and higher oligomers. For example, hetero-dimerization between two isoforms of the $GABA_B$ receptor has been shown to affect cell-surface localization (Margeta-Mitrovic, Jan *et al.* 2000). Co-immunoprecipitation techniques have been used in reports of receptor homodimerization in the case of metabotropic glutamate receptor (Romano, Yang *et al.* 1996) and β_2-adrenergic receptor (Hebert, Moffett

---

Material in this chapter has been previously published in: Banerjee S, Huber T, Sakmar TP. (2008) Rapid Incorporation of Functional Rhodopsin into Nanoscale Apolipoprotein Bound Bilayer (NABB) Particles. *J. Mol. Biol.* **377**(4): 1067-81.

et al. 1996) whereas cross-linking and bioluminescence resonance energy transfer (BRET) have been used in reports of oligomerization of dopamine D2 (Guo, Urizar *et al.* 2008). Most of the convincing reports of GPCR dimerization have dealt with family C GPCRs (section 1.1). Even in these cases, the functional consequences of a GPCR dimer towards G protein coupling, in a system free of accessory proteins, is not known.

For rhodopsin, a prototypical family A GPCR, a wide variety of assays have been applied by a number of research groups to determine whether rhodopsin exists as a monomer or a homo-dimer/ higher oligomers, similar to other known GPCRs in the native state (Fotiadis, Liang *et al.* 2003; Jastrzebska, Maeda *et al.* 2004; Chabre and le Maire 2005; Kota, Reeves *et al.* 2006). Attempts towards answering the question of whether rho dimerization is required for transducin signaling has not led to a consensus, primarily because it has not been possible to isolate rhodopsin monomers and dimers in a native-like well-defined environment that is free from interference of accessory proteins, yet tenable for biochemical assays. In this chapter, we describe the first demonstration of a novel single-particle electron microscopy imaging technique, coupled with ensemble biochemical assays, to probe G protein activation rates by rhodopsin monomers and dimers isolated in a nanoscale native-like membrane-mimetic systems, called NABBs (Chapter 3). We considered not only the oligomeric state, but also the relative orientation of two rhodopsins when they are incorporated in a NABB. We demonstrate that monomeric rhodopsin is sufficient for efficient activation of transducin, and infer the limits of G protein activity that

a putative physiological rhodopsin dimer may have. Defining the interaction of a G protein with the monomer or the oligomerization interface of a GPCR, in terms of catalytic center activity of the GPCR, could offer new pharmacological targets that modulate receptor dimerization without interfering with critical GPCR signaling pathways.

Figure 5-1. Gel-filtration Chromatography of Rho-NABBs

Gel-filtration chromatography of rhodopsin-NABBs made by Extracti-Gel D mediated detergent removal (Materials and Methods) using Alexa-488 labeled zap1Q26C, LRB-DOPE doped POPC and Atto-655 labeled rhodopsin on a Superose 6 10/30 column using an Akta Explorer 10 FPLC system. The incorporation ratio was approximately 0.1rho/NABB. Absorption at three wavelengths was recorded simultaneously: 280nm (protein absorbance), 570nm (LRB-DOPE absorbance) and 650nm (Atto 655 rho absorbance) indicating elution of total protein, lipid and rhodopsin from the column, respectively. (Top) Eluted fractions were analyzed by loading equal volumes on a NuPAGE 4-20% Bis-Tris gel run with SDS-MES running buffer. SDS-PAGE was followed by fluorescence detection using a Typhoon 9400 gel scanner.

Figure 5-1

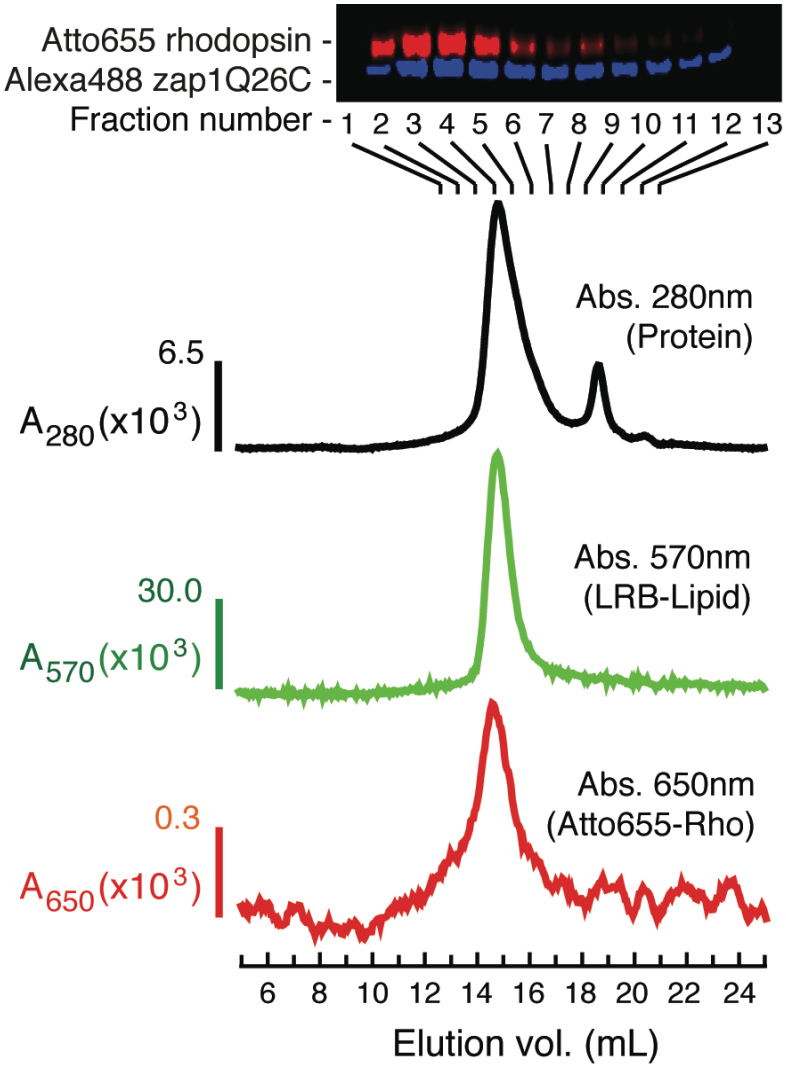
Atto655 rhodopsin -
Alexa488 zap1Q26C -
Fraction number - 1 2 3 4 5 6 7 8 9 10 11 12 13
Abs. 280nm
(Protein)
6.5
A280(x10^3)
Abs. 570nm
(LRB-Lipid)
30.0
A570(x10^3)
Abs. 650nm
(Atto655-Rho)
0.3
A650(x10^3)
6 8 10 12 14 16 18 20 22 24
Elution vol. (mL)

Table 2. Stoichiometry of Components for NABB Formation

Rho / NABB sample	Rho[a] (μM)	zap1[b] (μM)	POPC[c] (mM)	OG[d] (mM)	Cholate[e] (mM)
2 rho / NABB	80.0	80	3.3	51.0	34.8
1 rho / NABB	40.0	80	4.6	51.0	34.8
0.1 rho / NABB	4.0	80	5.8	51.0	34.8
0.01 rho / NABB	0.4	80	6.0	51.0	34.8
0 rho / NABB	0.0	80	6.0	51.0	34.8

(a) Rhodopsin was purified from bovine ROS using ConA-Sepharose affinity purification and stored as 400mM stock in 1.5% OG. **(b)** Zap1 (hexa-histidine tagged zebrafish apo A-I construct) was purified from *E. coli* using Ni-affinity and gel-filtration chromatography and stored as 0.6mM stock. **(c)** POPC was doped 1:100 with LRB-DOPE and stored as 13.1 mM stock in 1% sodium cholate. (**d, e**) OG and sodium cholate were stored as 10% (w/w) stocks in water. All components were stored at -80^{o}C and thawed on ice before mixing. The components were vortexed and incubated at room temperature for 30 min prior to detergent removal either dialysis or Extracti Gel D in buffer T (Materials and Methods).

Figure 5-2. Affinity Purification and Spectroscopic Characterization of Rho-NABBs

(A) Ni-NTA purification of a 1rho/NABB sample made with Atto-655 labeled rhodopsin and Alexa-488 labeled zap1Q26C. The sample was eluted with 10mM EDTA. **(B)** UV-visible spectra of Ni affinity purified rhodopsin-NABBs made with different starting stoichiometries of rhodopsin : zap1 with POPC stoichiometry adjusted accordingly (see **Table 2**). Zap1 is His tagged and the NABBs are purified by the Ni affinity purification. Spectra were normalized to unit absorbance at 280nm.

Figure 5-2

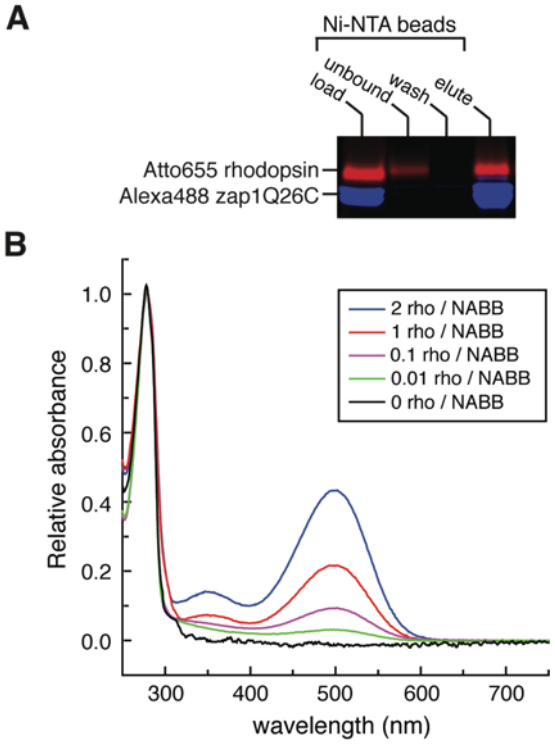
A
Ni-NTA beads
load
unbound
wash
elute
Atto655 rhodopsin
Alexa488 zap1Q26C
B
Relative absorbance
1.0
0.8
0.6
0.4
0.2
0.0
300
400
500
600
700
wavelength (nm)
2 rho / NABB
1 rho / NABB
0.1 rho / NABB
0.01 rho / NABB
0 rho / NABB

5.2 Results

5.2.1 Characterization of Rhodopsin Incorporation into NABBs

Dialysis (Method A) quantitatively removes detergents but can only be used efficiently for detergents with relatively high CMC values. We used a detergent removing gel, Extracti-Gel D (Pierce Biotechnology, Rockford, IL) to remove detergents with comparatively low CMC values and to accelerate the rate of NABB formation. The rate of detergent removal is expected to affect the pathway of discoidal self-assembly and the particle size distribution (Rigaud, Pitard *et al.* 1995). NABBs formed using Extracti-Gel D formed sharper gel-filtration profiles compared to detergent dialysis. **Fig. 5-1** shows gel-filtration of rho-NABB complexes made with Alexa-488 conjugated zap1Q26C, lissamine rhodamine B sulfonyl DOPE (LRB-DOPE)– doped POPC and Atto-655 labeled rhodopsin where the starting reconstitution stoichiometry was 1 rho per 10 NABBs. We used different starting molar ratios of rhodopsin to zap1 and POPC (NABB components) to form NABBs and subjected them to small-scale batch purifications using Ni affinity (**Fig. 5-2 A**). The unbound fraction contains rhodopsin in vesicles and/or aggregates. **Fig. 5-2 B** shows the UV-visible spectra of rho-NABBs made with different rhodopsin concentrations at a constant zap1

concentration after Ni affinity purification. The final A_{500}:A_{280} ratios are in good agreement with the initial stoichiometries of the reactions, indicating that rhodopsin incorporation in NABBs is efficient and controllable.

Figure 5-3. FRET between Multiple Rhodopsins in a NABB

(A) FRET emission profiles of Alexa-647 labeled rhodopsin in samples containing an equal mixture of Alexa-546 rho (R*d*) and Alexa-647 rho (R*a*), with decreasing rho/NABB ratios. In each NABB formation reaction, the rho concentration was constant and the relative proportion of POPC and apo A-I were increased. 10nM rho in NABBs was used in the cuvette for FRET measurements. The data are normalized to donor (Alexa-546) emission. **(B)** Ratio of Alexa-647 emission to Alexa-546 emission calculated from (A). The red bar corresponds to a 2 rho/NABB ratio and the blue bar to a 1 rho/NABB ratio. **(C)** FRET emission profiles of Alexa-647 labeled rho in samples containing similar amounts of lipids (POPC) as in (A) but with no apo A-I. **(D)** Ratio of Alexa-647 emission to Alexa-546 emission calculated from (C). The color of the bars correspond to the emission profile of the sample in (C).

Figure 5-3

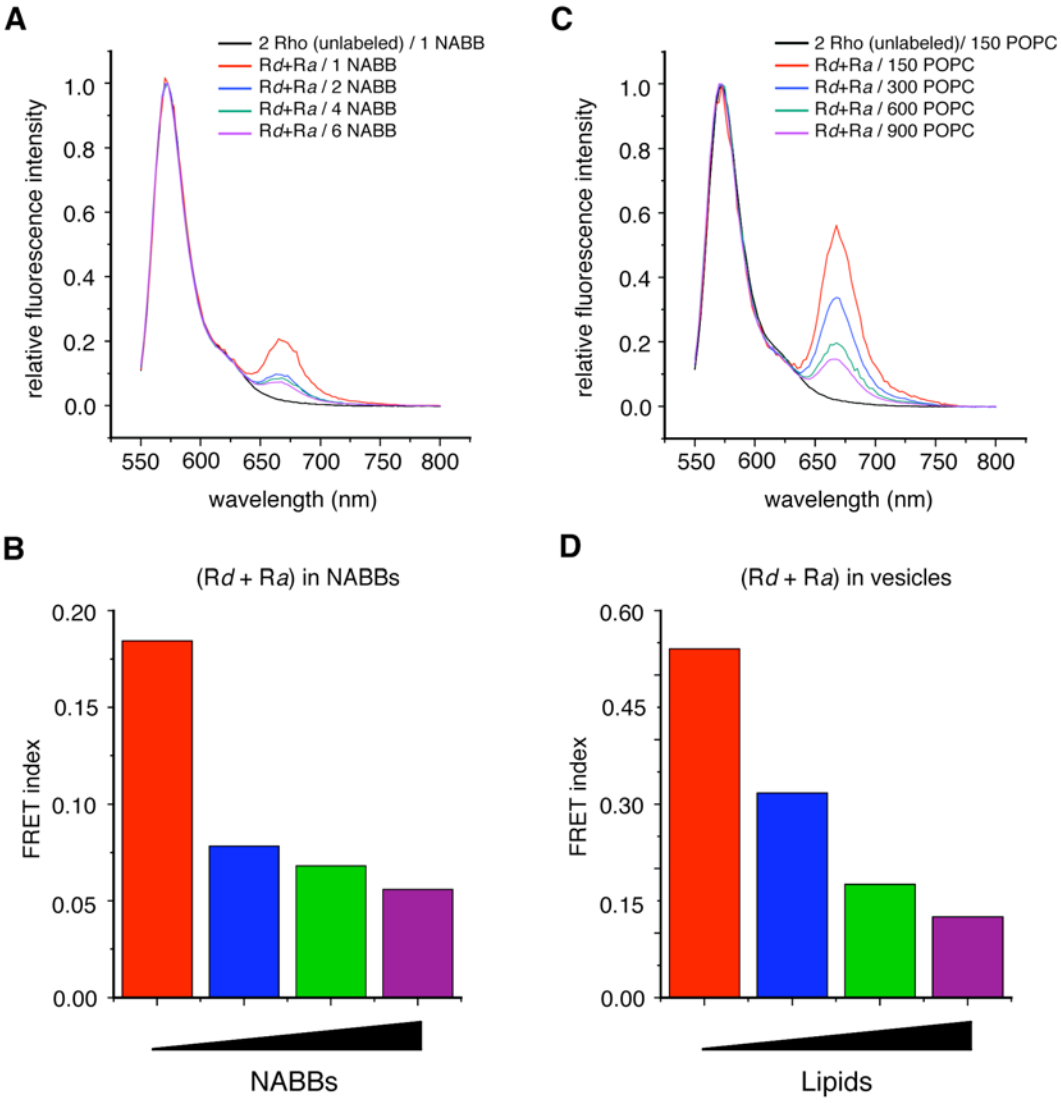
A
2 Rho (unlabeled) / 1 NABB
Rd+Ra / 1 NABB
Rd+Ra / 2 NABB
Rd+Ra / 4 NABB
Rd+Ra / 6 NABB
relative fluorescence intensity
1.0
0.8
0.6
0.4
0.2
0.0
550 600 650 700 750 800
wavelength (nm)
C
2 Rho (unlabeled)/ 150 POPC
Rd+Ra / 150 POPC
Rd+Ra / 300 POPC
Rd+Ra / 600 POPC
Rd+Ra / 900 POPC
relative fluorescence intensity
1.0
0.8
0.6
0.4
0.2
0.0
550 600 650 700 750 800
wavelength (nm)
B
(Rd + Ra) in NABBs
FRET index
0.20
0.15
0.10
0.05
0.00
NABBs
D
(Rd + Ra) in vesicles
FRET index
0.60
0.45
0.30
0.15
0.00
Lipids

5.2.2 FRET between Multiple Rhodopsins in a NABB

To determine whether rhodopsin forms constitutive dimers in a detergent solubilized form, we used increasing stoichiometry of NABB components (lipids + apo A-I) at a specific rho concentration in an attempt to form reactions where a 2 rho/NABB would be able to get 'diluted' out into 1 rho/NABB. We wanted to test whether the 2 rhodopsins stay in a single NABB when given the possibility of partitioning into separate NABBs. If rhodopsin had a strong, constitutive tendency to dimerize, it would not dissociate from the other rhodopsin in detergent, or when the detergent is removed to form NABBs. To test for rho dimerization, we carried out Fluorescence Resonance Energy Transfer (FRET) experiments between rho labeled with a donor fluorophore (Alexa-546) and rho labeled with an acceptor fluorophore (Alexa-647) mixed in equimolar ratio in the NABB formation reaction. Details about labeling and characterization of labeled rhodopsin are given in the preceding chapter. The Förster radius of the Alexa-546 – Alexa-647 pair has been reported to be 6.8nm (Molina, Barrera *et al.* 2006). If two rhodopsins with different labels were farther than 6.8nm apart from one another, a decrease in the emission signal of the acceptor fluorophore (therefore the FRET index) would be seen. The average diameter of a NABB is 10nm and since the rhodopsins were reconstituted into NABBs from a detergent-purified

state, a decrease in FRET index would also imply that the rhodopsins have been incorporated into distinct NABBs.

We observed a decrease in FRET between rhodopsins in reactions that contained increasing amounts of lipids and apo A-I compared to rho, as shown in **Fig. 5-3**. A sharp decrease in FRET was seen when the NABB stoichiometry is increased to accommodate 1 rho per NABB. Increasing the amount of unlabeled rhodopsin in the reaction, while keeping the relative ratio of lipids and apo A-I constant (corresponding to 2 rho/NABB) also showed a similar drop in FRET index.

The FRET data indicate that 2 rhodopsins do not constitutively dimerize when solubilized and purified in 1.5% octylglucoside containing buffer. When the ratio of lipids and apo A-I is increased such that the rhodopsins may either stay in the same NABB (maintain FRET) or distribute in separate NABBs (lose FRET), the rhodopsins tend to distribute into separate NABBs. A vesicle control was performed under similar rho and POPC concentrations but with no apo A-I added. The drop in FRET in vesicles is seen due to rhodopsin dispersion due to increasing lipid:rho ratio. Notably, the FRET values in vesicles are much higher than in NABBs, even though the same rho concentration was used in the cuvette in both experiments. The higher values are likely to be because of rhodopsin aggregates in vesicles where one donor may transfer energy to more than one acceptor in its vicinity. Since the Förster radius of the fluorophore pair (6.8nm) is larger than the thickness of a typical phospholipids bilayer (5nm), we expect efficient energy transfer to occur even if the 2 rhodopsins are incorporated anti-

parallel to one another, both in NABBs and in vesicles. Using the Alexa-546 – Alexa-647 fluorophore pair and ensemble FRET measurements, we were able to determine proximity of the rhodopsins within 6.8nm but not the ‘sidedness’ of incorporation of the rhodopsins.

Figure 5-4. Electron Microscopy of Rho-NABBs

(A) (Top) Nanogold-labeled rhodopsin in 2 rho-NABB samples imaged under negative stain in 0.5% uranyl acetate (UA). (Bottom) Histogram of number of nanogolds per NABB in 816 NABB particles chosen for analysis. 2 nanogold labels were visible in about 70% of the particles. **(B)** Single particles of 2 or 1 nanogold labeled rhodopsin-NABBs (NG-rho-NABBs) selected from nanogold labeled 2rho-NABB and 1rho-NABB EM images. Nanogold densities in the NABB are indicated with arrows. Outer edge of each box is 20nm in scale. **(C)** (Top) Gel-filtration of 2Fab-rho-NABB complexes on a Superose 6 10/30 column. The peak of 2rho-NABB is shown for comparison. (Bottom) Electron micrograph of 2Fab-rho-NABB shown under negative stain conditions using 1% UA. **(D)** Representative set of single particles obtained by epitope mapping of rhodopsin in NABBs using Fab. (Top) Single particles of 2Fab-rho-NABB grouped into anti-parallel and parallel orientation of rhodopsins in a NABB. A central 'hole' is clearly visible in the Fab fragments consistent with electron micrographs of Fab particles (Boisset, Radermacher *et al.* 1993). Orientation of Fab particles with respect to the central NABB density is depicted in a cartoon representation below each particle. Outer edge of each box is 30nm in length. (Bottom) Relative proportion of anti-parallel and parallel rhodopsins in 2Fab-rho-NABB samples determined by visual classification of Fab density with respect to NABB density from single particles of 2Fab-rho-NABB. Cartoon representations of the orientations of the particles on the grid considered for the analysis are shown on the *y*-axis. Representation **a** depicts anti-parallel rhodopsins in NABBs that are observed with the label on rhodopsin in a staggered or perpendicular position to the NABB density. Representation **b** depicts 2 rhodopsins in a parallel orientation.

Figure 5-4

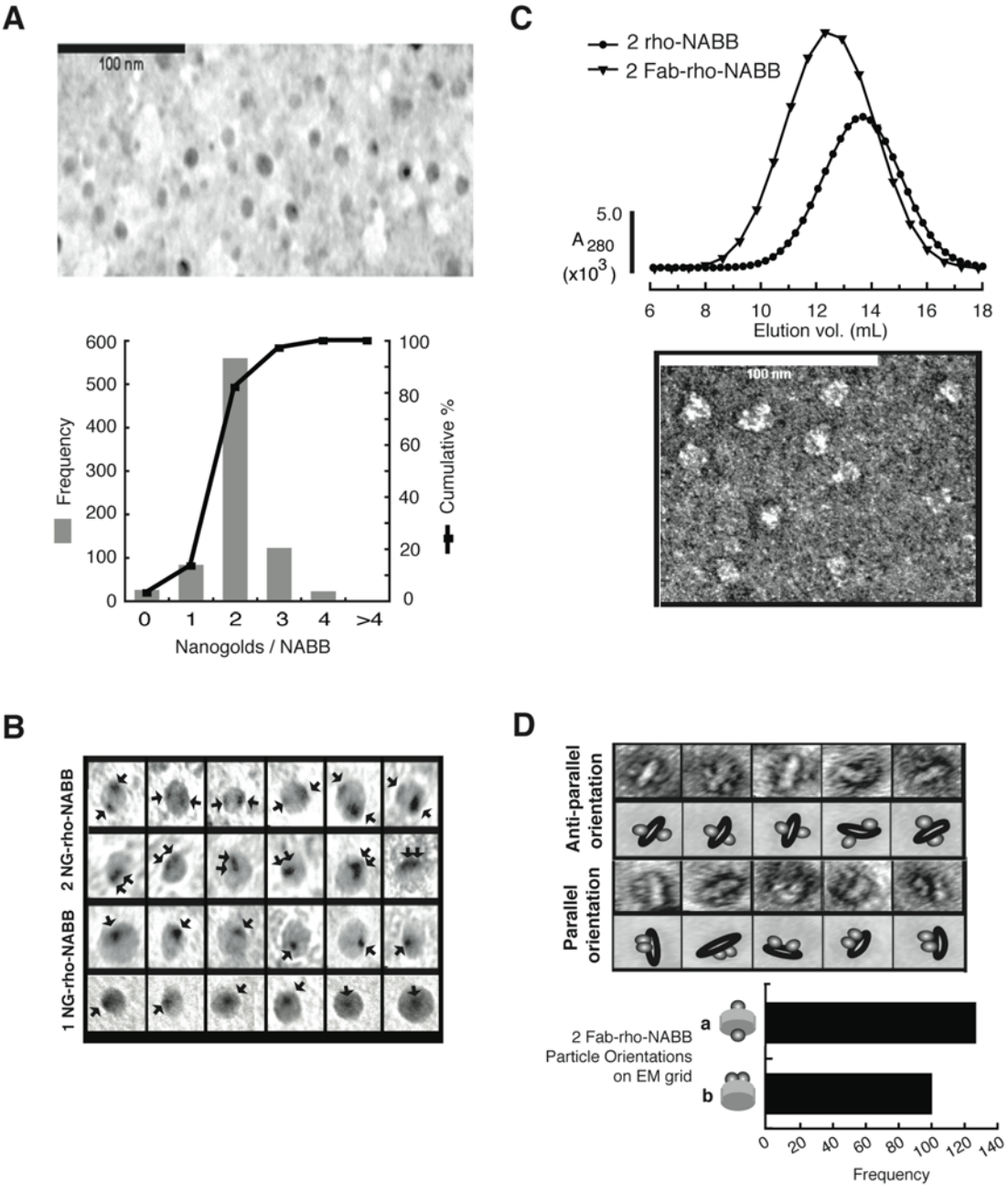
A
100 nm
Frequency
Cumulative %
Nanogolds / NABB
0
1
2
3
4
>4
B
2 NG-rho-NABB
1 NG-rho-NABB
C
2 rho-NABB
2 Fab-rho-NABB
5.0
A280
(x10^3)
Elution vol. (mL)
100 nm
D
Anti-parallel orientation
Parallel orientation
2 Fab-rho-NABB
Particle Orientations
on EM grid
a
b
Frequency

5.2.3 Determination of Orientation of Multiple Rhodopsins in a NABB

In order to visualize the incorporated rhodopsins in NABBs, rhodopsin-specific labels with no cross-reactivity with the lipid or apolipoprotein in the NABB were used. Rhodopsin was labeled site-specifically with nanogold and imaged by negative stain EM at very dilute rho-NABB concentrations (**Fig. 5-4 A** upper panel). The defocus used to image nanogold was typically less than the defocus used to visualize proteins (Hainfeld, Powell *et al.* 2002). At optimum underfocus values, the nanogold densities are clearly visible as high-density structures together with NABBs that appear as low-density structures over the background. Single particles were selected from individual micrographs using a semi-automatic selection ('boxing') procedure using the 'Boxer' software, part of the EMAN 1.7 suite of applications (Lüdtke, Baldwin *et al.* 1999). The nanogold labeled rho-NABBs were tenable to statistical analysis by counting the number of nanogolds per NABB. As shown in **Fig. 5-4 A** lower panel, more than 80% of the selected particles had at least two rhodopsins and approximately 70% of particles contained exactly two rhodopsins. 2 rho-NABBs and 1rho-NABBs can be clearly identified by the nanogold density (shown by arrows, **Fig. 5-4 B**) in the representative images. Thus, EM images may be used as further proof of stoichiometry of rhodopsin incorporation into NABBs.

In order to determine orientation of multiply incorporated rhodopsins, we chose to image rho-NABBs as a macromolecular assembly with anti-rhodopsin Fab fragments bound to the C-terminus of rhodopsin in NABBs. We confirmed

the formation of a stable 2Fab-rho-NABB complex by FPLC (**Fig. 5-4 C** upper panel). The EM image of the macromolecular complex with 1% UA staining is shown in **Fig. 5-4 C** lower panel. We propose that the NABBs are an effective tool to image complexes of transmembrane receptors with associated signaling molecules.

We analyzed Fab labeled rho-NABBs to ascertain the relative orientation of two rhodopsins in a single NABB. In the case of Fab labeled particles, only those particles were analyzed which have the NABB density approximately perpendicular to the plane of the grid in order to be able to be able to discern the Fab density which would be perpendicular to the characteristic NABB 'discoidal' density. The set of selected particles were subjected to visual inspection and classified into either anti-parallel or parallel from the relative orientation of nanogold or Fab density with respect to the central lipoprotein density. We analyzed single particles picked from high defocus (≈ –3μm) images of 2Fab-rho-NABB particles to classify the orientation of the C-termini of the two incorporated rhodopsins with respect to each other. For clarity, we chose only those particles where the zap1 belt was oriented perpendicular to the plane of the grid as these particles were the ones where the Fab positions could be detected unambiguously with respect to the belt (**Fig. 5-4 C** lower panel). Analysis of single particle images from Fab labeled 2rho-NABBs show that approximately half of all the NABBs containing two rhodopsins contained the rhodopsins in an antiparallel orientation with respect to each other (**Fig. 5-4 D**).

Figure 5-5. Thermal Stability of Rho-NABBs

Rho-NABB samples were made by detergent removal using Extracti-Gel D (Method 2.15). The samples were Ni affinity purified before analysis. Thermal stability of rhodopsin in various environments as indicated determined by UV-vis difference photobleaching spectroscopy. Each data point represents the average of three independent experiments. Note that rhodopsin reconstituted in NABBs has similar stability as in native ROS.

Figure 5-5

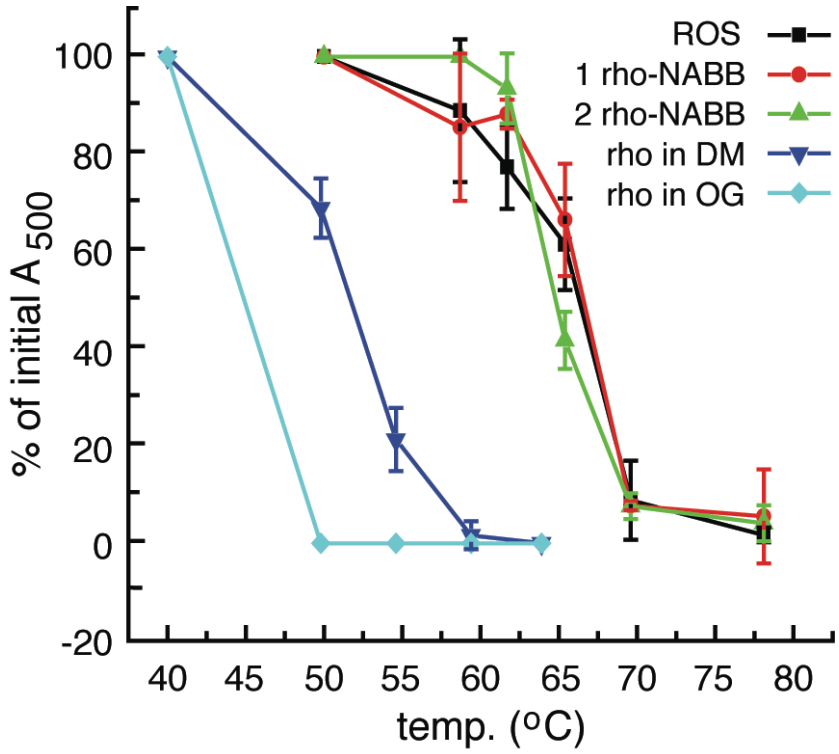
ROS
1 rho-NABB
2 rho-NABB
rho in DM
rho in OG
% of initial A 500
100
80
60
40
20
0
-20
40
45
50
55
60
65
70
75
80
temp. (°C)

5.2.4 Thermal Stability of Rho in NABBs

We compared thermal denaturation of rhodopsin in NABBs with rhodopsin in ROS and detergents commonly used for rhodopsin biochemistry. Thermal denaturation of rhodopsin occurs at a higher threshold temperature when it is in rod disc membranes compared with detergent (Hubbard 1958; Knudsen and Hubbell 1978). We observed that the denaturation temperature of rhodopsin in NABBs is similar to rhodopsin in ROS (**Fig. 5-5**). The data indicate that increasing the hydrophobic chain lengths of detergents (OG to DM), and substituting the non-ionic head group (OG or DM) by the zwitterionic head group of phospholipids (in NABBs or ROS membranes) both lead to substantial increase in thermal stability. There seems to be a slight decrease in the denaturation temperature when two rhodopsins inhabit a NABB compared to a single rhodopsin per NABB and this decrease may reflect the difference in the number of POPC molecules surrounding the rhodopsins and/or packing defects of the lipids in the reduced space between rho and apo A-I. The stoichiometry at the start of the self-assembly of the two rho per NABB particle has only 42 lipids surrounding each rhodopsin (21 per leaf of the bilayer). While this number of lipids may be comparable to the number of lipids surrounding rhodopsin in ROS (Miljanich and Dratz 1982), it is only 35% of the 116 lipids surrounding rhodopsin in a one rho/NABB case. The remarkable thermal stability of

rhodopsin(s) in a NABB indicate that a minimal amount of lipids surrounding rhodopsin is sufficient to preserve its conformational state and thermal stability may not depend upon long range lipid interactions.

Figure 5-6. Meta-II Decay and Opsin Regeneration

(A) Meta-II decay kinetics of one or two rhodopsins in NABBs probed by Trp fluorescence increase as a function of time after bleaching. Excitation wavelength 295nm, emission wavelength 330nm, integration time 2 s. Data were fit to a pseudo first-order kinetics to determine the half-life times of Meta-II decay. Values are averages of three independent experiments. **(B)** Regeneration of opsin in NABBs (1 opsin per NABB) probed by absorbance spectroscopy at 520nm. Absorbance was recorded in 3 s intervals with an integration time of 1 s. Opsin formed by photobleaching a 1rho-NABB sample (Method 2.21) was regenerated by stoichiometric amount of 11-*cis*-retinal dissolved in empty NABBs (red curve). Addition of 11-*cis*-retinal to empty NABBs is also shown (black curve). The regenerated rhodopsin in NABBs was stable to treatment with hydroxylamine and could be photobleached.

Figure 5-6

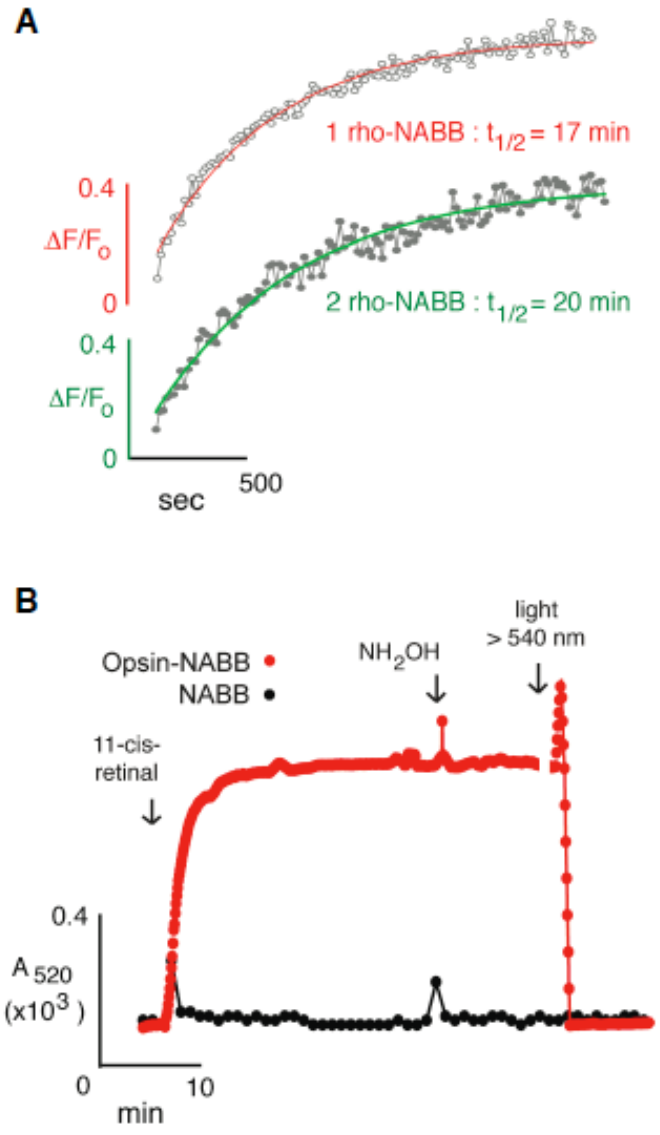
A
1 rho-NABB : t1/2 = 17 min
2 rho-NABB : t1/2 = 20 min
0.4
ΔF/Fo
0
0.4
ΔF/Fo
0
sec
500
B
Opsin-NABB
NABB
11-cis-
retinal
NH2OH
light
> 540 nm
0.4
A520
(x10^3)
0
10
min

5.2.5 Meta-II Decay and Regeneration of Opsin in NABBs

Meta-II decay of rhodopsin was followed by monitoring the change in Trp fluorescence to determine the Meta-II decay kinetics of rhodopsin(s) incorporated in a NABB. We found that the Meta-II intermediate in one rho-NABBs has a half-life of 17 min and Meta-II in two rho-NABBs has a slightly longer half-life of 20 min (**Fig. 5-6 A**). These values correlate with our data showing differences in the fraction of deprotonated Schiff base formed upon actinic light exposure and are in good agreement with previous reports of rhodopsin Meta-II decay assays (Heck, Schädel *et al.* 2003; Jastrzebska, Maeda *et al.* 2004).

Opsin-NABB formed after Meta-II decay of rhodopsin was able to regenerate rapidly and quantitatively in the presence of stoichiometric amounts of 11-*cis*-retinal (**Fig. 5-6 B**). Absorbance at 520nm was not affected by the absorption peak of free retinal (378nm) or nonspecific Schiff base formation. The rapid regeneration of opsin in NABBs compared with opsin in DM is probably a result of the dramatic difference in the partial volume fraction of the lipidic environment. A recovery of the characteristic difference spectra and lack of hydroxylamine sensitivity under conditions minimizing photobleaching implies that the added 11-*cis*-retinal forms a specific, protonated Schiff base linkage at Lys-296 of opsin to form regenerated rhodopsin. Photobleaching the sample in the presence of hydroxylamine greatly accelerates the decay of Meta-II. In the

presence of the deprotonated Schiff base form of retinal, hydroxylamine leads to the formation of a stable retinal oxime, a phenomenon that efficiently sequesters the chromophore out of the opsin.

Figure 5-7. Transducin Activation by One and Two Rho-NABBs

The rho-NABB samples were 1D4 affinity purified to remove 'empty' NABBs from interfering in the assay. Transducin activation by one and two rhodopsins per NABB probed by Trp fluorescence. 10nM rhodopsin(s) in NABB were photobleached in the presence of 100nM holotransducin and non-hydrolysable GTP analog (GTP-γS). Fluorescence change of transducin due to 1rho-NABB (red curve) and 2rho-NABB (blue curve) and empty NABB (black trace) is shown. The rates are averages of three independent experiments.

Figure 5-7

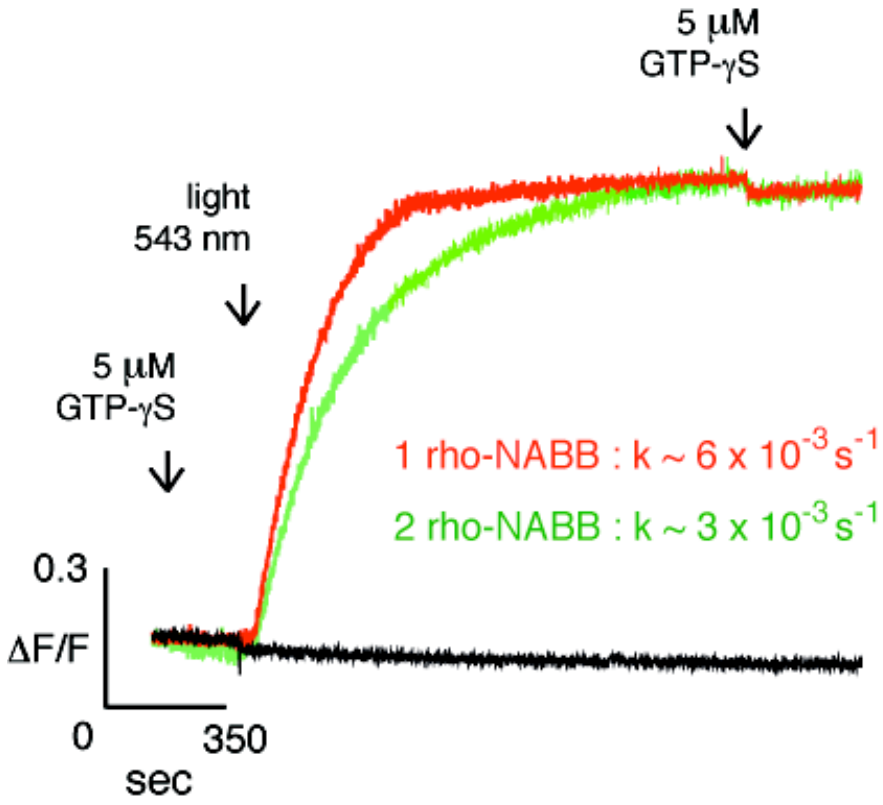
5 μM
GTP-γS
light
543 nm
5 μM
GTP-γS
1 rho-NABB : k ~ 6 x 10-3 s-1
2 rho-NABB : k ~ 3 x 10-3 s-1
0.3
ΔF/F
0
350
sec

5.2.6 G protein Activation by Rhodopsin Monomers and Dimers

We measured the rates of transducin activation by rho-NABBs containing predominantly either one or two rhodopsins per particle (**Fig. 5-7**). The data were fit to an exponential of the form:

$$y = a_1 - a_2 e^{-kx}$$

with rate constant *k*. 1rho-NABB gave an apparent pseudo first-order rate constant ($k_{obs}^{(1)}$) of 6×10^{-3} s^{-1} and the 2rho-NABB sample gave a value ($k_{obs}^{(1)}$) of 3×10^{-3} s^{-1}. Since both samples contain the same rhodopsin concentration, the number of catalytic centers for transducin activation is the same in the monomers and dimers. If the dimers are a mixture of *N* different equally probable species and only one of them is active, then the activity of this species is *N*-times the activity of the monomer. The maximum activity of the parallel (physiologically relevant) rho dimer may thus be calculated by assuming that only the parallel dimer is responsible for the observed transducin activity. As suggested by EM imaging, *N* equals two, and considering only the parallel dimer to be active, the catalytic center activity (Segel 1993) of the dimer is same as that of the monomer. Consequently, the dimer is equally efficient in activating transducin compared with the monomer.

The statements above may be rationalized further by comparison of transducin activation by rhodopsin in monomer and dimer form assuming it to be

an enzyme-catalyzed reaction between rho (enzyme) and transducin (substrate). Catalytic efficiencies of two enzymes may be compared by the ratio k_{cat}/K_m for the two enzymatic reactions. This ratio is also called the specificity constant and it is an apparent second-order rate constant with the units $M^{-1}s^{-1}$ (Nelson and Cox 2004). The Turnover Number (k_{cat}) may be specified as Molecular Activity or Catalytic Center Activity, depending on the definition of enzyme concentration (Segel 1993). *Molecular Activity* is defined as the number of moles of substrate transformed per minute per mole of enzyme. *Catalytic Center Activity* is defined as the number of moles of substrate transformed per minute per mole of active subunit or catalytic center. In the following derivations, we adopt the Catalytic Center Activity convention, since it has been hypothesized that a rho dimer interacts with a single transducin (Filipek 2005). The observed pseudo first-order rates of transducin activation are the products of k_{cat}/K_m and the rhodopsin concentration.

The observed rate of transducin activation by the rhodopsin monomer and dimer may be considered proportional to the concentration of rhodopsin in the samples according to the following mathematical relations:

$$k_{obs}^{(1)} = \sum_{i=1}^{N} k_i^{(2)} c_i \qquad (1)$$

$$c_0 = \sum_{i=1}^{N} c_i = c_0 \sum_{i=1}^{N} p_i \qquad (2)$$

where,

$k_{obs}^{(1)}$ is the observed pseudo-first order rate constant of rho-NABBs for transducin activation,

$k_i^{(2)}$ is the second-order rate constant of i^{th} species of rho-NABBs for transducin activation,

c_i is the concentration of rhodopsin in the i^{th} species of rho-NABB,

c_0 is the total concentration of rhodopsin in rho-NABB,

p_i is the probability of occurrence of the i^{th} species in a rho-NABB sample, and

N is the total number of species possible in each rho-NABB sample.

Consider two different cases of distribution of rhodopsin in rho-NABBs:

Case 1: N species are equally probable and all N species are equally active (homogeneous case).

$$p_i = 1/N$$

$$k^{(2)} = k_1^{(2)} = k_2^{(2)} = \ldots = k_N^{(2)} > 0$$

$$k_{obs}^{(1)} = c_0 \sum_{i=1}^{N} p_i k_i^{(2)}$$

$$k_{obs}^{(1)} = c_0 N \frac{1}{N} k^{(2)}$$

$$k^{(2)} = \frac{k_{obs}^{(1)}}{c_0} \qquad (3)$$

For rho monomer in 1rho-NABB (*mon*), only 1 species exists, thus *N*=1 (Case 1)

$$k_{mon}^{(2)} = \frac{k_{obs,mon}^{(1)}}{c_{mon}} \qquad (4)$$

From our experimental observations:

The same rhodopsin concentration is present in the dimer (*dim*) and monomer (*mon*) samples:

$$c_{\dim} = c_{mon}$$

Transducin activation rate of rho dimer is half of that of the monomer:

$$k_{obs,\dim}^{(1)} = \frac{1}{2} k_{obs,mon}^{(1)}$$

For rho dimer in 2rho-NABB, two species exist, thus

$$N = 2$$

Assuming both species in the dimer are equally active, from Eqn. (3) and (4) we get:

$$k_{\dim}^{(2)} = \frac{k_{obs,\dim}^{(1)}}{c_{\dim}}$$

$$k_{\dim}^{(2)} = \frac{\frac{1}{2} k_{obs,mon}^{(1)}}{c_{mon}} \qquad (\textit{from exp. observations a and b})$$

$$k_{\dim}^{(2)} = \frac{1}{2} k_{mon}^{(2)} \qquad (5)$$

Thus in this case, the dimer is half as active as the monomer.

Case 2: *N* species are equally probable and only one out of the *N* species is active.

$$p_i = 1/N$$

$$k_1^{(2)} > 0$$

$$k_i^{(2)} = 0 \text{ for } i > 1$$

$$k_{obs}^{(1)} = c_0 \sum_{i=1}^{N} p_i k_i^{(2)}$$

$$k_{obs}^{(1)} = c_0 \frac{1}{N} k_1^{(2)}$$

$$k_1^{(2)} = N \frac{k_{obs}^{(1)}}{c_0} \qquad (6)$$

Assuming only the parallel (physiological) dimer is active (Case 2), we get:

$$k_{\text{dim}}^{(2)} = N \frac{k_{obs,\text{dim}}^{(1)}}{c_{\text{dim}}}$$

$$k_{\text{dim}}^{(2)} = 2 \frac{k_{obs,\text{dim}}^{(1)}}{c_{\text{dim}}} \qquad (\textit{from exp. observation c})$$

$$k_{\text{dim}}^{(2)} = 2\left(\frac{\frac{1}{2} k_{obs,mon}^{(1)}}{c_{mon}} \right) \qquad (\textit{from exp. observations a and b})$$

$$k_{\text{dim}}^{(2)} = k_{mon}^{(2)} \qquad (7)$$

Thus in this case, the active dimer has the same activity as the monomer.

The rationale for using *N* may be generalized further. It has been reported that a rhodopsin molecule may have three oligomerization interfaces and only one of them form the 'true' rhodopsin dimer physiologically (Liang, Fotiadis *et al.* 2003; Suda, Filipek *et al.* 2004). Each oligomerization interface will lead to a distinct dimer where one rhodopsin may be considered to be rotated in-plane with respect to the other (see **Fig. 1-4**). These dimers may or may not be active towards transducin. To arrive at the maximum activity of the 'true' dimer, we assume that only the 'true' parallel dimer is active in a population of anti-parallel and parallel (N=2) and three sub-populations of parallel dimers (N=6). The 'true' dimer will then have 3-times the catalytic center activity of the monomer. If any of the subpopulations are active towards transducin, then the 'true' dimer will have a correspondingly lower activity, until all the subpopulations have equal activity and the activity of the dimer becomes equal to the monomer.

In conclusion, we propose that the rhodopsin dimer in a lipid environment does not have dramatically higher activity compared with rhodopsin monomer as reported in detergents (Jastrzebska, Fotiadis *et al.* 2006). Earlier experiments performed in detergents which reported long-range rhodopsin oligomerization and markedly higher activity toward transducin by these oligomers (Jastrzebska, Fotiadis *et al.* 2006) are difficult to interpret since the detergent concentration effects may explain some, if not all, observations (Ernst, Gramse *et al.* 2007). Our experiments in NABBs do not suffer from this detergent concentration artifact

and hence we can propose the upper and lower limits of the G protein activity of the putative (physiologically relevant) rhodopsin dimer.

5.3 Discussion

5.3.1 Characterization of Rhodopsin-NABBs

We have demonstrated a method of rapidly incorporating the prototypical 7-TM GPCR rhodopsin from a detergent purified state into a soluble, controllable, nanoscale lipid bilayer at high efficiency using apolipoprotein A-I, which we cloned from zebrafish. We have discussed a strategy for high-yield heterologous expression, purification and site-specific labeling of zebrafish apo A-I (zap1, zap1Q26C). Zap1 has favorable thermodynamics of interaction with POPC and proceeds to interact with POPC via an increase in its α-helical character (Chapter 3). A discoidal Nanoscale Apolipoprotein Bound Bilayer (NABB) is formed by a self-assembly process between lipids and zap1 triggered by detergent removal. Integral or peripheral membrane proteins present in the detergent mixture at a certain concentration become incorporated into the NABB.

The enhancement of thermal stability of rhodopsin upon incorporation into NABBs is particularly striking. Many GPCRs show time-dependent loss of activity in detergents (Navratilova, Sodroski *et al.* 2005). Using our method of rapid incorporation into the phospholipid matrix of NABBs, long-term exposure to detergents may be avoided, thereby extending the resilience of the reconstituted

GPCR for *in vitro* studies. Thermal stability of rhodopsin is likely to be enhanced by shielding of the transmembrane hydrophobic area from water and satisfying specific chemical interactions with phospholipids on the protein surface. Local coupling of phospholipids to rhodopsin (Huber, Botelho *et al.* 2004; Soubias, Teague *et al.* 2006) results in long-range curvature elastic deformations in a bilayer membrane (Brown 1994), which influences the conformational energetics of the Meta-I/Meta-II transition and rhodopsin oligomerization (Botelho, Huber *et al.* 2006; Periole, Huber *et al.* 2007). Furthermore, we have demonstrated that the NABBs may be utilized for isolating either one or two receptors in absence of excess empty NABBs—a phenomenon that is not possible to achieve in detergent micelles.

5.3.2 Single-Particle Analysis of EM Images

The negative staining technique in electron microscopy has the advantage that the particles appear with high contrast, which enables a clear visualization of Fab fragments on the edge of discoidal NABB structures. However, this technique suffers from some shortcomings. A certain amount of flattening of the particles is usually observed in negatively stained, air-dried samples. The extent of flattening is lower in regions of higher concentration of the negative stain (Boisset, Radermacher *et al.* 1993). Air drying and stain properties may cause aggregates of the molecules on the grid and exaggeration of the particle sizes, which limits the number of well-separated particles that can be obtained from a micrograph for

analysis. While a visual classification was possible, the lipoprotein particles had sufficient heterogeneity in shape to be intractable to more rigorous statistical analyses. In the technique of cryo-EM, the molecules are entrapped in their native orientation in a layer of vitreous ice. The densities measured in cryo-EM reflect the projections of the biological material without any staining agent around the particle. However, while using charged lipoproteins like NABBs made with POPC as the lipid, the strong electron density of the lipid headgroups overwhelms the densities of proteins that are not sufficiently separated from the lipid bilayer. Cryo-negative staining may be an emerging technical improvement for imaging lipoprotein particles. Embedding the sample in vitreous ice after negative staining could reverse the strong electron density of the lipid headgroups under cryo-EM conditions, and allow acquisition of medium to high-resolution structural data of membrane proteins incorporated in these discoidal lipoprotein particles.

An important unanswered question from previous work on putative rho dimers was the relative orientation of the two rhodopsins incorporated in a discoidal lipoprotein. Ensemble fluorescence based proximity methods (like FRET) could not be used since the properties of most commercially available fluorophores do not allow a clear resolution between parallel and anti-parallel dimers in a mixed population. We chose to undertake EM imaging followed by single-particle selection from the micrographs. We experimented with two complementary labeling techniques of rhodopsin which would enable us to measure the stoichiometry of rho incorporation and the position of the C-termini of rho when 2 rho were incorporated into a NABB. We chose previously

characterized NABB densities in EM images to select particles for our analyses. Our EM observations indicate that in approximately one-half of the NABBs with two rhodopsins, the rhodopsins are oriented anti-parallel to each other. This ratio was independent of whether the samples were prepared by dialysis or over Extracti Gel D columns, indicating that the process of 'rhodopsin scrambling' does not depend on the rate of detergent removal. The anti-parallel orientation in the 2Fab-rho-NABB (**Fig. 5-4**) had a profound impact when we attempted to determine the structure of the complex using the 'common lines' algorithm of single-particle averaging (Lüdtke, Baldwin *et al.* 1999), as seen in Appendix Fig A. The barrel shape of the complex is due to the influence of Fab density above and below the plane of the NABB. Averaging the Fourier Transform of the image class averages by imposing a C_6 symmetry axis perpendicular to the plane of the NABB gives rise to a heavy 'smear' of density on both sides of the NABB.

5.3.3 Insights into G protein Activity of a Putative Rhodopsin Dimer Compared to a Monomer

Dimerization of family A GPCRs, particularly rhodopsin, is still a matter of intense debate (Chabre, Cone *et al.* 2003; Fotiadis, Liang *et al.* 2003; Jastrzebska, Maeda *et al.* 2004; Ernst, Gramse *et al.* 2007). A key question in the field is whether the rhodopsin monomer or putative dimer is the signaling unit for G protein activation. Model systems used to address this question are receptors in

detergent micelles, proteoliposomes, and recently, apo A-I stabilized phospholipid bilayer particles. Using detergent micelles, it has been claimed that dimeric rhodopsins have higher Gt activation rates than monomers (Jastrzebska, Maeda *et al.* 2004; Jastrzebska, Fotiadis *et al.* 2006). However, others have pointed out that the method is inappropriate to support the conclusions (Chabre and le Maire 2005; Ernst, Gramse *et al.* 2007). Work with rhodopsin in proteoliposomes has shown that dispersed rhodopsin is more active (Botelho, Huber *et al.* 2006). In line with this observation, Whorton *et al.* showed, using β_2-adrenergic receptor (β_2-AR) reconstituted into HDL particles, that monomeric receptor is sufficient to activate G protein (Whorton, Bokoch *et al.* 2007). However, their work cannot exclude the possibility that receptor dimers may have substantially higher activity than monomers. Using a similar approach, Bayburt *et al.* have used one and two rhodopsins in Nanodiscs, and have concluded that dimerization is not necessary for efficient coupling of rhodopsin to transducin (Bayburt, Leitz *et al.* 2007). However, this conclusion is based on the assumption that two rhodopsins per Nanodisc form a physiologically relevant, parallel dimer. Here we show, using NABBs, that such structures formed with two rhodopsins contain a mixture of parallel and anti-parallel dimers.

Together with the Gt activation results, and assuming that the parallel dimer is inactive, it follows that the active dimer has the same catalytic center activity as the monomer. As proposed in the rhodopsin “rows of dimers” model (Liang, Fotiadis *et al.* 2003), a rhodopsin molecule may have three oligomerization interfaces. If the parallel dimer consists of subpopulations of

dimers using these dimerization interfaces then only a fraction (1/3) will contain the postulated 'true' dimer. Consequently, the catalytic center activity of this structure could be at most (assuming all other subpopulations to be inactive) 3-times the activity of the monomer.

In a GPCR like rhodopsin which does not constitutively dimerize in detergent, an accurate estimation of G protein activation rates due to the physiological dimer can only occur when the correct dimeric interface between the 2 rho in a NABB can be detected (for example, by using high-resolution EM techniques). Our method presented here cannot conclusively determine the rate of the putative physiologically relevant rho dimer. We proceeded by assuming that the aforementioned dimer is a part of the mixture of rho configurations that we detect using electron microscopy. Thus, we provide a conceptual model for the possible limits of G protein activity of a GPCR dimer in a NABB compared with a monomer.

5.3.4 Rho Dimerization is an Assay Dependent Phenomenon

We have offered proof in this chapter that rhodopsin does not form constituitive dimers when reconstituted into NABBs from a detergent solubilized, purified state. Our EM studies also show that any detergent-based *in-vitro* dimer or oligomerization based functional assays must take into account the relative orientation of the GPCRs, in order to be meaningful.

What is the cause of the underlying artifacts associated with detergent solubilized membrane proteins, specifically regarding their tendency to adopt an anti-parallel orientation? One explanation takes the topological asymmetry of biological membranes, and its subsequent disruption, into account. The asymmetry of native membranes of membrane proteins is manifested by differential distribution of phospholipids between the two leaflets of the bilayer. The lipid arrangement provides the membrane proteins not only with maximum interaction forces with phospholipids but also with additional stability of their quarternary structure (Klingenberg 1981). After detergent solubilization, the asymmetric environment of the membrane is lost, as the detergent forms a micelle around the membrane protein. The uniform detergent may not allow a differential binding of molecules to different parts of the protein. The absence of this differentiation may cause instability of detergent-solubilized proteins, forcing them to form an anti-parallel (non-physiological) orientation to satisfy the hydrophobic interactions in their structure. A similar argument of satisfying hydrophobic interactions between two rho monomers may be used to explain why two rhodopsins incorporated in a NABB adopt an anti-parallel arrangement. If the extent of hydrophobic contacts and other non-covalent forces in a physiologically relevant, parallel rho dimer were sufficiently strong, it would have resisted the need to reorient itself in detergent.

Rhodopsin reconstitution in asolectin produced self-associated, symmetric oligomers (Mansoor, Palczewski *et al.* 2006). However, this phenomenon is not unique to rhodopsin and seems to be a property of the lipid mixture comprising

asolectin (24% saturated, 14% mono-unsaturated and 62% polyunsaturated) at a certain lipid to protein ratio only which is not generally applicable to other lipids (e.g- egg PC, POPC, DMPC) (Huang, Bayley *et al.* 1980; Niu, Kim *et al.* 2002). Biophysical and Molecular Dynamics of rhodopsin with a range of lipids (Botelho, Huber *et al.* 2006) (Periole, Huber *et al.* 2007), has shown that the hydrophobic mismatch between lipid chains and the rhodopsin transmembrane region, as well as local deformations in the bilayer thickness as a result of accommodation of phospholipids to the hydrophobic and polar faces of rhodopsin, drive rhodopsin aggregation. Finally, it has been proposed that some experiments consisting of cellular overexpression of GPCRs may have overestimated dimerization due to transient, non-specific protein contacts (James, Oliveira *et al.* 2006). In our approach, we isolated and purified two rhodopsins in close proximity (less than 10nm apart) using NABBs. However, this is possible due to excess rho present during NABB formation (**Table 2**), and limited by the diameter of a NABB.

Comparisons of dimerization potential of rhodopsin (and other family A GPCRs) with GPCRs that are currently known to form strong dimers (Romano, Yang *et al.* 1996; Kaupmann, Malitschek *et al.* 1998) and higher order oligomers (Guo, Urizar *et al.* 2008) are often made in support of the rhodopsin dimer model. However such comparisons are not strictly valid since most of the latter GPCRs possess distinct structural elements that facilitate dimerization. These elements include extended N termini, folded into distinct motifs, as well as extended C-termini (Bockaert and Pin 1999; Bockaert 2003). The constitutive homo or

heterodimers are often disulfide linked or associated with their large extracellular domains which include the ligand binding site. These structural features and phenomena have not been reported in rhodopsin.

Another major factor that tends to be overlooked in comparative reports between rhodopsins and other GPCRs is the issue of GPCR trafficking to the cell surface. For instance, in the case of one of the best known GPCR dimers, the $GABA_B$ receptor, two isoforms $GABA_BR1$ (GBR1) and $GABA_BR2$ (GBR2) dimerize to form the functional receptor (Jones, Borowsky *et al.* 1998; Kaupmann, Malitschek *et al.* 1998; White, Wise *et al.* 1998). When the isoforms are expressed alone in cells, GBR1 is retained intracellularly (Couve, Filippov *et al.* 1998) while GBR2 is transported to the surface but cannot bind GABA or initiate signaling (White, Wise *et al.* 1998). It is hypothesized that GBR2 acts as a molecular chaperone that masks the ER retention signal of GBR1 using the C-terminal end thus allowing transport of the dimer to the cell surface in a functional form (Margeta-Mitrovic, Jan *et al.* 2000). In contrast, rhodopsin is trafficked from rod inner segments (site of synthesis) to mature rod outer segments (ROS) in the retina using a specialized pathway involving a series of coordinated fusions (Boesze-Battaglia 2000). This process of fusion is likely optimized for high density of rhodopsins that is required for close to single-photon sensitivity to dim light.

From our experiments, we deduce that dimerization of rhodopsin may not be required for transducin activation. It is, however, interesting to speculate whether oligomerization of other GPCRs has been an evolutionary process that

may have led to fine-tuning of the G protein signaling rate in cells. A computational study of possible dimeric interfaces of GPCRs using a chimeric muscarinic M3 and adrenergic α_2 receptor system predicts a parallel orientation of the third intracellular loop (IL 3) in each monomer, with the orientation preserved even across different putative dimerization interfaces (Gouldson, Higgs *et al.* 2000). This may have important functional consequences in terms of G protein interaction with this domain. Interestingly, the arrangement of transmembrane helices in the helix IV-V rho dimerization model (**Fig. 1-4**) does not appear to be one of the several possible of the dimerization motifs presented.

6.0

Chemokine Receptor 5 (CCR5) Incorporation and Activity in NABBs

6.1 Introduction

Chemokine receptor 5 (CCR5) is a clinically important GPCR but only limited experimental reports exist about its molecular mechanism in a purified, cell-free state (Mirzabekov, Bannert *et al.* 1999; Stenlund, Babcock *et al.* 2003; Navratilova, Dioszegi *et al.* 2006). The lack of information about CCR5 compared with other membrane proteins may be due to the inability to get high amounts of CCR5 for purification and *in-vitro* studies. CCR5 requires unique posttranslational modifications for function (Farzan, Mirzabekov *et al.* 1999), which varies depending upon the cell type used for heterologous expression. CCR5 also shows a marked loss of activity when purified in detergents (Mirzabekov, Bannert *et al.* 1999). We have previously shown that rhodopsin exhibits a significant increase in thermal stability when reconstituted into NABBs (Banerjee, Huber *et al.* 2008). We reasoned that NABBs may be the ideal

platform for *in-vitro* studies of CCR5 by providing the detergent-labile receptor a stable, soluble, lipid environment for biochemical assays.

CCR5 has many known ligands (Rossi and Zlotnik 2000), but the most well-characterized agonists are RANTES, MIP-1α and MIP-1β. These ligands are able to suppress HIV-1 infection *in-vitro* (Wilkinson 1996; Princen and Schols 2005). While RANTES is basic at physiological pH, MIP-1α and MIP-1β are acidic under those conditions. However all three interact with CCR5. *In-vitro* receptor binding and activation studies show a large overlap in receptor and chemokine specificities. This effect is not echoed *in-vivo* according to gene knockout and antagonist assays (Gerard and Rollins 2001; Proudfoot 2002). Traditional methods of screening receptor activity use radiolabeled ligands or nucleotide, which are hazardous, costly and cumbersome to use. We made use of a recently developed fluorescent GTP analog (McEwen, Gee *et al.* 2001) to design an assay that is able to detect ligand mediated G protein activation. The ideas and methods presented in this chapter will enable us to answer pertinent and long-standing questions about the effect of G protein on binding affinity of CCR5 ligands and differential activation of G proteins by different chemokines.

Figure 6-1. Sandwich-ELISA Strategies used for Characterizing CCR5-NABBs

Sandwich ELISA uses dual epitopes on the CCR5-NABB in a high-throughput, antibody-based screening protocol. The two antibodies are selected based on the assay performed. The fluorimetric quantitation is made possible by a colorless substrate that is converted into a fluorescent product by a catalytic reaction of Horseradish peroxidase (HRP) in the presence of excess H_2O_2. **(A)** 2D7 / 1D4 ELISA. The capture antibody is 2D7, a conformation sensitive antibody to the extracellular side of CCR5. The amount of correctly folded CCR5 bound to 2D7 is detected by probing with HRP-tagged 1D4 antibody, which recognizes a linear epitope engineered at the C-terminus of CCR5. **(B)** 6xHis / 1D4 ELISA. The capture antibody is a hexa-histidine (6xHis) tag recognizing antibody that binds to His tags present on zap1 which form NABBs. The amount of NABBs containing CCR5 (or any other 1D4-epitope tagged receptor) is detected by probing with 1D4-HRP antibody. **(C)** 1D4 / 6xHis ELISA. Switching the order of antibodies in (B) results in an assay that estimates the proportion of the total CCR5 in NABBs.

Figure 6-1

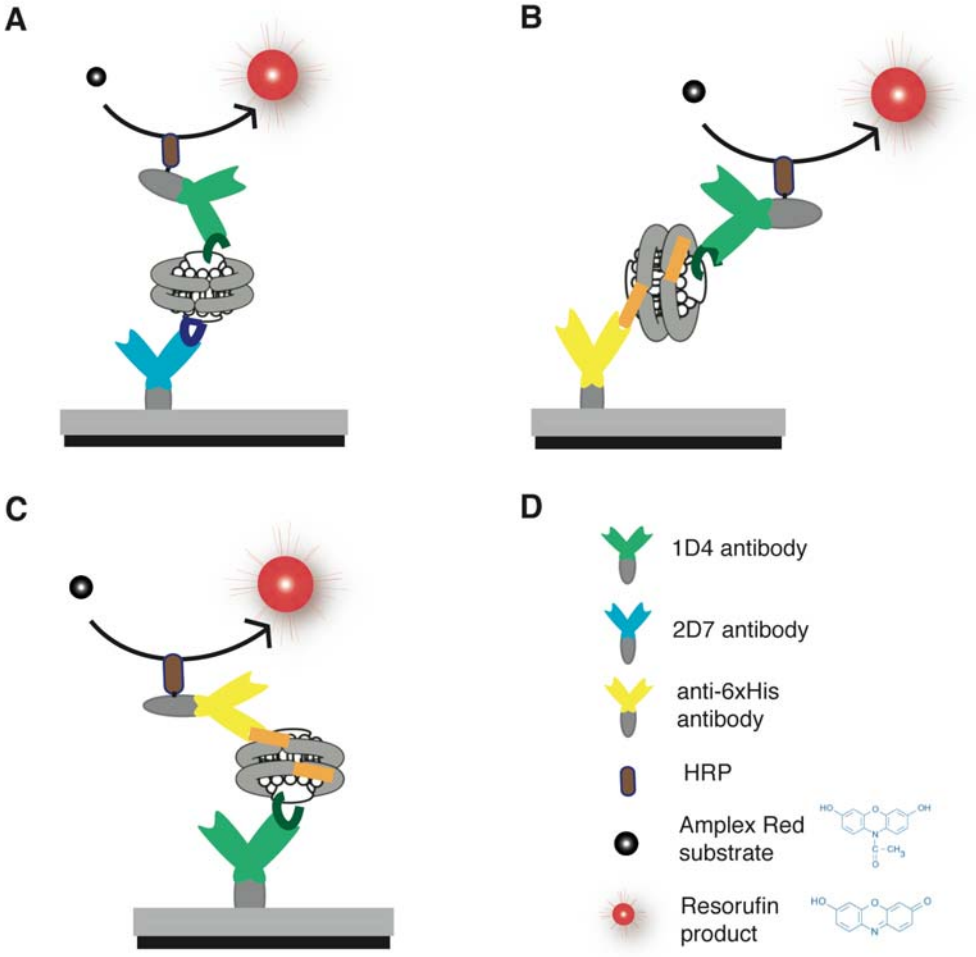
A
B
C
D
1D4 antibody
2D7 antibody
anti-6xHis antibody
HRP
Amplex Red substrate
Resorufin product

6.2 Results

6.2.1 Rapid Incorporation of CCR5 into NABBs

A stable cell line was established and used for the purpose of optimizing incorporation of CCR5 into NABBs. HEK-293 cells were labeled with FITC conjugated anti-CCR5 antibody and the highest expressing clone (R5-18) was selected and amplified. Unlike rhodopsin, CCR5 does not have a characteristic spectroscopic signal. Therefore, to characterize CCR5 incorporation into NABBs, we first developed a high-throughput sandwich ELISA assay (**Fig. 6-1**). We designed the screen to quantify both the correctly folded CCR5 in NABBs as well as total CCR5 using different antibodies commercially available for CCR5 in order to detect nanomolar concentrations of CCR5.

We were able to incorporate CCR5 in NABBs starting from cell-pellets derived from 6-10 10 cm diameter (approx. 314 cm^2 area) plates. The cells were lysed in a mixture of lipids and detergents that has been reported to preserved CCR5 stability (Navratilova, Sodroski *et al.* 2005; Navratilova, Dioszegi *et al.* 2006). The CCR5 fraction was enriched using 1D4-sepharose beads and the buffer was exchanged to buffer H1 containing POPC/POPS and CHAPS.

Figure 6-2. Gel-filtration of CCR5-NABBs

Gel-filtration chromatography of CCR5-NABBs made by Extracti-Gel D mediated detergent removal (Method 2.24) using NBD-DOPE doped POPC on a Superose 6 PC 3.2/30 column on an Akta Explorer 10 FPLC system. Absorption at two wavelengths was recorded simultaneously: 280nm (protein absorbance), 460nm (NBD-DOPE absorbance) indicating elution of total protein and lipid from the column. The eluted fractions were analyzed by sandwich ELISA, using 2D7 as the capture antibody and 1D4-HRP as the probe. Since 2D7 is a conformation sensitive antibody, the ELISA profile indicates the amount of correctly folded CCR5 in the eluted fractions. The basal response was calculated using empty NABBs, prepared under identical conditions and assayed on the same ELISA plate at similar protein concentration.

Figure 6-2

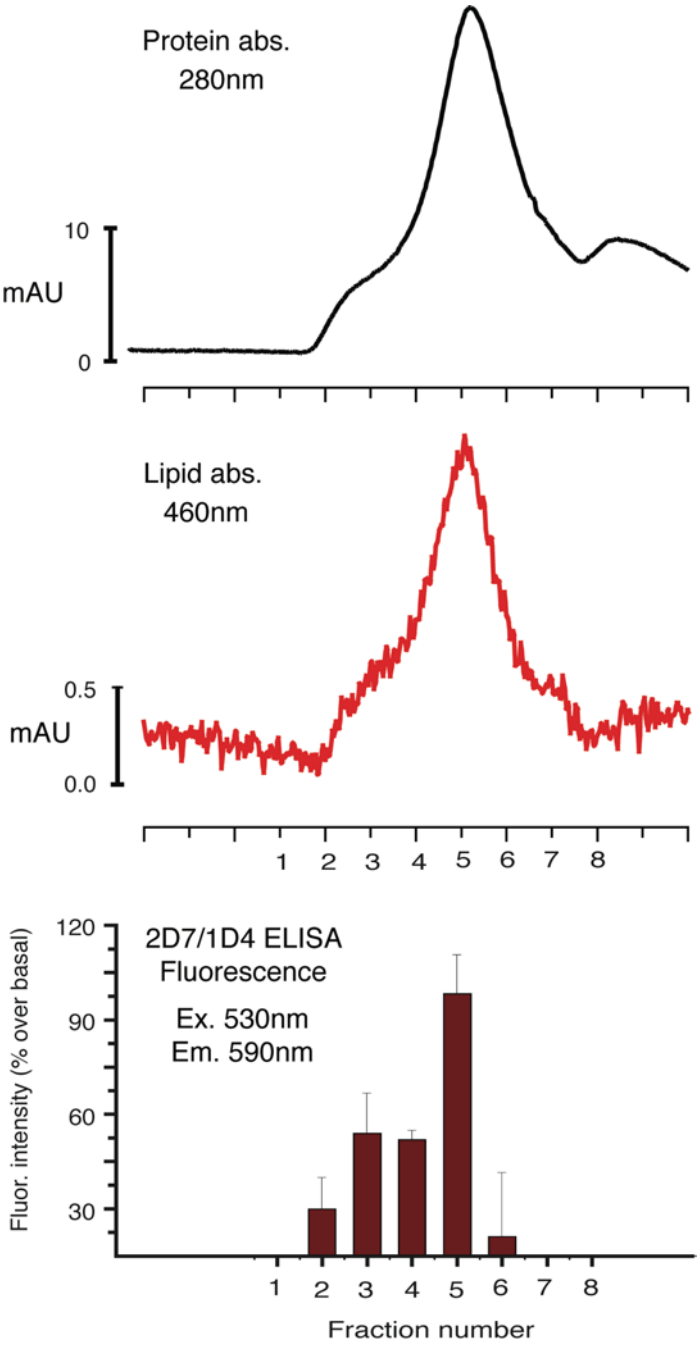
Protein abs.
280nm
10
mAU
0
Lipid abs.
460nm
0.5
mAU
0.0
1 2 3 4 5 6 7 8
2D7/1D4 ELISA
Fluorescence
Ex. 530nm
Em. 590nm
Fluor. intensity (% over basal)
120
90
60
30
1 2 3 4 5 6 7 8
Fraction number

The CCR5 was eluted with 1D5 nonapeptide, and purified zap1 was added. Detergent removal from this solution was done by passing over an Extracti Gel-D resin, yielding NABBs, as determined by a single peak in the gel-filtration step (**Fig. 6-2**). Correctly folded CCR5 was detected in the fractions using ELISA with 2D7 capture and 1D4 probing. 2D7 recognizes a split epitope on the extracellular side of CCR5 when parts of the epitope are spatially close, and is therefore considered to bind to the correct conformation of CCR5 (Khurana, Kennedy *et al.* 2005).

The CCR5 elutes at the molecular weight region (retention volume) characteristic of NABBs, as well as at higher molecular weight regions using a Superose 6 column. The cumulative signal of CCR5 in fractions 2-4 is higher than the CCR5 signal in fraction 5 (NABB peak). This distribution indicates that most of the CCR5 may be incorporated in larger discs, or multiple CCR5 may have been incorporated in the NABBs. The latter possibility is less likely given the high NABB / CCR5 ratio used for NABB formation (>100:1), unless CCR5 forms constitutive dimers in detergents used for cell lysis.

Figure 6-3. Conformational Stability of CCR5 in NABBs

Conformational stability of the extracellular side of CCR5 after exposure to different detergents was determined by a sandwich ELISA using 2D7 and 1D4 (Fig. 6-1 A, Method 2.25). HEK-293 (clone 18) cell aliquots were lysed using Buffer (20mM Tris pH 7, 150mM NaCl, 1mM EDTA) supplemented with detergents (1% w/v) and lipids (1% w/v total lipid) as shown at 4°C for 1 h. The samples were incubated at room temperature for 30 min before loading on the 96-well plate. Sample 2 was kept in a 95°C water bath immediately after lysis for 5 min, followed by 30 min room temperature incubation. Sample 7 was processed from a cell aliquot lysed under conditions of Sample 1, followed by detergent removal as described in Method 2.24 (Materials and Methods).

Figure 6-3

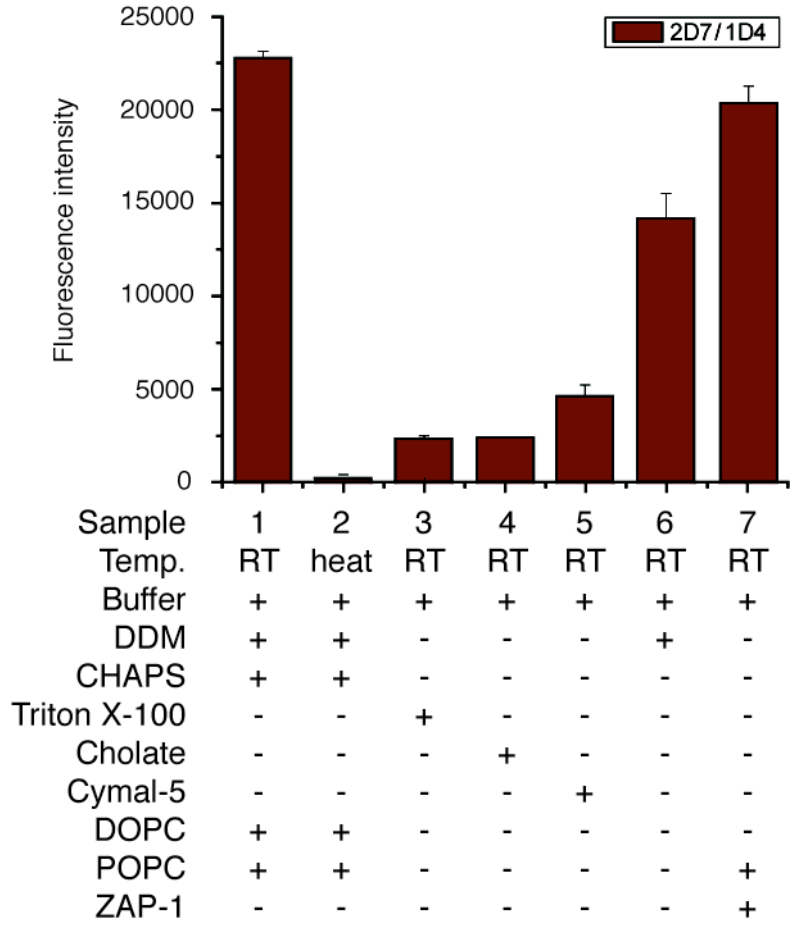
25000
20000
15000
10000
5000
0
Fluorescence intensity
2D7/1D4
Sample 1 2 3 4 5 6 7
Temp. RT heat RT RT RT RT RT
Buffer + + + + + + +
DDM + + - - - + -
CHAPS + + - - - - -
Triton X-100 - - + - - - -
Cholate - - - + - - -
Cymal-5 - - - - + - -
DOPC + + - - - - -
POPC + + - - - - +
ZAP-1 - - - - - - +

6.2.2 Detection of correctly folded CCR5 in NABBs

We optimized an ELISA protocol where the antigen (CCR5-NABBs) was sequentially sandwiched between two antibodies recognizing specific, distinct epitopes on the CCR5-NABB assembly. 2D7 is a monoclonal antibody that has been shown to recognize a split epitope on the extracellular side of CCR5 only when the epitopes are in proximity to each other (Wu, LaRosa *et al.* 1997; Khurana, Kennedy *et al.* 2005), which would be the case in a correctly folded form of CCR5. Heat denaturation abolishes 2D7 binding to CCR5, and the 2D7 binding may be competitively inhibited by chemokines. 1D4 monoclonal antibody recognizes an engineered linear amino-acid sequence at the C-terminal tail of CCR5. We measured the binding of CCR5-NABBs to 2D7 (capture antibody) as an indication of correctly folded CCR5. The amount of CCR5 bound to the capture antibody was measured by detecting the binding of the second antibody–HRP-linked 1D4, and adding a fluorogenic HRP substrate in the microplate wells. The sandwich ELISA data is shown in **Fig. 6-3**. Equivalent volumes were used for each sample.

To measure total amount of CCR5 in NABBs, 1D4 antibody was used as the capture antibody and HRP-linked hexa-histidine binding antibody (6H) was used as the detection antibody to recognize the hexa-histidine tag on zap1. HEK cells solubilized in buffer containing dodecyl maltoside (DDM), CHAPS and a

1:1 (w/w) mixture of DOPC and POPC lipids gave the highest ELISA signal (sample 1). Heat treatment of this sample, followed by thawing at room temperature destroyed binding to 2D7 antibody (sample 2). Sample 2 served as a negative control for this ELISA, since it shows that the final ELISA signal is due to specific initial binding to 2D7, and not because of non-specific binding to the microplate well. Heat denaturation of CCR5 destroys the native conformation of the extracellular loops (including ECL 2) resulting in loss of binding to 2D7. We also tested solubilization conditions where different detergents were used (samples 3-6) at 1% (w/v) concentrations. At these concentrations, all the detergents studied were above their CMC values. The samples were incubated for 30 min at room temperature. DDM was seen to be the best detergent for stabilizing the 2D7 epitope, with a signal that was 65% of sample 1. Reconstitution of a sample solubilized in conditions identical to sample 1 into NABBs using POPC and zap1 (Method 2.24) gave a signal that was 92% the signal of sample 1. The ELISA data implies that rapid incorporation of CCR5 into NABBs preserves the native conformational state of the receptor. It should be mentioned that there is likely to be a difference in the extent of antibody binding by receptors in detergent and in NABBs. We expect the binding of receptor in NABBs to be less than that of receptor in detergent micelles because of lesser accessibility of the epitope to the antibody, and the charged phospholipids headgroups. If this binding difference is considered, then the signal of sample 1 and sample 7 will be virtually identical.

Figure 6-4. Ligand Mediated Activation of CCR5 in NABBs

CCR5 activation of G protein was measured by binding of a fluorescently labeled nucleotide analog BODIPY-FL-GTPγS. BODIPY-FL-GTPγS binds to activated G protein and undergoes an increase in fluorescence quantum yield. The fluorescence increase of BODIPY-FL-GTPγS was measured using CCR5-NABBs with or without ligand. **(A)** Change in BODIPY-FL-GTPγS fluorescence using CCR5-NABBs and different G protein components is shown in the absence or presence of ligand (RANTES). Rhodopsin-NABBs and holotransducin were used as a positive control. Gi_1 α-subunit ($Gi_1\alpha$) was heterologously expressed and purified from *E. coli* (Method 2.8.1). Holotransducin (Gt) was isolated from bovine retinae (Method 2.5), and transducin beta-gamma subunits (Gtβγ) were derived from holotransducin (Method 2.6). Fluorescence intensity was calculated relative to that of a mixture of G protein and empty NABBs. **(B)** Specific RANTES mediated increase in G protein activity derived from panel A.

Figure 6-4

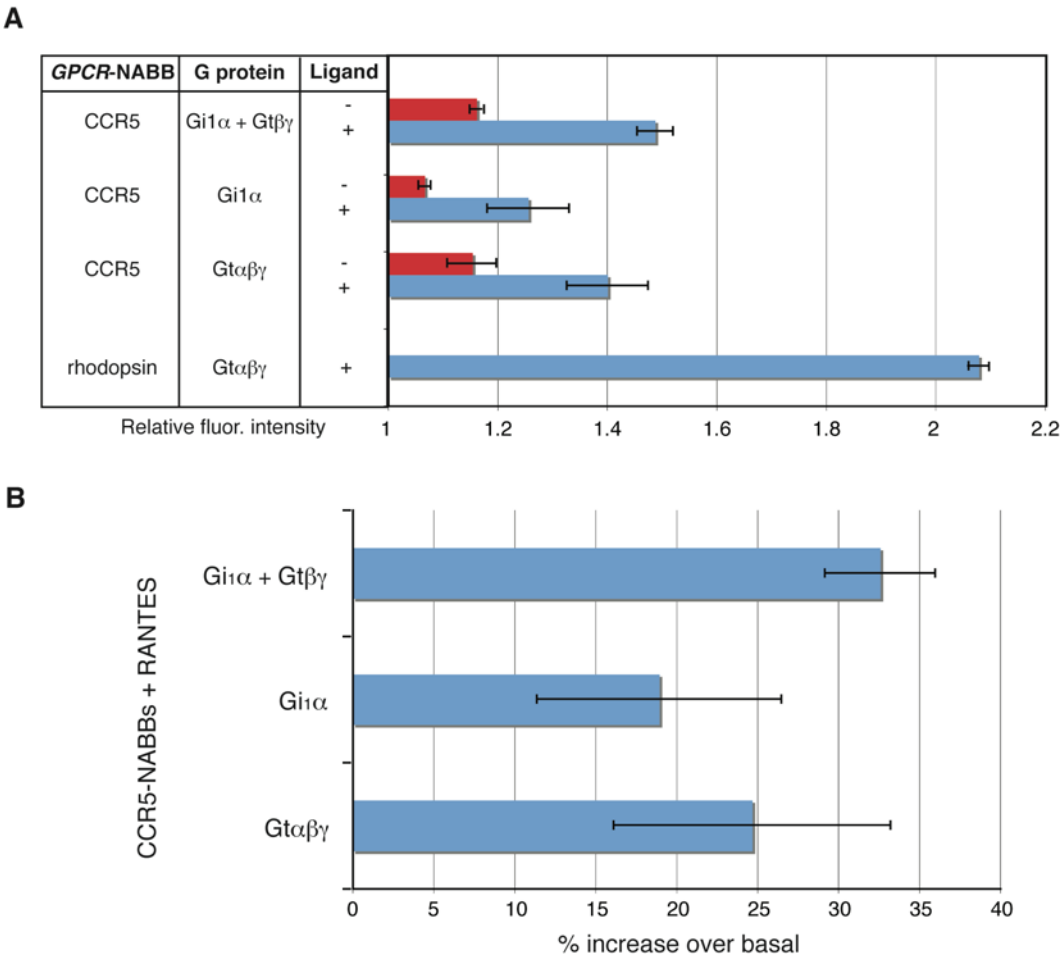
A
GPCR-NABB
G protein
Ligand
CCR5
Gi1α + Gtβγ
CCR5
Gi1α
CCR5
Gtαβγ
rhodopsin
Gtαβγ
Relative fluor. intensity
1
1.2
1.4
1.6
1.8
2
2.2
B
CCR5-NABBs + RANTES
Gi1α + Gtβγ
Gi1α
Gtαβγ
0
5
10
15
20
25
30
35
40
% increase over basal

6.2.3 Ligand-mediated G protein Activity of CCR5 in NABBs

A fluorescent, non-hydrolysable, non-radioactive GTP analog was used to measure guanine nucleotide exchange by the G-protein in the presence or absence of ligand-stimulated receptor. The BODIPY-FL-GTPγS (B-GTPγS) nucleotide undergoes an increase in fluorescence quantum yield upon binding to the G-protein α-subunit (McEwen, Gee *et al.* 2001). The fluorescence increase occurs presumably due to de-quenching of the fluorophore from the guanine ring, which occurs in the extended conformation of the nucleotide when it resides in the nucleotide binding pocket. The maximum increase in quantum yield of B-GTPγS upon binding to $G_{i1}\alpha$ has been reported to be 3-4 times over B-GTPγS alone. Unlike (unlabeled) GTPγS, binding of B-GTPγS has been hypothesized to form an intermediate activated state of Gt between the inactive and fully-activated states (Ramachandran and Cerione 2004). The nucleotide may be used to follow the steady-state enzyme kinetics of the Gα subunits (Jameson, Roof *et al.* 2005). In this case, we adapted the reagent concentrations and reaction time to enable us to monitor increase in fluorescence of B-GTPγS in an end-point assay. The assay was optimized using rhodopsin-NABBs and holotransducin.

CCR5 is known to couple to the G_i class of G-proteins (Cardaba, Kerr *et al.* 2008). We observed efficient G-protein activation by CCR5-NABBs in the presence of the heterotrimeric Gi protein, as well as holotransducin. Stimulation

of CCR5 in NABBs by 50mM RANTES produced upto 30% enhancement of B-GTPγS binding to the G protein, compared with unstimulated CCR5-NABBs (**Fig. 6-4**). The largest increase in BODIPY-FL-GTPγS was seen when βγ subunits from transducin were mixed in equimolar ratio with *E. coli* expressed and purified $G_{i1}\alpha$. The *E. coli* expressed G_{i1} α subunit used in this experiment did not contain post-translational modifications (prenylation or myristoylation) that are present in native Gα subunits. The results indicate the requirement of a heterotrimeric G protein to observe the activity of CCR5. The α-subunit of the G protein is mostly in contact with the cytoplasmic side of the GPCR. However, CCR5 does not seem to couple efficiently with $G_i\alpha$ alone. We noticed a requirement of the βγ subunits for efficient activation of the G protein α subunit. In our assay, the role of βγ subunits may be to increase the accessibility of the G_{i1} α subunit to the NABB due to the lipid anchor present on the γ-subunit. Isoprenylated peptides have approximately 10-fold higher affinity for lipids than their unmodified versions (Silvius and l'Heureux 1994). The γ_1 subunit (present in transducin) contains a farnesyl (15 carbons) modification at its C-terminus. Other γ-subunits have geranygeranylations (20 carbons) at the same location (Wedegaertner, Wilson *et al.* 1995). It is also plausible that the βγ-subunits modulate an increase in the receptor mediated GTP uptake by the α-subunit by affecting the conformational change in the G protein.

We detected B-GTPγS uptake in the presence of unstimulated CCR5-NABBs (**Fig. 6-4 A**). A certain basal level of constitutive GPCR activity is

common for GPCRs in the absence of an inverse agonist (Bartfai, Benovic *et al.* 2004). Under the conditions of our assay, a 10-15% greater binding of B-GTPγS was seen in the presence of CCR5-NABBs without ligand compared with empty NABBs alone. Samples with RANTES showed a significantly higher increase in signal.

6.3 Discussion

6.3.1 A General Incorporation and Detection Strategy for Expressed Membrane Proteins into NABBs

Unlike rhodopsin, CCR5 and other known GPCRs do not contain an internal chromophore with which to accurately estimate their concentration in a mixture of other proteins. We therefore chose to work in small volumes for NABB formation (50 – 100 μL) and make the concentration of NABBs high enough such that there are always excess of empty NABBs compared to membrane proteins in that volume. Using this approach, we can approximate that most, if not all, membrane proteins in the cell lysate will be incorporated into NABBs. The GPCR containing NABBs were then isolated using immunoaffinity purification. We have also refined this method by adding a short immunoaffinity step for the GPCR prior to NABB formation. This modification enabled us to work with larger volumes of lysate and higher concentrations of the GPCR, as

well as do a convenient buffer exchange from the cell lysis buffer to the NABB formation buffer while the GPCR was on the solid immunoaffinity bead support. The method developed for rapid incorporation of CCR5 in NABBs may be generalized to other membrane proteins that are expressed in cells at similar or higher levels. The method is also scalable to larger volumes, using the same strategies of cell lysis, initial enrichment, NABB formation, final purification, and antibody-based characterization.

Conventional methods of characterization of macromolecular protein complexes commonly involve SDS-PAGE and immunoblotting. In these methods, any information about activity is lost and quantitation of the signal is difficult, and relatively few samples may be analyzed simultaneously. We developed a sandwich ELISA technique which may be easily adapted to different membrane proteins in NABBs by using appropriate antibodies. The screening process was adapted for a microplate due to which many conditions may be analyzed in replicates in a rapid and quantitative way. We chose an antibody (2D7) that recognizes the biologically relevant conformation of CCR5 in order to analyze the amount of active receptor incorporated in NABBs. 2D7 has also been shown to effectively compete with RANTES and gp120 from HIV for binding to CCR5 (Wu, LaRosa *et al.* 1997; Rossi and Zlotnik 2000; Zhang, Rao *et al.* 2007). This property enables us to focus on those conditions that are most likely to yield CCR5-NABBs which can be analyzed for relevant biological assays.

6.3.2 G protein Activation by CCR5-NABBs

The presence of G protein may serve to modulate ligand affinity in the GPCR, probably by making high-affinity sites accessible to agonist (Whorton, Bokoch *et al.* 2007). *In-vitro* assays of small-molecules affecting ligand binding to CCR5 in the absence of G proteins may not be accurate in predicting the *in-vivo* effects. A series of cell-based and membrane-based assays have determined that CCR5 couples to both Gi as well as Gq class of G proteins (Mueller, Mahmoud *et al.* 2006; Springael, de Poorter *et al.* 2007). Whether a CCR5 facilitated HIV infection involves G protein signaling by CCR5 is not resolved (Gosling, Monteclaro *et al.* 1997; Kinter, Catanzaro *et al.* 1998). Further, CCR5 has been shown to interact with CD4 and CXCR4 in assays where HIV entry is accompanied by either Gi or Gq signaling (Lin, Mettling *et al.* 2006; Harmon and Ratner 2008). However, there have been no reports of assays of CCR5 with purified G proteins. The BODIPY-FL-GTPγS binding assay presented here is a convenient and rapid method to assay for effector mediated G protein activation using purified CCR5-NABBs with purified G proteins.

7.0 Future Perspectives

7.1 Introduction

Nanoscale, water-soluble, well-defined lipid bilayer particles like NABBs have tremendous potential in a variety of applications in spectroscopy, cell-biology and medicine. Based on work done by other groups on similar nanoscale structures and membrane proteins, and our own data and experience, this chapter presents the near and long term experimental approaches that will be made possible using NABBs.

7.2 Novel Assay Development

7.2.1 Infra-Red Spectroscopy of Membrane Proteins

Fourier transformed infrared spectroscopy (FTIR) difference spectroscopy is a widely used technique to investigate secondary structure and conformational changes upon interaction with substrates (Fahmy, Siebert *et al.* 1995; Siebert

1995; Zvyaga, Fahmy *et al.* 1996). However, the standard FTIR technique (transmission mode) is limited to studying thin films to avoid the strong background IR absorbance of water. FTIR in an attenuated total reflection (ATR) mode solves this problem and allows for solvent accessibility to the protein. But FTIR-ATR studies too have been limited by difficult sample preparation (poor protein film formation, hydration induced swelling of sample and lack of preservation of protein native state). The signal to noise ratio in a typical FTIR-ATR experiment is sufficient to study protein multilayers but not monolayers. Surface enhanced infrared absorption spectroscopy (SEIRA) is a modification of the FTIR-ATR method that can reliably measure spectra in protein monolayers (Ataka and Heberle 2006). The SEIRA technique involves enhancement of the interaction of IR by the sample with surface plasmons (collective electronic oscillations from a colloidal metal film). The signal enhancement is restricted to 8-10 nm above the colloidal metal surface; therefore the bulk solution is not enhanced. The enhancement of signal is affected by the size, shape and proximity of the protein 'islands' to the metal film, provided that the islands are smaller than the wavelength of IR light (15-30 nm).

For SEIRA measurements, a colloidal gold film is used as the surface. The surface is often modified with linkers to avoid protein denaturation and to provide selective protein orientation for measurements. The gold film used for SEIRA may be conveniently modified with Ni-NTA groups. The NABB system meets all the criteria to be an ideal sample for SEIRA studies. They are small in size, may have a high concentration of proteins incorporated per NABB and the zap1 is

histidine tagged, which can easily bind to a Ni-NTA surface. Accessibility to both sides of the incorporated receptor is preserved for studies of complex conformational changes. Initial experiments with rho-NABBs have shown that the NABBs oriented parallel to the gold surface (probably due to two his tags per NABB), and no significant loss in the rhodopsin IR spectrum was detected (Vogel R- unpublished results).

7.2.2 Single-molecule Fluorescence of GPCRs

'Nanosizing' a traditional bulk-phase assay may lead to previously unanticipated results. For example, a notable decrease in G protein activation rates was reported in the presence of excess 'empty' HDL particles in assays where rhodopsin were incorporated in HDL-like nanodisc particles (Bayburt, Leitz *et al.* 2007). The reason of the lower rate of activation was hypothesized to be partitioning of Gt into empty NABBs. Using β_2-adrenergic receptor monomers in HDL particles, and in the absence of empty HDL particles, only 6% of the total Gs was bound to β_2-AR containing HDL particles (Whorton, Bokoch *et al.* 2007). In this case, it was hypothesized that excess Gs precipitates in the absence of sufficient number of HDL particles, probably due to the hydrophobic modifications present on Gs. In our experience with ensemble G protein assays with rho-NABBs, we observed lower activation rates in the presence of empty NABBs using the Trp fluorescence assay. Using the high-throughput BODIPY-FL-GTPγS assay with CCR5-NABBs, we did not observe a significant change in

G protein activation in the presence or absence of empty NABBs. Further, our control experiments using rho-NABBs did not show any difference in the basal BODIPY-GTPγS binding rate of Gt in buffer alone or Gt in the presence of empty NABBs (Grunbeck A- unpublished data).

Fluorescence measurements carried out at single-particle resolution can provide information of structural distributions in a direct fashion, since emitted photons from individual molecules can be recorded and analyzed. The molecular systems can be studied in a molecule-by-molecule manner, which enables evaluation of biological processes in a model-free fashion (Mukhopadhyay and Deniz 2007). The well-defined structure of NABBs and the ability to study individual GPCRs either under constant flow conditions or by tethering the NABBs to a functionalized surface make this an ideal system for single-molecule fluorescence assays.

Single-molecule fluorescence studies also require the use of a novel class of fluorophores that are photostable to intense laser excitation and do not form non-emitting triplet states upon excitation (Eggeling, Fries *et al.* 1998). We have used the Atto-655 dye for derivatization of rhodopsin (Chapter 4), which is part of a series of dyes that fulfill the characteristics above and are hence ideally suited for single-molecule fluorescence studies. Atto-655 is an oxazine-backbone based dye that has lower molecular weight than most commercially available dyes that are fluorescent at long wavelengths. The Atto dyes have been reported to show significantly lower self-quenching, and have a rigid backbones that do not show *cis*-trans isomerization common to cyanine based fluorophores (usually, only the

trans conformation of a fluorophore is responsible for its fluorescence properties). Quantitative studies of GPCRs in NABBs will thus depend on a combination of ensemble assays like those presented in the preceding chapters, alongwith single-particle techniques using appropriate fluorophore reporters, to understand signal transduction events at a level proximal to the GPCR.

7.3 Future Research Aims

7.3.1 G protein Effects on Ligand Affinity of a GPCR

How can we detect a small change in ligand affinity of a GPCR under the influence of purified G proteins using an ensemble fluorescence assay? When fluorescently modified ligands are available (for example, RANTES for CCR5), the sensitive technique of fluorescence anisotropy may be used to determine even small changes in the anisotropy of the labeled ligand (in this case, a chemokine). In a homogeneous solution the ground-state fluorophores will all be randomly oriented. When exposed to polarized light, those fluorophores which have their absorption transition moments oriented along the electric vector of the incident light are preferentially excited (Lakowicz 1999). Hence, the excited state population is no longer randomly oriented. Depolarization of emission can be caused by a number of phenomena. Depending upon the conditions of this type of

experiment, depolarization may be chiefly be determined by the rotational diffusion of the fluorophore (attached to the ligand).

To measure fluorescence anisotropy (*r*), the sample is excited with polarized light and the intensity of emission is measured through a polarizer.

$$r = \frac{I_{\parallel} - I_{\perp}}{I_{\parallel} + 2I_{\perp}}$$

where, $I_{\parallel}$ is the measured intensity when the emission polarizer is oriented parallel to the direction of the polarized excitation, and $I_{\perp}$ is the measured intensity when the polarizer is perpendicular to the excitation polarization.

The labeled molecule is considered a spehere for the purpose of calculating the average anisotropy in the sample. Following pulsed excitation, the decay of fluorescence anisotropy, the decay of fluorescence anisotropy of a sphere is given by:

$$r(t) = r_0 e^{-t/\theta}$$

where r_0 is the anisotropy at $t = 0$ (also called fundamental anisotropy). θ is the rotational correlation time of the sphere, given by

$$\theta = \frac{\eta V}{RT}$$

where η is the viscosity, V is the volume of the rotating unit, T is the temperature in Kelvin and R is the gas constant.

Considering the simplest mode of anisotropy, where the intensity follows a single-exponential intensity decay, the expression for measured anisotropy *r* (derived from Perrin equations) (Lakowicz 1999) is:

$$r = \frac{r_0}{1 + (\tau / \theta)}$$

where τ is fluorescence lifetime of the fluorophore. If the correlation time is larger than the lifetime ($\theta >> \tau$) then $r = r_0$. If the correlation time is shorter than the lifetime ($\theta << \tau$), then $r = 0$.

For globular proteins, the rotational correlation time is related to the molecular weight (*M*) by:

$$\theta = \frac{\eta V}{RT} = \frac{\eta M}{RT}(\bar{v} + h)$$

where $\bar{v}$ is the specific volume of the protein (typically 0.73 mL/g) and *h* is the hydration (near 0.23 g of H_2O per gram of protein).

For small fluorophores in a low viscosity solution, the emission is highly depolarized because of very low rotational correlation times (determined by molecular weight, as described above). The average molecular weight of a fluorescently labeled chemokine is 8 kD. Upon binding to CCR5 in NABBs, the molecular weight of the fluorophore-containing system increases to around 250 kD, or roughly 30 times the mass of the fluorescent chemokine alone. The NABB not only stabilizes the CCR5, but in this case, adds the required bulk to increase the rotational diffusion time of the bound fluorophore resulting in a net increase in anisotropy, compared with a free (unbound) ligand. A heterotrimeric G protein bound to the CCR5-NABB will increase the molecular mass of the system even

further. Using this assay with an appropriately chosen fluorophore, it could be possible to detect changes in ligand binding to CCR5 by the relative change in anisotropy signal of the fluorophore as a measure of binding affinity to the CCR5-NABBs.

7.3.2 Functional Consequences of GPCR Dimerization

NABBs may be designed to contain one or two GPCRs based on the stoichiometry of GPCR to zap1 and lipids. The NABBs are formed by a self-assembly process mediated by hydrophobic association of the zap1 with the lipid acyl chains and extensive salt-bridging between two anti-parallel, amphiphatic alpha-helices of zap1, resulting in a soluble, disocidal structure of lipids with the GPCR(s) incorporated. NABB assembly starts from a detergent solubilized state of GPCR, lipids and zap1, therefore any artifactual aggregation of the GPCR with other protein components can be minimized. The NABBs with or without the GPCR may be affinity purified on Ni-NTA beads, or the affinity tag on the GPCR may be used to obtain high purity of GPCR containing NABBs. In chapter 5, we have characterized rhodopsin-NABBs using a variety of biophysical and biochemical methods to detect G protein activation by one or two rhodopsins in NABBs. We have demonstrated that a GPCR in NABBs has significantly higher thermal stability compared to commonly used detergents (Chapter 5, 6). We have also developed a method to rapidly incorporate CCR5 in NABBs from solubilized

HEK-293 cell membranes, thereby minimizing the exposure of the GPCR to detergents (Chapter 6).

Knowledge of the GPCR oligomeric state responsible for G protein activation may be key to a novel class of therapeutic interventions, which perform either by blocking GPCR dimerization directly or by modulating G protein affinity for one of the oligomeric states. It is difficult to distinguish between dimerization requirements for trafficking and for G protein activation using cell-based assays. NABBs may be used to isolate one or two GPCRs to perform G protein activations in ultra small volumes and concentrations of all components.

7.3.3 Structures of a GPCR–G protein Assembly in a NABB

The study of membrane proteins in general, and GPCRs in particular, has been hampered by the lack of a well-defined, soluble, model membrane. In the absence of a membrane, even relatively soluble membrane proteins tend to oligomerize or aggregate. On the other hand, if liposomes or detergent micelles are used to stabilize proteins, the situation is complicated by these systems' inherent polydispersity, inconsistency and instability. It has therefore been challenging to obtain unambiguous information about GPCR structure and function experimentally. NABBs may serve as a versatile adjunct to and extend the use of conventional membrane technologies.

Electron microscopy is a powerful emerging field of image-based structure deconvolution. Over the last decade, a convergence has taken place

between the diverse fields of statistical optics, theory of linear systems, and multivariate data analysis and classification with EM imaging (Frank 2002). Determination of structure at a biologically meaningful resolution with single-particle averaging techniques requires a good control of sample preparation (homogeneous sample) and classification methods (often more than one method). Negative stain EM is useful mainly for revealing only the surface contour of a protein (Henderson 1995). This is because predominantly low-resolution information is preserved by the negative stain due to the limitations associated with embedding a biological sample in a heavy-ion based high contrast medium. While we were able to perform a visual classification using negative-stained NABBs (**Fig. 5-4**), the lipoprotein particles had sufficient heterogeneity in shape to be intractable to more rigorous statistical analyses or structure prediction (Appendix Fig. A). In cryo-EM, the molecules are entrapped in their native orientation in a layer of vitreous ice. The densities measured in cryo-EM reflect the projections of the biological material without any staining agent around the particle. However, while using charged lipoproteins like NABBs made with POPC as the lipid, the strong electron density of the lipid headgroups overwhelms the densities of proteins that are not sufficiently separated from the lipid bilayer. Cryo-negative staining may be a promising technique that would reverse the strong electron density of the lipid headgroups under cryo-EM conditions, and allow acquisition of medium to high resolution structural data of membrane proteins incorporated in these discoidal lipoprotein particles.

NMR spectroscopy is a complementary technique to X-ray crystallography for high resolution structure determination. NMR of discoidal lipoprotein complexes presents the challenge of long rotational correlation times of the relatively large sizes of lipoprotein complexes to be solved by solution NMR. Solid-state NMR (SSNMR) has evolved as a powerful tool for structural studies of protein and large complexes with slow tumbling rates. The limitation of using isotope labels at a small number of sites on a protein in SSNMR has been overcome in the last decade by the introduction of high magnetic field (greater than 14 Tesla) and high-frequency magic-angle spinning (MAS) in combination with multi-dimensional dipolar recoupling sequences (Opella and Marassi 2004). NMR on lipoprotein particles has been successfully performed (Li, Kijac *et al.* 2006; Mishra, Anantharamaiah *et al.* 2006) although full assignments of the peaks have not been reported in the case of membrane protein embedded in these structures (Kijac, Li *et al.* 2007).

7.3.4 Tailoring Apolipoproteins to form NABBs of Diverse Properties

Apolipoproteins are called protein detergents for their unique ability to form defined discoidal lipoprotein complexes. How can the properties of apo A-I be modulated to form discs that have long-term stability, or are able to be triggered to fuse and deliver their cargo (for example, to a Giant Unilamellar Vesicle)? The amino-acid sequence of apo A-I is well-conserved throughout evolution. Exploring apo A-I sequences of animals that evolved differently may

provide us with clues as to which regions in the sequence may be critical for stability of the structure. In one such attempt, the lipid binding helical stretches in human apo A-I were repeated in different numbers to form a series of engineered constructs called Membrane Scaffold Protein (MSP) series by the Sligar group (Denisov, Grinkova *et al.* 2004). However, the net effect of these duplications was not observed on the weighted salt-bridging scores, indicating that this strategy may not be sufficient to increase disc stability. Methods to detect small changes in disc stability and lipid affinity will also have to be developed simultaneously.

APPENDIX A

3D Model of 2Fab-rho-NABB from Negative stain EM images

The EMAN suite of programs (Lüdtke, Baldwin *et al.* 1999) was used to determine a preliminary structure of purified 2Fab-rho-NABBs (Chapter 5). 12 electron micrographs were used to select 516 single particles using the Boxer program. The defocus of the micrographs was approximately

-5 μm. The selected particles were arranged into 8 class averages, and these classes were averaged to give the final model as shown. A C_6 axis of symmetry perpendicular to the plane of the assumed disc was imposed during calculation of the 3D model in order to converge the calculations to form a cylindrical shape. The volume errors arising from the 'common-lines' approach to calculating the structure was not corrected for. The model was not refined any further.

A barrel shape of the 2Fab-rho-NABB complex can be seen. The outline of the NABB can be discerned from the structure. The smear of density above and below the plane is likely due to C_6 symmetry imposed while calculating the model.

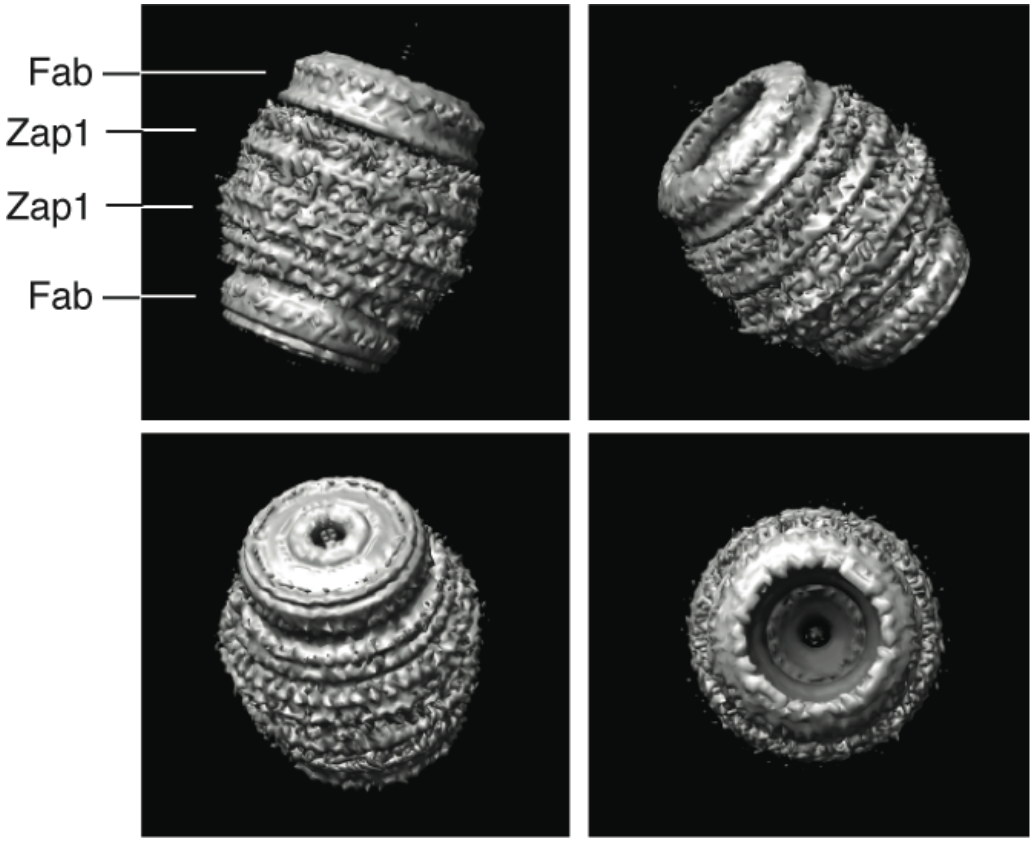
Fab
Zap1
Zap1
Fab

APPENDIX B

Sandwich ELISA Calibration using Rho-NABBs

Detection of 1 rho-NABBs may be done using the sandwich ELISA technique (Chapter 6). 6xHis antibody was used to capture NABBs and 1D4-HRP was used to detect the rhodopsin present. **(A)** Scatter plot of log of the rho concentration in NABBs in each well (x-axis) vs the percentage of the maximum fluorescence intensity obtained. Each point is the average of 4 wells. Black points show binding of 1D4 purified 1 rho-NABB (from a 0.01 rho/NABB sample) and red points show binding of 0.01 rho/NABB (including excess NABBs) to 1μg/mL of 6xHis antibody inside the microplate wells. Rho-NABBs compete for 6xHis binding with empty NABBs as seen by the requirement of higher rho concentration to achieve the same signal when excess empty NABBs are present (red). **(B)** Image of the microplate region corresponding to the black data points in (A) using a Typhoon 9400 scanner showing the fluorescence intensity of the Amplex Red product as a function of rho concentration. The sample plate was prepared by serially diluting 10nM of rho in NABBs (rightmost wells) from right to left.

A

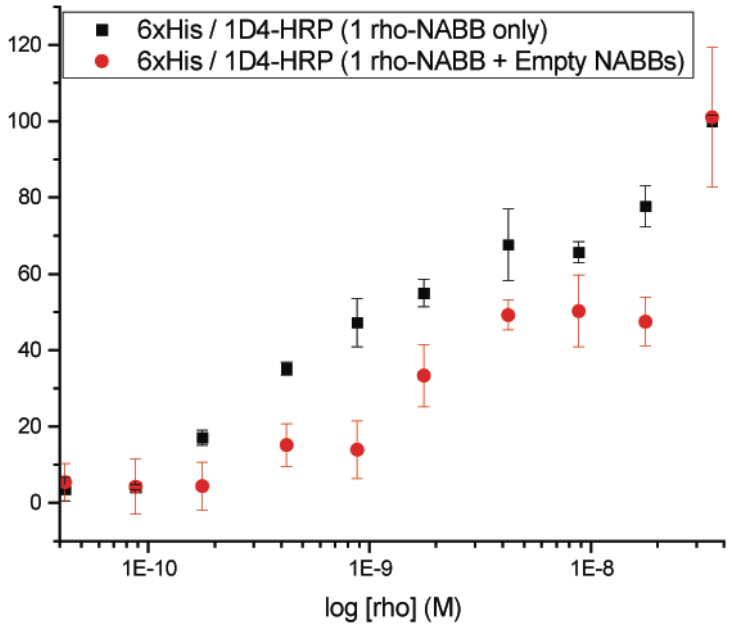
6xHis / 1D4-HRP (1 rho-NABB only)
6xHis / 1D4-HRP (1 rho-NABB + Empty NABBs)
120
100
80
60
40
20
0
1E-10
1E-9
1E-8
log [rho] (M)

B

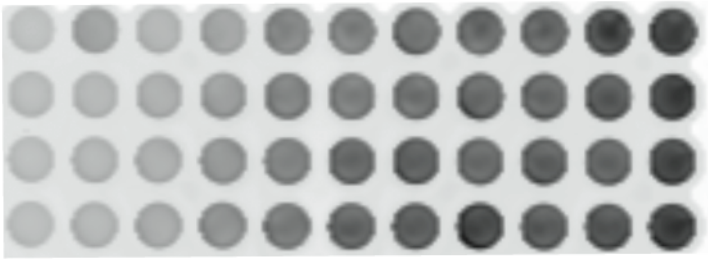

Bibliography

1. Ajees A.A., Anantharamaiah G.M., Mishra V.K., Hussain M.M. and Murthy H.M. (2006). Crystal structure of human apolipoprotein A-I: insights into its protective effect against cardiovascular diseases. *Proc. Natl. Acad. Sci. USA* **103**(7): 2126-2131.

2. Arnulphi C., Jin L.H., Tricerri M.A. and Jonas A. (2004). Enthalpy-driven apolipoprotein A-I and lipid bilayer interaction indicating protein penetration upon lipid binding. *Biochemistry* **43**(38): 12258-12264.

3. Ataka K. and Heberle J. (2006). Use of surface enhanced infrared absorption spectroscopy (SEIRA) to probe the functionality of a protein monolayer. *Biopolymers* **82**(4): 415-419.

4. Banerjee S., Huber T. and Sakmar T.P. (2008). Rapid incorporation of functional rhodopsin into nanoscale apolipoprotein bound bilayer (NABB) particles. *J. Mol. Biol.* **377**(4): 1067-1081.

5. Bartfai T., Benovic J.L., Bockaert J., Bond R.A., Bouvier M., Christopoulos A., Civelli O., Devi L.A., George S.R., Inui A., Kobilka B., Leurs R., Neubig R., Pin J.P., Quirion R., Roques B.P., Sakmar T.P., Seifert R., Stenkamp R.E. and Strange P.G. (2004). The state of GPCR research in 2004. *Nat. Rev. Drug Discovery* **3**(7): 574-626.

6. Bayburt T.H., Grinkova Y.V. and Sligar S.G. (2002). Self-assembly of discoidal phospholipid bilayer nanoparticles with membrane scaffold proteins. *Nano Lett.* **2**(8): 853-856.

7. Bayburt T.H., Leitz A.J., Xie G., Oprian D.D. and Sligar S.G. (2007). Transducin activation by nanoscale lipid bilayers containing one and two rhodopsins. *J. Biol. Chem.* **282**(20): 14875-14881.

8. Bayburt T.H. and Sligar S.G. (2002). Single-molecule height measurements on microsomal cytochrome P450 in nanometer-scale phospholipid bilayer disks. *Proc. Natl. Acad. Sci. USA* **99**(10): 6725-6730.

9. Bayburt T.H. and Sligar S.G. (2003). Self-assembly of single integral membrane proteins into soluble nanoscale phospholipid bilayers. *Protein Sci.* **12**(11): 2476-2481.

10. Benkirane M., Jin D.Y., Chun R.F., Koup R.A. and Jeang K.T. (1997). Mechanism of transdominant inhibition of CCR5-mediated HIV-1 infection by CCR5Δ32. *J. Biol. Chem.* **272**(49): 30603-30606.

11. Bergendahl V., Anthony L.C., Heyduk T. and Burgess R.R. (2002). On-column tris(2-carboxyethyl)phosphine reduction and IC5-maleimide labeling during purification of a RpoC fragment on a nickel-nitrilotriacetic acid column. *Anal. Biochem.* **307**(2): 368-374.

12. Berger E.A., Murphy P.M. and Farber J.M. (1999). Chemokine receptors as HIV-1 coreceptors: Roles in viral entry, tropism, and disease. *Ann. Rev. Immunol.* **17**: 657-700.

13. Bhat S., Sorci-Thomas M.G., Alexander E.T., Samuel M.P. and Thomas M.J. (2005). Intermolecular contact between globular N-terminal fold and C-terminal domain of Apo A-I stabilizes its lipid-bound conformation: studies employing chemical cross-linking and mass spectrometry. *J. Biol. Chem.* **280**(38): 33015-33025.

14. Bockaert J. (2003). The 'magic tail' of G protein-coupled receptors: an anchorage for functional protein networks. *FEBS Lett.* **546**: 65-72.

15. Bockaert J. and Pin J.P. (1999). Molecular tinkering of G protein-coupled receptors: an evolutionary success. *EMBO J.* **18**: 1723-1729.

16. Boesze-Battaglia K. (2000). Fusion between retinal rod outer segment membranes and model membranes: Functional assays and role for peripherin/rds. Vertebrate Phototransduction and the Visual Cycle, Pt B. San Diego, Academic Press Inc. **316:** 65-86.

17. Boguski M.S., Elshourbagy N., Taylor J.M. and Gordon J.I. (1985). Comparative-analysis of repeated sequences in rat apolipoprotein A-I, apolipoprotein A-IV and apolipoprotein E. *Proc. Natl. Acad. Sci. USA* **82**(4): 992-996.

18. Boisset N., Radermacher M., Grassucci R., Taveau J.C., Liu W.P., Lamy J., Frank J. and Lamy J.N. (1993). 3-Dimensional immunoelectron microscopy of scorpion hemocyanin labeled with a monoclonal Fab fragment. *J. Struct. Biol.* **111**(3): 234-244.

19. Borhani D.W., Rogers D.P., Engler J.A. and Brouillette C.G. (1997). Crystal structure of truncated human apolipoprotein A-I suggests a lipid-bound conformation. *Proc. Natl. Acad. Sci. USA* **94**(23): 12291-12296.

20. Botelho A.V., Gibson N.J., Thurmond R.L., Wang Y. and Brown M.F. (2002). Conformational energetics of rhodopsin modulated by nonlamellar-forming lipids. *Biochemistry* **41**(20): 6354-6368.

21. Botelho A.V., Huber T., Sakmar T.P. and Brown M.F. (2005). Direct effect of membrane stress on lipid-rhodopsin organization and function. *Biophys. J.* **88**(1): 579A-579A.

22. Botelho A.V., Huber T., Sakmar T.P. and Brown M.F. (2006). Curvature and hydrophobic forces drive oligomerization and modulate activity of rhodopsin in membranes. *Biophys. J.* **91**(12): 4464-4477.

23. Bouvier M. (2001). Oligomerization of G-protein-coupled transmitter receptors. *Nat. Rev. Neurosci.* **2**: 274-286.

24. Brasseur R., De Meutter J., Vanloo B., Goormaghtigh E., Ruysschaert J.M. and Rosseneu M. (1990). Mode of assembly of amphipathic helical segments in model high-density lipoproteins. *Biochim. Biophys. Acta.* **1043**(3): 245-252.

25. Brown M.F. (1994). Modulation of rhodopsin function by properties of the membrane bilayer. *Chem. Phys. Lipids* **73**(1-2): 159-180.

26. Cardaba C.M., Kerr J.S. and Mueller A. (2008). CCR5 internalization and signaling have different dependence on membrane lipid raft integrity. *Cell. Signal.* **20**(9): 1687-1694.

27. Carnemolla R., Ren X.F., Biswas T.K., Meredith S.C., Reardon C.A., Wang J.J. and Getz G.S. (2008). The specific amino acid sequence between helices 7 and 8 influences the binding specificity of human apolipoprotein A-I for high density lipoprotein (HDL) subclasses – A potential for HDL preferential generation. *J. Biol. Chem.* **283**(23): 15779-15788.

28. Catte A., Patterson J.C., Jones M.K., Jerome W.G., Bashtovyy D., Su Z., Gu F., Chen J., Aliste M.P., Harvey S.C., Li L., Weinstein G. and Segrest J.P. (2006). Novel changes in discoidal high density lipoprotein morphology: a molecular dynamics study. *Biophys. J.* **90**(12): 4345-4360.

29. Chabre M., Cone R. and Saibil H. (2003). Biophysics - Is rhodopsin dimeric in native rods? *Nature* **426**(6962): 30-31.

30. Chabre M. and le Maire M. (2005). Monomeric G-protein-coupled receptor as a functional unit. *Biochemistry* **44**(27): 9395-9403.

31. Cherezov V., Rosenbaum D.M., Hanson M.A., Rasmussen S.G., Thian F.S., Kobilka T.S., Choi H.J., Kuhn P., Weis W.I., Kobilka B.K. and Stevens R.C. (2007). High-resolution crystal structure of an engineered human β_2-adrenergic G protein-coupled receptor. *Science* **318**(5854): 1258-1265.

32. Cohen G.B., Oprian D.D. and Robinson P.R. (1992). Mechanism of activation and inactivation of opsin: role of Glu113 and Lys296. *Biochemistry* **31**(50): 12592-12601.

33. Couve A., Filippov A.K., Connolly C.N., Bettler B., Brown D.A. and Moss S.J. (1998). Intracellular retention of recombinant GABA(B) receptors. *J. Biol. Chem.* **273**(41): 26361-26367.

34. Daemen F.J., Van Breugel P.J., Jansen P.A. and Bonting S.L. (1976). Biochemical aspects of the visual process. XXXIV. Relation between sulfhydryl groups and properties of rhodopsin studied by means of methylmercuric iodide. *Biochim Biophys Acta* **453**(2): 374-382.

35. De Grip W.J. (1982). [38] Thermal stability of rhodopsin and opsin in some novel detergents. *Methods Enzymol.*, Academic Press**:** 256-265.

36. De Grip W.J. and Daemen F.J.M. (1982). [33] Sulfhydryl chemistry of rhodopsin. *Methods Enzymol.*, Academic Press**:** 223-236.

37. Denisov I.G., Grinkova Y.V., Lazarides A.A. and Sligar S.G. (2004). Directed self-assembly of monodisperse phospholipid bilayer nanodiscs with controlled size. *J. Amer. Chem. Soc.* **126**(11): 3477-3487.

38. Devanathan S., Yao Z., Salamon Z., Kobilka B. and Tollin G. (2004). Plasmon-waveguide resonance studies of ligand binding to the human β_2-adrenergic receptor. *Biochemistry* **43**(11): 3280-3288.

39. Doms R.W. and Trono D. (2000). The plasma membrane as a combat zone in the HIV battlefield. *Genes Dev.* **14**(21): 2677-2688.

40. Dowhan W. (1997). Molecular basis for membrane phospholipid diversity: why are there so many lipids? *Ann. Rev. Biochem.* **66**: 199-232.

41. Duronio R.J., Jackson-Machelski E., Heuckeroth R.O., Olins P.O., Devine C.S., Yonemoto W., Slice L.W., Taylor S.S. and Gordon J.I. (1990). Protein N-myristoylation in Escherichia coli: reconstitution of a eukaryotic protein modification in bacteria. *Proc. Natl. Acad. Sci. USA* **87**(4): 1506-1510.

42. Eggeling C., Fries J.R., Brand L., Gunther R. and Seidel C.A. (1998). Monitoring conformational dynamics of a single molecule by selective fluorescence spectroscopy. *Proc. Natl. Acad. Sci. USA* **95**(4): 1556-1561.

43. Ernst O.P., Gramse V., Kolbe M., Hofmann K.P. and Heck M. (2007). Monomeric G protein-coupled receptor rhodopsin in solution activates its G protein transducin at the diffusion limit. *Proc. Natl. Acad. Sci. USA* **104**(26): 10859-10864.

44. Fahmy K. and Sakmar T.P. (1993). Light-dependent transducin activation by an ultraviolet-absorbing rhodopsin mutant. *Biochemistry* **32**(35): 9165-9171.

45. Fahmy K., Siebert F. and Sakmar T.P. (1995). Photoactivated state of rhodopsin and how it can form. *Biophys. Chem.* **56**(1-2): 171-181.

46. Farrens D.L., Altenbach C., Yang K., Hubbell W.L. and Khorana H.G. (1996). Requirement of rigid-body motion of transmembrane helices for light activation of rhodopsin. *Science* **274**(5288): 768-770.

47. Farzan M., Mirzabekov T., Kolchinsky P., Wyatt R., Cayabyab M., Gerard N.P., Gerard C., Sodroski J. and Choe H. (1999). Tyrosine sulfation of the amino terminus of CCR5 facilitates HIV-1 entry. *Cell* **96**(5): 667-676.

48. Fielding C. and Fielding P. (1995). Molecular physiology of reverse cholesterol transport. *J. Lipid Res.* **36**(2): 211-228.

49. Fielding P.E. and C.J. F. (2002). Dynamics of lipoprotein transport in the human circulatory system. Biochemistry of lipids, Lipoproteins and Membranes. Vance D.E and J.E. V. Amsterdam, Elsevier Science. **36:** 527-552.

50. Filipek S. (2005). Organization of rhodopsin molecules in native membranes of rod cells - an old theoretical model compared to new experimental data. *J. Mol. Model.* **11**(4-5): 385-391.

51. Filipek S., Stenkamp R.E., Teller D.C. and Palczewski K. (2003). G protein-coupled receptor rhodopsin: A prospectus. *Ann. Rev. Physiol.* **65**: 851-879.

52. Filipek S., Teller D.C., Palczewski K. and Stenkamp R. (2003). The crystallographic model of rhodopsin and its use in studies of other G protein-coupled receptors. *Ann. Rev. Biophys. Biomol. Struct.* **32**: 375-397.

53. Findlay J.B., Barclay P.L., Brett M., Davison M., Pappin D.J. and Thompson P. (1984). The structure of mammalian rod opsins. *Vision Res.* **24**(11): 1501-1508.

54. Forte T.M., Nichols A.V., Gong E.L., Lux S. and Levy R.I. (1971). Electron microscopic study on reassembly of plasma high density apoprotein with various lipids. *Biochim. Biophys. Acta. (BBA) - Lipids and Lipid Metabolism* **248**(2): 381-386.

55. Fotiadis D., Liang Y., Filipek S., Saperstein D.A., Engel A. and Palczewski K. (2003). Atomic-force microscopy: Rhodopsin dimers in native disc membranes. *Nature* **421**(6919): 127-128.

56. Fotiadis D., Liang Y., Filipek S., Saperstein D.A., Engel A. and Palczewski K. (2004). The G protein-coupled receptor rhodopsin in the native membrane. *FEBS Letters* **564**(3): 281-288.

57. Frank J. (2002). Single-particle imaging of macromolecules by cryo-electron microscopy. *Ann. Rev. Biophys. Biomol. Struc.* **31**: 303-319.

58. Frank P.G. and Marcel Y.L. (2000). Apolipoprotein A-I: structure-function relationships. *J. Lipid Res.* **41**(6): 853-872.

59. George S.R., O'Dowd B.F. and Lee S.P. (2002). G-protein-coupled receptor oligomerization and its potential for drug discovery. *Nat. Rev. Drug Discovery* **1**: 808-820.

60. Gerard C. and Rollins B.J. (2001). Chemokines and disease. *Nat. Immunology* **2**(2): 108-115.

61. Ghanouni P. (2001). Functionally different agonists induce distinct conformations in the G protein coupling domain of the β_2-adrenergic receptor. *J. Biol. Chem.* **276**: 24433-24436.

62. Glick B.R. and Pasternak J.J. (1994). Molecular Biotechnology: Principles and Applications of Recombinant DNA. Washington, DC, ASM Press.

63. Gosling J., Monteclaro F.S., Atchison R.E., Arai H., Tsou C.L., Goldsmith M.A. and Charo I.F. (1997). Molecular uncoupling of C-C chemokine receptor 5-induced chemotaxis and signal transduction from HIV-1 coreceptor activity. *Proc. Natl. Acad. Sci. USA* **94**(10): 5061-5066.

64. Gouldson P.R., Higgs C., Smith R.E., Dean M.K., Gkoutos G.V. and Reynolds C.A. (2000). Dimerization and domain swapping in G-protein-coupled receptors: A computational study. *Neuropsychopharmacology* **23**(4): S60-S77.

65. Greentree W.K. and Linder M.E. (2004). Purification of recombinant G protein alpha subunits from Escherichia coli. *Methods Mol. Biol.* **237**: 3-20.

66. Guo W., Urizar E., Kralikova M., Mobarec J.C., Shi L., Filizola M. and Javitch J.A. (2008). Dopamine D2 receptors form higher order oligomers at physiological expression levels. *EMBO J.* **27**(17): 2293-2304.

67. H. Beverley Osborne C.S.A.H. (1974). Bovine rhodopsin: characterization of the complex formed with Triton X-100. *Eur. J. Biochem.* **44**(2): 383-390.

68. Hainfeld J.F. and Powell R.D. (2000). New frontiers in gold labeling. *J. Histochem. Cytochem.* **48**(4): 471-480.

69. Hainfeld J.F., Powell R.D. and Furuya F.R. (2002). Microscopic Uses of Nanogold. Gold and Silver Staining: Techniques in Molecular Morphology. Hacker G.W. and Gu J. Boca Raton, CRC Press**:** 85-106.

70. Hargrave P.A., McDowell J.H., Feldmann R.J., Atkinson P.H., Rao J.K. and Argos P. (1984). Rhodopsin's protein and carbohydrate structure: selected aspects. *Vision Res.* **24**(11): 1487-1499.

71. Harmon B. and Ratner L. (2008). HIV envelope induction of the $G\alpha_q$ signaling cascade is required for virus entry. *J. Virol*. **82**(18): 9191-9205.

72. Harris J.R. (1997). Negative Staining and Cryoelectron Microscopy: The Thin Film Techniques. Oxford, UK, Bios Scientific Publishers Limited.

73. Hebert T.E., Moffett S., Morello J.P., Loisel T.P., Bichet D.G., Barret C. and Bouvier M. (1996). A peptide derived from a β_2-adrenergic receptor transmembrane domain inhibits both receptor dimerization and activation. *J. Biol. Chem.* **271**(27): 16384-16392.

74. Heck M., Schädel S.A., Maretzki D., Bartl F.J., Ritter E., Palczewski K. and Hofmann K.P. (2003). Signaling states of rhodopsin – Formation of the storage form metarhodopsin III, from active metarhodopsin II. *J. Biol. Chem.* **278**(5): 3162-3169.

75. Henderson R. (1995). The potential and limitations of neutrons, electrons and X-rays for atomic resolution microscopy of unstained biological molecules. *Quart. Rev. Biophys.* **28**(2): 171-193.

76. Hong K. and Hubbell W.L. (1973). Lipid requirements for rhodopsin regenerability. *Biochemistry* **12**(22): 4517-4523.

77. Howard A.D., McAllister G., Feighner S.D., Liu Q., Nargund R.P., Van der Ploeg L.H. and Patchett A.A. (2001). Orphan G-protein-coupled receptors and natural ligand discovery. *Trends Pharmacol. Sci.* **22**(3): 132-140.

78. Huang K.S., Bayley H. and Khorana H.G. (1980). Delipidation of bacteriorhodopsin and reconstitution with exogenous phospholipid. *Proc. Natl. Acad. Sci. USA* **77**(1): 323-327.

79. Hubbard R. (1958). The thermal stability of rhodopsin and opsin. *J. Gen. Physiol.* **42**(2): 259-280.

80. Huber T., Botelho A.V., Beyer K. and Brown M.F. (2004). Membrane model for the G-protein-coupled receptor rhodopsin: hydrophobic interface and dynamical structure. *Biophys. J.* **86**(4): 2078-2100.

81. Huber T., Menon S. and Sakmar T.P. (2008). Structural basis for ligand binding and specificity in adrenergic receptors: implications for GPCR-targeted drug discovery. *Biochemistry* **47**(42): 11013-11023.

82. Huber T. and Sakmar T.P. (2008). Rhodopsin's active state is frozen like a DEER in the headlights. *Proc. Natl. Acad. Sci. USA* **105**(21): 7343-7344.

83. Imamoto Y., Kataoka M., Tokunaga F. and Palczewski K. (2000). Light-induced conformational changes of rhodopsin probed by fluorescent Alexa594 immobilized on the cytoplasmic surface. *Biochemistry* **39**(49): 15225-15233.

84. Jaakola V.P., Griffith M.T., Hanson M.A., Cherezov V., Chien E.Y., Lane J.R., Ijzerman A.P. and Stevens R.C. (2008). The 2.6 Angstrom Crystal Structure of a Human A2A Adenosine Receptor Bound to an Antagonist. *Science*. *In Press.*

85. James J.R., Oliveira M.I., Carmo A.M., Iaboni A. and Davis S.J. (2006). A rigorous experimental framework for detecting protein oligomerization using bioluminescence resonance energy transfer. *Nat. Methods* **3**(12): 1001-1006.

86. Jameson E.E., Roof R.A., Whorton M.R., Mosberg H.I., Sunahara R.K., Neubig R.R. and Kennedy R.T. (2005). Real-time detection of basal and stimulated G protein GTPase activity using fluorescent GTP analogues. *J. Biol. Chem.* **280**(9): 7712-7719.

87. Jastrzebska B., Fotiadis D., Jang G.-F., Stenkamp R.E., Engel A. and Palczewski K. (2006). Functional and structural characterization of rhodopsin oligomers. *J. Biol. Chem.* **281**(17): 11917-11922.

88. Jastrzebska B., Maeda T., Zhu L., Fotiadis D., Filipek S., Engel A., Stenkamp R.E. and Palczewski K. (2004). Functional characterization of rhodopsin monomers and dimers in detergents. *J. Biol. Chem.* **279**(52): 54663-54675.

89. Jonas A. and Drengler S.M. (1980). Kinetics and mechanism of Apolipoprotein A-I interaction with L-Alpha-Dimyristoylphosphatidylcholine vesicles. *J. Biol. Chem.* **255**(5): 2190-2194.

90. Jonas A., Kezdy K.E. and Wald J.H. (1989). Defined Apolipoprotein A-I Conformations in Reconstituted High-Density Lipoprotein Disks. *J. Biol. Chem.* **264**(9): 4818-4824.

91. Jonas A., Krajnovich D.J. and Patterson B.W. (1977). Properties of molecular complexes of A-I apolipoproteins with L-Alpha-Dimyristoyl Phosphatidylcholine. *Federation Proceedings* **36**(3): 829-829.

92. Jonas A., Steinmetz A. and Churgay L. (1993). The number of amphipathic alpha-helical segments of Apolipoprotein A-I, Apolipoprotein E, and Apolipoprotein A-IV determines the size and functional properties of their reconstituted lipoprotein particles. *J. Biol. Chem.* **268**(3): 1596-1602.

93. Jones K.A., Borowsky B., Tamm J.A., Craig D.A., Durkin M.M., Dai M., Yao W.J., Johnson M., Gunwaldsen C., Huang L.Y., Tang C., Shen Q.R., Salon J.A., Morse K., Laz T., Smith K.E., Nagarathnam D., Noble S.A., Branchek T.A. and Gerald C. (1998). GABA(B) receptors function as a heteromeric assembly of the subunits GABA(B)R1 and GABA(B)R2. *Nature* **396**(6712): 674-679.

94. Jones M.K., Anantharamaiah G.M. and Segrest J.P. (1992). Computer-programs to identify and classify amphipathic alpha-helical domains. *J. Lipid Res.* **33**(2): 287-296.

95. Karathanasis S.K., Zannis V.I. and Breslow J.L. (1983). Isolation and characterization of the human apolipoprotein A-I gene. *Proc. Natl. Acad. Sci. USA* **80**(20): 6147-6151.

96. Kaupmann K., Malitschek B., Schuler V., Heid J., Froestl W., Beck P., Mosbacher J., Bischoff S., Kulik A., Shigemoto R., Karschin A. and Bettler B. (1998). GABA(B)-receptor subtypes assemble into functional heteromeric complexes. *Nature* **396**(6712): 683-687.

97. Khurana S., Kennedy M., King L.R. and Golding H. (2005). Identification of a linear peptide recognized by monoclonal antibody 2D7 capable of generating CCR5-specific antibodies with human immunodeficiency virus-neutralizing activity. *J. Virol.* **79**(11): 6791-6800.

98. Kijac A.Z., Li Y., Sligar S.G. and Rienstra C.M. (2007). Magic-angle spinning solid-state NMR spectroscopy of nanodisc-embedded human CYP3A4. *Biochemistry* **46**(48): 13696-13703.

99. Kinter A., Catanzaro A., Monaco J., Ruiz M., Justement J., Moir S., Arthos J., Oliva A., Ehler L., Mizell S., Jackson R., Ostrowski M., Hoxie J., Offord R. and Fauci A.S. (1998). CC-chemokines enhance the replication of T-tropic strains of HIV-1 in CD4(+) T cells: role of signal transduction. *Proc. Natl. Acad. Sci. USA* **95**(20): 11880-11885.

100. Klingenberg M. (1981). Membrane protein oligomeric structure and transport function. *Nature* **290**(5806): 449-454.

101. Klon A.E., Jones M.K., Segrest J.P. and Harvey S.C. (2000). Molecular belt models for the apolipoprotein A-I Paris and Milano mutations. *Biophys. J.* **79**(3): 1679-1685.

102. Klon A.E., Segrest J.P. and Harvey S.C. (2002). Molecular dynamics simulations on discoidal HDL particles suggest a mechanism for rotation in the apo A-I belt model. *J. Mol. Biol.* **324**(4): 703-721.

103. Knudsen P. and Hubbell W.L. (1978). Stability of rhodopsin in detergent solutions. *Membrane Biochem.* **1**(3-4): 297-322.

104. Konno T., Meguro H. and Tuzimura K. (1975). D-Pantolactone as a circular dichroism (CD) calibration. *Anal. Biochem.* **67**(1): 226-232.

105. Kota P., Reeves P.J., RajBhandary U.L. and Khorana H.G. (2006). Opsin is present as dimers in COS1 cells: Identification of amino acids at the dimeric interface. *Proc. Natl. Acad. Sci. USA* **103**(9): 3054-3059.

106. Lakowicz J.R. (1999). Fluorescence Anisotropy. Principles of Fluorescence Spectroscopy. New York, Kluwer Academic. **1:** 291-318.

107. Leekumjorn S. and Sum A.K. (2007). Molecular characterization of gel and liquid-crystalline structures of fully hydrated POPC and POPE bilayers. *J. Phys. Chem. B.* **111**(21): 6026-6033.

108. Leng J., Egelhaaf S.U. and Cates M.E. (2003). Kinetics of the micelle-to-vesicle transition: Aqueous lecithin-bile salt mixtures. *Biophys. J.* **85**(3): 1624-1646.

109. Lewis J.W. and Kliger D.S. (2000). Absorption spectroscopy in studies of visual pigments: spectral and kinetic characterization of intermediates. *Methods Enzymol.* **315**: 164-178.

110. Li H.H., Lyles D.S., Thomas M.J., Pan W. and Sorci-Thomas M.G. (2000). Structural determination of lipid-bound ApoA-I using fluorescence resonance energy transfer. *J. Biol. Chem.* **275**(47): 37048-37054.

111. Li L., Chen J.G., Mishra V.K., Kurtz J.A., Cao D.F., Klon A.E., Harvey S.C., Anantharamaiah G.M. and Segrest J.P. (2004). Double belt structure of discoidal high density lipoproteins: Molecular basis for size heterogeneity. *J. Mol. Biol.* **343**(5): 1293-1311.

112. Li W.H., Tanimura M., Luo C.C., Datta S. and Chan L. (1988). The apolipoprotein multigene family – biosynthesis, structure, structure-function relationships, and evolution. *J. Lipid Res.* **29**(3): 245-271.

113. Li Y., Kijac A.Z., Sligar S.G. and Rienstra C.M. (2006). Structural analysis of nanoscale self-assembled discoidal lipid bilayers by solid-state NMR spectroscopy. *Biophys. J.* **91**(10): 3819-3828.

114. Liang Y., Fotiadis D., Filipek S., Saperstein D.A., Palczewski K. and Engel A. (2003). Organization of the G protein-coupled receptors rhodopsin and opsin in native membranes. *J. Biol. Chem.* **278**(24): 21655-21662.

115. Lin Y.L., Mettling C., Portales P., Reant B., Robert-Hebmann V., Reynes J., Clot J. and Corbeau P. (2006). The efficiency of R5 HIV-1 infection is determined by CD4 T-cell surface CCR5 density through Gαi-protein signalling. *AIDS* **20**(10): 1369-1377.

116. Liu R., Paxton W.A., Choe S., Ceradini D., Martin S.R., Horuk R., MacDonald M.E., Stuhlmann H., Koup R.A. and Landau N.R. (1996). Homozygous defect in HIV-1 coreceptor accounts for resistance of some multiply-exposed individuals to HIV-1 infection. *Cell* **86**(3): 367-377.

117. Lüdtke S.J., Baldwin P.R. and Chiu W. (1999). EMAN: semiautomated software for high-resolution single-particle reconstructions. *J. Struct. Biol.* **128**(1): 82-97.

118. Luttrell L.M. and Lefkowitz R.J. (2002). The role of β-arrestins in the termination and transduction of G-protein-coupled receptor signals. *J. Cell. Sci.* **115**: 455-465.

119. Mansoor S.E., Palczewski K. and Farrens D.L. (2006). Rhodopsin self-associates in asolectin liposomes. *Proc. Natl. Acad. Sci. USA* **103**(9): 3060-3065.

120. Margeta-Mitrovic M., Jan Y.N. and Jan L.Y. (2000). A trafficking checkpoint controls GABA(B) receptor heterodimerization. *Neuron* **27**(1): 97-106.

121. Matz C.E. and Jonas A. (1982). Micellar complexes of human apolipoprotein A-I with phosphatidylcholines and cholesterol prepared from cholate-lipid dispersions. *J. Biol. Chem.* **257**(8): 4535-4540.

122. McCaslin D.R. and Tanford C. (1981). Different states of aggregation for unbleached and bleached rhodopsin after isolation in two different detergents. *Biochemistry* **20**(18): 5212-5221.

123. McEwen D.P., Gee K.R., Kang H.C. and Neubig R.R. (2001). Fluorescent BODIPY-GTP analogs: real-time measurement of nucleotide binding to G proteins. *Anal. Biochem.* **291**(1): 109-117.

124. McGuire K.A., Davidson W.S. and Jonas A. (1996). High yield overexpression and characterization of human recombinant proapolipoprotein A-I. *J. Lipid Res.* **37**(7): 1519-1528.

125. McLachlan A.D. (1977). Repeated helical pattern in apolipoprotein-A-I. *Nature* **267**(5610): 465-466.

126. McVey M., Kellet E., Rees S., Wilson S., Pope A.J. and Milligan G. (2001). Monitoring receptor oligomerization using time-resolved fluorescence resonance energy transfer and bioluminescence resonance energy transfer: The human delta-opioid receptor displays constitutive oligomerization at the cell surface which is not regulated by receptor occupancy. *J. Biol. Chem.* **276**: 14092-14095.

127. Melia T.J., Malinski J.A., He F. and Wensel T.G. (2000). Enhancement of phototransduction protein interactions by lipid surfaces. *J. Biol. Chem.* **275**(5): 3535-3542.

128. Menon S.T., Han M. and Sakmar T.P. (2001). Rhodopsin: structural basis of molecular physiology. *Physiol. Rev.* **81**: 1659-1688.

129. Mercier J.F., Salahpour A., Angers S., Breit A. and Bouvier M. (2002). Quantitative assessment of β1- and β2-adrenergic receptor homo- and heterodimerization by bioluminescence resonance energy transfer. *J. Biol. Chem.* **277**: 44925-44931.

130. Miljanich G.P. and Dratz E.A. (1982). Fatty acid composition and pairing in phospholipids of rod outer segments. *Methods Enzymol.* **81**: 806-815.

131. Mirzabekov T., Bannert N., Farzan M., Hofmann W., Kolchinsky P., Wu L.J., Wyatt R. and Sodroski J. (1999). Enhanced expression, native purification, and characterization of CCR5, a principal HIV-1 coreceptor. *J. Biol. Chem.* **274**(40): 28745-28750.

132. Mishra V.K., Anantharamaiah G.M., Segrest J.P., Palgunachari M.N., Chaddha M., Sham S.W.S. and Krishna N.R. (2006). Association of a model class A apolipoprotein amphipathic α helical peptide with lipid. *J. Biol. Chem.* **281**(10): 6511-6519.

133. Molina M.L., Barrera F.N., Fernandez A.M., Poveda J.A., Renart M.L., Encinar J.A., Riquelme G. and Gonzalez-Ros J.M. (2006). Clustering and coupled gating modulate the activity in KcsA, a potassium channel model. *J. Biol. Chem.* **281**(27): 18837-18848.

134. Mueller A., Mahmoud N.G. and Strange P.G. (2006). Diverse signalling by different chemokines through the chemokine receptor CCR5. *Biochem. Pharmacol.* **72**(6): 739-748.

135. Mukhopadhyay S. and Deniz A.A. (2007). Fluorescence from diffusing single molecules illuminates biomolecular structure and dynamics. *J. Fluoresc.* **17**(6): 775-783.

136. Muller A. (2001). Involvement of chemokine receptors in breast cancer metastasis. *Nature* **410**: 50-56.

137. Navratilova I., Dioszegi M. and Myszka D.G. (2006). Analyzing ligand and small molecule binding activity of solubilized GPCRs using biosensor technology. *Anal. Biochem.* **355**(1): 132-139.

138. Navratilova I., Sodroski J. and Myszka D.G. (2005). Solubilization, stabilization, and purification of chemokine receptors using biosensor technology. *Anal. Biochem.* **339**(2): 271-281.

139. Nelson D.L. and Cox M.M. (2004). Enzymes. Lehninger Principles of Biochemistry. New York, Worth Publishers**:** 263-264.

140. Nion S., Demoor L., Boutillon C., Luchoomun J., Vanloo B., Fievet C., Castro G., Rosseneu M., Fruchart J.-C., Tartar A. and Clavey V. (1998). Branched synthetic peptide constructs mimic cellular binding and efflux of apolipoprotein AI in reconstituted high density lipoproteins. *Atherosclerosis* **141**(2): 227-235.

141. Niu L., Kim J.M. and Khorana H.G. (2002). Structure and function in rhodopsin: Asymmetric reconstitution of rhodopsin in liposomes. *Proc. Natl. Acad. Sci. USA* **99**(21): 13409-13412.

142. O'Brien S.J. and Moore J.P. (2000). The effect of genetic variation in chemokines and their receptors on HIV transmission and progression to AIDS. *Immunol. Reviews* **177**: 99-111.

143. Okada T., Takeda K. and Kouyama T. (1998). Highly selective separation of rhodopsin from bovine rod outer segment membranes using combination of divalent cation and alkyl(thio)glucoside. *Photochem. Photobiol.* **67**(5): 495-499.

144. Opella S.J. and Marassi F.M. (2004). Structure determination of membrane proteins by NMR spectroscopy. *Chem. Rev.* **104**(8): 3587-3606.

145. Oppermann M. (2004). Chemokine receptor CCR5: insights into structure, function, and regulation. *Cell. Signal.* **16**(11): 1201-1210.

146. Osborne H.B., Sardet C., Michel-Villaz M. and Chabre M. (1978). Structural study of rhodopsin in detergent micelles by small-angle neutron scattering. *J. Mol. Biol.* **123**(2): 177-206.

147. Palanche T. (2001). The neurokinin A receptor activates calcium and cAMP responses through distinct conformational states. *J. Biol.Chem.* **276**: 34853-34861.

148. Palczewski K. (2000). Crystal structure of rhodopsin: a G protein-coupled receptor. *Science* **289**: 739-745.

149. Palczewski K., Kumasaka T., Hori T., Behnke C.A., Motoshima H., Fox B.A., Le Trong I., Teller D.C., Okada T., Stenkamp R.E., Yamamoto M. and Miyano M. (2000). Crystal structure of rhodopsin: A G protein-coupled receptor. *Science* **289**(5480): 739-745.

150. Papermaster D.S. (1982). Preparation of retinal rod outer segments. *Methods Enzymol.* **81**: 48-52.

151. Periole X., Huber T., Marrink S.J. and Sakmar T.P. (2007). G protein-coupled receptors self-assemble in dynamics simulations of model bilayers. *J. Amer. Chem. Soc.* **129**(33): 10126-10132.

152. Phillips J.C., Wriggers W., Li Z., Jonas A. and Schulten K. (1997). Predicting the structure of apolipoprotein A-I in reconstituted high-density lipoprotein disks. *Biophys. J.* **73**(5): 2337-2346.

153. Phillips W. and Cerione R. (1988). The intrinsic fluorescence of the alpha subunit of transducin. Measurement of receptor-dependent guanine nucleotide exchange. *J. Biol. Chem.* **263**(30): 15498-15505.

154. Princen K. and Schols D. (2005). HIV chemokine receptor inhibitors as novel anti-HIV drugs. *Cytokine Growth Factor Rev.* **16**(6): 659-677.

155. Proudfoot A.E.I. (2002). Chemokine receptors: Multifaceted therapeutic targets. *Nat. Rev. Immunology* **2**(2): 106-115.

156. Ramachandran S. and Cerione R.A. (2004). Stabilization of an intermediate activation state for transducin by a fluorescent GTP analogue. *Biochemistry* **43**(27): 8778-8786.

157. Reschly E.J., Sorci-Thomas M.G., Davidson W.S., Meredith S.C., Reardon C.A. and Getz G.S. (2002). Apolipoprotein A-I alpha -helices 7 and 8 modulate high density lipoprotein subclass distribution. *J. Biol. Chem.* **277**(12): 9645-9654.

158. Ridge K.D., Abdulaev N.G., Sousa M. and Palczewski K. (2003). Phototransduction: crystal clear. *Trends in Biochemical Sciences* **28**(9): 479-487.

159. Rigaud J.L., Pitard B. and Levy D. (1995). Reconstitution of Membrane-Proteins into Liposomes - Application to Energy-Transducing Membrane-Proteins. *Biochim. Biophys. Acta* **1231**(3): 223-246.

160. Rodriguez-Frade J.M., del Real G., Serrano A., Hernanz-Falcon P., Soriano S.F., Vila-Coro A.J., de Ana A.M., Lucas P., Prieto I., Martinez A.C. and Mellado M. (2004). Blocking HIV-1 infection via CCR5 and CXCR4 receptors by acting in trans on the CCR2 chemokine receptor. *EMBO J.* **23**(1): 66-76.

161. Rogers D.P., Brouillette C.G., Engler J.A., Tendian S.W., Roberts L., Mishra V.K., Anantharamaiah G.M., LundKatz S., Phillips M.C. and Ray M.J. (1997). Truncation of the amino terminus of human apolipoprotein A-I substantially alters only the lipid-free conformation. *Biochemistry* **36**(2): 288-300.

162. Rogers D.P., Roberts L.M., Lebowitz J., Datta G., Anantharamaiah G.M., Engler J.A. and Brouillette C.G. (1998). The lipid-free structure of apolipoprotein A-I: Effects of amino-terminal deletions. *Biochemistry* **37**(34): 11714-11725.

163. Romano C., Yang W.L. and O'Malley K.L. (1996). Metabotropic glutamate receptor 5 is a disulfide-linked dimer. *J. Biol. Chem.* **271**(45): 28612-28616.

164. Rossi D. and Zlotnik A. (2000). The biology of chemokines and their receptors. *Ann. Rev. Immunol.* **18**: 217-243.

165. Rubin J.B., Kung A.L., Klein R.S., Chan J.A., Sun Y.P., Schmidt K., Kieran M.W., Luster A.D. and Segal R.A. (2003). A small-molecule antagonist of CXCR4 inhibits intracranial growth of primary brain tumors. *Proc. Natl. Acad. Sci. USA* **100**(23): 13513-13518.

166. Saibil H., Chabre M. and Worcester D. (1976). Neutron diffraction studies of retinal rod outer segment membranes. *Nature* **262**(5566): 266-270.

167. Sakmar T.P. (2002). Structure of rhodopsin and the superfamily of seven-helical receptors: the same and not the same. *Curr. Op. Cell Biol.* **14**(2): 189-195.

168. Salom D., Lodowski D.T., Stenkamp R.E., Le Trong I., Golczak M., Jastrzebska B., Harris T., Ballesteros J.A. and Palczewski K. (2006). Crystal structure of a photoactivated deprotonated intermediate of rhodopsin. *Proc. Natl. Acad. Sci. USA* **103**(44): 16123-16128.

169. Samson M., Libert F., Doranz B.J., Rucker J., Liesnard C., Farber C.M., Saragosti S., Lapoumeroulie C., Cognaux J., Forceille C., Muyldermans G., Verhofstede C., Burtonboy G., Georges M., Imai T., Rana S., Yi Y.J., Smyth R.J., Collman R.G., Doms R.W., Vassart G. and Parmentier M. (1996). Resistance to HIV-1 infection in Caucasian individuals bearing mutant alleles of the CCR-5 chemokine receptor gene. *Nature* **382**(6593): 722-725.

170. Scheerer P., Park J.H., Hildebrand P.W., Kim Y.J., Krauss N., Choe H.W., Hofmann K.P. and Ernst O.P. (2008). Crystal structure of opsin in its G-protein-interacting conformation. *Nature* **455**(7212): 497-502.

171. Scholtz J.M., Hong Q., York E.J., Stewart J.M. and Baldwin R.L. (1991). Parameters of helix-coil transition theory for alanine-based peptides of varying chain lengths in water. *Biopolymers* **31**(13): 1463-1470.

172. Schulz G.E. and R.H. S. (1979). Noncovalant Forces Determining Protein Structure. Principles of Protein Structure. C.R. C. New York, Springer. **1:** 27-44.

173. Scotton C.J., Wilson J.L., Scott K., Stamp G., Wilbanks G.D., Fricker S., Bridger G. and Balkwill F.R. (2002). Multiple actions of the chemokine CXCL12 on epithelial tumor cells in human ovarian cancer. *Cancer Res.* **62**(20): 5930-5938.

174. Seelig J. (2004). Thermodynamics of lipid-peptide interactions. *Biochim. Biophys. Acta-Biomembranes* **1666**(1-2): 40-50.

175. Segel I.H. (1993). Turnover Number. Enzyme Kinetics. New York, Wiley-Interscience. **1:** 79-80.

176. Segrest J.P., Garber D.W., Brouillette C.G., Harvey S.C. and Anantharamaiah G.M. (1994). The amphipathic alpha-helix - a multifunctional structural motif in plasma apolipoproteins. *Adv. Protein Chem.* **45**: 303-369.

177. Segrest J.P., Jones M.K., Deloof H., Brouillette C.G., Venkatachalapathi Y.V. and Anantharamaiah G.M. (1992). The amphipathic helix in the exchangeable apolipoproteins - a review of secondary structure and function. *J. Lipid Res.* **33**(2): 141-166.

178. Segrest J.P., Jones M.K., Klon A.E., Sheldahl C.J., Hellinger M., De Loof H. and Harvey S.C. (1999). A detailed molecular belt model for apolipoprotein A-I in discoidal high-density lipoprotein. *J. Biol. Chem.* **274**(45): 31755-31758.

179. Segrest J.P., Li L., Anantharamaiah G.M., Harvey S.C., Liadaki K.N. and Zannis V. (2000). Structure and function of apolipoprotein A-I and high-density lipoprotein. *Curr. Op. Lipidology* **11**(2): 105-115.

180. Seifert R., Wenzel-Seifert K. and Kobilka B.K. (1999). GPCR–Gα fusion proteins: molecular analysis of receptor–G-protein coupling. *Trends Pharmacol. Sci.* **20**: 383-389.

181. Sheldahl C. and Harvey S.C. (1999). Molecular dynamics on a model for nascent high-density lipoprotein: role of salt bridges. *Biophys. J.* **76**(3): 1190-1198.

182. Shih A.Y., Denisov I.G., Phillips J.C., Sligar S.G. and Schulten K. (2005). Molecular dynamics simulations of discoidal bilayers assembled from truncated human lipoproteins. *Biophys. J.* **88**(1): 548-556.

183. Shimamura T., Hiraki K., Takahashi N., Hori T., Ago H., Masuda K., Takio K., Ishiguro M. and Miyano M. (2008). Crystal structure of squid rhodopsin with intracellularly extended cytoplasmic region. *J. Biol. Chem.* **283**(26): 17753-17756.

184. Siebert F. (1995). Infrared spectroscopy applied to biochemical and biological problems. *Methods Enzymol.* **246**: 501-526.

185. Silva R., Hilliard G.M., Li L., Segrest J.P. and Davidson W.S. (2005). A mass spectrometric determination of the conformation of dimeric apolipoprotein A-I in discoidal high density lipoproteins. *Biochemistry* **44**(24): 8600-8607.

186. Silvius J.R. and l'Heureux F. (1994). Fluorimetric evaluation of the affinities of isoprenylated peptides for lipid bilayers. *Biochemistry* **33**(10): 3014-3022.

187. Smith R.W., Wood C.M., Cash P., Diao L. and Part P. (2005). Apolipoprotein A-I could be a significant determinant of epithelial integrity in rainbow trout gill cell cultures: A study in functional proteomics. *Biochim. Biophys. Acta* **1749**(1): 81-93.

188. Sorci-Thomas M.G., Curtiss L., Parks J.S., Thomas M.J. and Kearns M.W. (1997). Alteration in apolipoprotein A-I 22-mer repeat order results in a decrease in lecithin:cholesterol acyltransferase reactivity. *J. Biol. Chem.* **272**(11): 7278-7284.

189. Soubias O., Teague W.E. and Gawrisch K. (2006). Evidence for specificity in lipid-rhodopsin interactions. *J. Biol. Chem.* **281**(44): 33233-33241.

190. Springael J.Y., de Poorter C., Deupi X., Van Durme J., Pardo L. and Parmentier M. (2007). The activation mechanism of chemokine receptor CCR5 involves common structural changes but a different network of interhelical interactions relative to rhodopsin. *Cell. Signal.* **19**(7): 1446-1456.

191. Steinberg S.F. and Brunton L.L. (2001). Compartmentation of G-protein-coupled signaling pathways in cardiac myocytes. *Ann. Rev. Pharmacol. Toxicol.* **41**: 751-773.

192. Stenlund P., Babcock G.J., Sodroski J. and Myszka D.G. (2003). Capture and reconstitution of G protein-coupled receptors on a biosensor surface. *Anal. Biochem.* **316**(2): 243-250.

193. Stryer L., Hurley J.B. and Fung B.K. (1983). Transducin and the cyclic GMP phosphodiesterase of retinal rod outer segments. *Methods Enzymol.* **96**: 617-627.

194. Suda K., Filipek S., Palczewski K., Engel A. and Fotiadis D. (2004). The supramolecular structure of the GPCR rhodopsin in solution and native disc membranes. *Mol. Membr. Biol.* **21**(6): 435-446.

195. Suryanarayana S., von Zastrow M. and Kobilka B.K. (1992). Identification of intramolecular interactions in adrenergic receptors. *J. Biol. Chem.* **267**(31): 21991-21994.

196. Swaminath G. (2004). Sequential binding of agonists to the β2 adrenoceptor. Kinetic evidence for intermediate conformational states. *J. Biol. Chem.* **279**: 686-691.

197. Tricerri M.A., Agree A.K.B., Sanchez S.A., Bronski J. and Jonas A. (2001). Arrangement of apolipoprotein A-I in reconstituted high-density lipoprotein disks: An alternative model based on fluorescence resonance energy transfer experiments. *Biochemistry* **40**(16): 5065-5074.

198. Tricerri M.A., Toledo J.D., Sanchez S.A., Hazlett T.L., Gratton E., Jonas A. and Garda H.A. (2005). Visualization and analysis of apolipoprotein A-I interaction with binary phospholipid bilayers. *J. Lipid Res.* **46**(4): 669-678.

199. van Meer G., Voelker D.R. and Feigenson G.W. (2008). Membrane lipids: where they are and how they behave. *Nat. Rev. Mol. Cell Biol.* **9**(2): 112-124.

200. Vila-Coro A.J., Mellado M., Martin de Ana A., Lucas P., del Real G., Martinez A.C. and Rodriguez-Frade J.M. (2000). HIV-1 infection through the CCR5 receptor is blocked by receptor dimerization. *Proc. Natl. Acad. Sci. USA* **97**(7): 3388-3393.

201. Vuong T.M., Chabre M. and Stryer L. (1984). Millisecond activation of transducin in the cyclic nucleotide cascade of vision. *Nature* **311**(5987): 659-661.

202. Warne T., Serrano-Vega M.J., Baker J.G., Moukhametzianov R., Edwards P.C., Henderson R., Leslie A.G., Tate C.G. and Schertler G.F. (2008). Structure of a β1-adrenergic G-protein-coupled receptor. *Nature* **454**(7203): 486-491.

203. Wedegaertner P.B., Wilson P.T. and Bourne H.R. (1995). Lipid modifications of trimeric G Proteins. *J. Biol. Chem.* **270**(2): 503-506.

204. White J.H., Wise A., Main M.J., Green A., Fraser N.J., Disney G.H., Barnes A.A., Emson P., Foord S.M. and Marshall F.H. (1998). Heterodimerization is required for the formation of a functional GABA(B) receptor. *Nature* **396**(6712): 679-682.

205. White S.H. and Wimley W.C. (1999). Membrane protein folding and stability: Physical principles. *Ann. Rev. Biophys. Biomol. Struct.* **28**: 319-365.

206. Whorton M.R., Bokoch M.P., Rasmussen S.G., Huang B., Zare R.N., Kobilka B. and Sunahara R.K. (2007). A monomeric G protein-coupled receptor isolated in a high-density lipoprotein particle efficiently activates its G protein. *Proc. Natl. Acad. Sci. USA* **104**(18): 7682-7687.

207. Wieprecht T., Beyermann M. and Seelig J. (2002). Thermodynamics of the coil-[alpha]-helix transition of amphipathic peptides in a membrane environment: the role of vesicle curvature. *Biophys. Chem.* **96**(2-3): 191-201.

208. Wilkinson D. (1996). Cofactors provide the entry keys. HIV-1. *Curr. Biol.* **6**(9): 1051-1053.

209. Wlodawer A., Segrest J.P., Chung B.H., Chiovetti R. and Weinstein J.N. (1979). High-density lipoprotein recombinants: evidence for a bicycle tire micelle structure obtained by neutron scattering and electron microscopy. *FEBS Lett.* **104**(2): 231-235.

210. Wool G.D., Reardon C.A. and Getz G.S. (2008). Apolipoprotein A-I mimetic peptide helix number and helix linker influence potentially anti-atherogenic properties. *J. Lipid Res.* **49**(6): 1268-1283.

211. Wu L., LaRosa G., Kassam N., Gordon C.J., Heath H., Ruffing N., Chen H., Humblias J., Samson M., Parmentier M., Moore J.P. and Mackay C.R. (1997). Interaction of chemokine receptor CCR5 with its ligands: Multiple domains for HIV-1 gp120 binding and a single domain for chemokine binding. *J. Exp. Med.* **186**(8): 1373-1381.

212. Yan E.C., Kazmi M.A., Ganim Z., Hou J.M., Pan D., Chang B.S., Sakmar T.P. and Mathies R.A. (2003). Retinal counterion switch in the photoactivation of the G protein-coupled receptor rhodopsin. *Proc Natl Acad Sci USA* **100**(16): 9262-9267.

213. Zhang J., Rao E., Dioszegi M., Kondru R., DeRosier A., Chan E., Schwoerer S., Cammack N., Brandt M., Sankuratri S. and Ji C. (2007). The second extracellular loop of CCR5 contains the dominant epitopes for highly potent anti-human immunodeficiency virus monoclonal antibodies. *Antimicrob. Agents Chemother.* **51**(4): 1386-1397.

214. Zhang Z.X., Melia T.J., He F., Yuan C., McGough A., Schmid M.F. and Wensel T.G. (2004). How a G protein binds a membrane. *J. Biol. Chem.* **279**(32): 33937-33945.

215. Zou Y.R., Kottmann A.H., Kuroda M., Taniuchi I. and Littman D.R. (1998). Function of the chemokine receptor CXCR4 in haematopoiesis and in cerebellar development. *Nature* **393**(6685): 595-599.

216. Zvyaga T.A., Fahmy K., Siebert F. and Sakmar T.P. (1996). Characterization of the mutant visual pigment responsible for congenital night blindness: a biochemical and Fourier-transform infrared spectroscopy study. *Biochemistry* **35**(23): 7536-7545.